

# MASS TRANSFER

## 1. Introduction

Mass transfer phenomena impact upon all facets of chemical technology. Transport effects often determine the productivity of reactors and the downstream product recovery operations. Gas–liquid mass transfer problems arise during supply of oxygen and other gases from a gas phase to a liquid medium in processes, eg, oxidation, chlorination, and catalytic hydrogenation. Similarly, gas–liquid mass transfer issues must be faced again during recovery operations, eg, distillation. Liquid–liquid mass transfer occurs during emulsion polymerization, liquid–liquid extraction, and supply of oxygen using liquid carriers, eg, perfluorocarbons. Solid–liquid mass transfer problems are faced in adsorption processes and operations, eg, crystallization. Performance of solid-phase catalysts in numerous processes is limited by solid–liquid mass transfer. Solid–liquid mass transfer effects influence membrane separations, eg, microfiltration and ultrafiltration. Transport within solid particles, or intraparticle mass transfer, can become limiting in heterogeneous catalysis. Gas–solid transport is seen during some drying situations. Some of these transport issues are the focus of this article.

Ultimately, the transport of a solute through any fluid or space is governed by the molecular diffusivity or the diffusion coefficient of the solute in the fluid or solution. How diffusivity is affected by factors, eg, temperature and viscosity, and the estimation of diffusivities in various situations are discussed below.

## 2. Diffusion Coefficient or Diffusivity

Mass diffusivity,  $D$ , is a measure of a solute's mobility in a solvent. Mass diffusivity is the equivalent of thermal diffusivity ( $\alpha_H = (k_H/C_p\rho)$ ) of heat transfer problems and the momentum diffusivity (ie, kinematic viscosity,  $\mu/\rho$ ) of momentum transfer. For diffusion of a solute through a fluid (or a continuous phase), the diffusion coefficient depends on temperature, the type of fluid and its viscosity, and the concentration of solute in solution. Diffusivities in liquids and gases generally increase with temperature. At atmospheric pressure, the diffusivity ( $D$ ) in a gas depends on the absolute temperature as follows:  $D \propto T^b$ , where the  $b$  value varies between 1.66 and 2.00. Liquid-phase diffusivities are little affected by pressure, but in gases diffusivities decline approximately linearly as pressure increases. Typically, liquid-phase diffusivities are only about a hundredth of those in gases.

When a fluid is confined in a porous solid, the effects of pore walls and tortuosity reduce diffusivity value relative to that in the unconfined fluid. Diffusion in homogeneous solids occurs exceedingly slowly. As an approximate guide, Table 1 lists the typical magnitudes of diffusivity values for a solute diffusing in various continuous phases. A component A may diffuse in a continuous phase of the same component (ie, diffusion in itself), or a different component B. Self-diffusivity,  $D_{AA}$ , refers to the diffusion of a component in itself. When the components A and B are of similar molecular properties (molar mass, polarity), self-diffusion coefficients of A and B are approximately equal to the mutual diffusivity,

## 2 MASS TRANSFER

$D_{AB}$  (1). Also, if A and B are the more and the less mobile components, respectively, then the mutual diffusivity  $D_{AB}$  tends to have a value between the upper and the lower limits of  $D_{AA}$  and  $D_{BB}$  (1).

Diffusion coefficients of common solute–solvent combinations are available in handbooks. Tables 2 and 3 provide some typical data. Methods of measuring diffusion coefficients have been described by Geankoplis (2) and Pratt (3). When diffusion coefficients are not available, they can be estimated as discussed in the next section.

**2.1. Diffusivity in Solvents, Polymer Solutions, and Gels.** The diffusivity of a small solute A diffusing in a dilute liquid B can be estimated using the Wilke–Chang equation (4),

$$D_{AB} = 1.173 \times 10^{-16} \frac{(\xi M_B)^{0.5} T}{\mu_B V_A^{0.6}} \quad (1)$$

where  $M_B$  and  $\mu_B$  are the molecular weight and the viscosity of the solvent, respectively;  $T$  is the absolute temperature,  $V_A$  is the molar volume of the solute at its boiling point, and  $\xi$  is the association parameter—a measure of polar interactions among molecules—of the solvent. Association parameters of some common solvents are noted in Table 4 (4). The molar volumes are given in handbooks, or, for organic solutes, they are easily calculated by the group contribution method (2,3). Equation 1 is suitable for small solutes with  $V_A \leq 0.500 \text{ m}^3/\text{kmol}$ . When molar volumes are larger, as with globular proteins, Stokes–Einstein equation may be used to estimate diffusivities; thus,

$$D_{AB} = \frac{9.96 \times 10^{-16} T}{\mu_B V_A^{1/3}} \quad (2)$$

Larger molecules diffuse more slowly than small ones. For example, the diffusivities of globular proteins (Table 3) are much smaller than those of the solutes listed in Table 2.

Small solutes, eg, sugar or oxygen, diffusing in solutions of polymers move more slowly than in water. Diffusion coefficient  $D_{AP}$  of a small solute in a solution of a globular protein can be approximated as

$$D_{AP} = D_A(1 - 1.81 \times 10^{-3} C) \quad (3)$$

where  $D_A$  is the diffusivity of the solute in water and  $C \text{ (kg/m}^3\text{)}$  is the concentration of protein in solution (2). Equation 3 is suitable only when the diffusing solute does not associate with the protein molecule. When a solute associates with the protein, a part of the observed diffusivity of solute is due to diffusion of the protein molecules and a part is due to diffusion of unassociated solute.

Small molecules diffusing through gels such as agar, gelatin, and alginate, diffuse more slowly than in water. The diffusion coefficient declines with increasing concentration of the gelling agent; however, in typically formulated gels, diffusivities are only 20–50% lower than in water. Inorganic salts and electrolytes

that dissociate in water actually diffuse as ‘molecules’ in the absence of electric fields. Diffusivities of electrolytes may be estimated using methods discussed by Pratt (3) and Knudsen and co-workers (1).

**2.2. Diffusivity in Gases and Vapors.** Diffusion in gases and vapors depends on pressure because pressure affects the mean free path or the average distance traveled by molecules between molecular collisions. Also, the mean free path  $\lambda_m$  (m) varies with temperature, the molecular weight, and the viscosity of the gas, as follows:

$$\lambda_m = \frac{3.2\mu_G}{P_g} \left( \frac{R_G T}{2\pi M_G} \right)^{1/2} \quad (4)$$

In equation 4,  $P_g$  is the pressure,  $R_G$  is the gas constant,  $\mu_G$  is the gas viscosity, and  $M_G$  is the molar mass of the gas.

Many correlations are available for estimating diffusivity of one gas in another (1), but no single correlation is satisfactory for every situation. For mutual diffusion of binary mixtures of nonpolar gases at low pressure, a suitable equation for diffusivity is the Fuller–Schettler–Giddings equation (1), as follows:

$$D_{AB} = \frac{0.001T^{1.75}(M_A M_B)^{1/2}}{P_g \left[ (\Sigma v_A)^{1/3} + (\Sigma v_B)^{1/3} \right]^2} \quad (5)$$

In equation 5,  $T$  is the absolute temperature,  $M_A$  and  $M_B$  are the molar masses of A and B, respectively,  $P_g$  is the pressure, and  $\Sigma v_A$  and  $\Sigma v_B$  are diffusion volumes ( $\text{cm}^3/\text{mol}$ ) of A and B. The diffusion volume of a component is estimated using diffusion volumes of the atoms in the molecule. Some atomic diffusion volumes ( $\text{cm}^3/\text{mol}$ ) are C, 16.5; H, 1.98; O, 5.48; N, 5.69; Cl, 19.5; S, 17.0; aromatic ring,  $-20.2$ ; and heterocyclic ring,  $-20.2$ .

For estimating mutual diffusivity of polar gases in binary mixtures at low pressure, a suitable equation is the Brokaw equation (1):

$$D_{AB} = \frac{18.58 \times 10^{-4} T^{3/2} (M_A M_B)^{1/2}}{P_g \sigma_{AB}^2 \Omega_D} \quad (6)$$

where  $\sigma_{AB}$  is a characteristic length ( $\text{\AA}$ ), calculated as follows:

$$\sigma_{AB} = \frac{\sigma_A + \sigma_B}{2} \quad (7)$$

and

$$\sigma_i = 1.18 V_b^{1/3} \quad (8)$$

## 4 MASS TRANSFER

The parameter  $V_b$  is the molar volume ( $\text{cm}^3/\text{mol}$ ) of a component at its normal boiling point. The parameter  $\Omega_D$  in equation 6 is related to the absolute temperature, as follows:

$$\Omega_D = \left[ 44.54 \left( \frac{k_B T}{(\varepsilon_A \varepsilon_B)^{1/2}} \right)^{-4.909} + 1.911 \left( \frac{k_B T}{(\varepsilon_A \varepsilon_B)^{1/2}} \right)^{-1.575} \right]^{0.1} \quad (9)$$

In equation 9,  $k_B$  is Boltzman constant ( $8.9308 \times 10^{-10}$  g equiv  $\Omega/\text{s}$ ) and  $\varepsilon$  is the characteristic Lennard-Jones energy. The latter depends on the normal boiling temperature ( $T_b$ , K), as follows:

$$\varepsilon = 1.15 T_b k_B \quad (10)$$

For supercritical binary gas mixtures, the mutual diffusivity can be estimated using Sun-Chen equation (1), as follows:

$$D_{AB} = \frac{1.23 \times 10^{-10} T}{\mu_B^{0.799} V_A^{0.49}} \quad (11)$$

where  $V_A$  is the molar volume of A at its critical point and  $\mu_B$  is the viscosity of the continuous phase. The typical diffusivity values for some gases and vapors in air are noted in Table 5.

## 3. Gas–Liquid Mass Transfer

Gas–liquid reactions and contacting operations are exceedingly common in the processing of chemicals. Reactions, eg, oxidations, chlorinations, hydrogenations, and polymerization of alkenes require efficient contacting of gases and liquids. Gas–liquid mass transfer without reaction occurs typically in separation processes, eg, distillation and absorption. Biotechnology processes for culturing microorganisms often require transfer of oxygen and carbon dioxide (5). Gas–liquid mass transfer can be especially difficult in viscous fluids, eg, fermentation broths and polymer solutions (5,6).

Generally, gases are sparingly soluble in liquids. Consequently, the supply of a dissolved gas in a reactor is rapidly exhausted by the reaction and the dissolved gas must be replenished continuously by bubbling. The transport route of a soluble gas from the gas to the liquid-phase is schematically illustrated in Fig. 1. The gas may be imagined as passing through stagnant gas and liquid films on either side of the gas–liquid interface. The resistance to transfer is localized within the stagnant films and the gas–liquid interface itself is assumed to offer no resistance to mass transfer. Mass transfer in the films occurs solely by diffusion; therefore, at steady state, linear concentration profiles exist in the

films (Fig. 1). The transport flux ( $J$ ) of the diffusing species is related to the concentration gradient ( $\Delta C$ ) in the film and to the film thickness ( $\delta$ ) as follows:

$$J = \frac{D}{\delta} \Delta C \quad (12)$$

In equation 12,  $D$  is the diffusivity of the transferring component in the film. The ratio  $D/\delta$  is known as the mass transfer coefficient,  $k$ . For an ideal gas, the thickness  $\delta_G$  of the laminar gas film at the gas–liquid interface is related with diffusivity ( $D_G$ ) and pressure ( $P_g$ ), as follows:

$$\delta_G = \frac{P_g D_G}{k_G R_G T} \quad (13)$$

where  $k_G$  ( $\text{kmol} \cdot \text{s}^{-1} \text{m}^{-2}$ ) is the gas–film mass transfer coefficient.

At steady state, the flux of the diffusing component—or the rate of transfer per unit cross-sectional area—is the same through the gas and the liquid films; thus, equation 12 may be written for each of the two films:

$$J = k_G (C_G - C_{Gi}) \quad (14)$$

$$= k_L (C_{Li} - C_L) \quad (15)$$

where  $k_G$  and  $k_L$  are the gas and the liquid film mass transfer coefficients, respectively. The overall mass flux from the gas to the liquid-phase may be written as follows:

$$J = K_L (C^* - C_L) \quad (16)$$

where  $C^*$  is the saturation concentration (ie, the maximum possible value) of the diffusing component in the liquid in equilibrium with the gas phase and  $K_L$  is the overall mass transfer coefficient based on the liquid film. The saturation concentration  $C^*$  in the liquid is related to the gas phase concentration ( $C_G$ ) of the diffusing component by Henry's law:

$$C_G = H C^* \quad (17)$$

where  $H$  is the dimensionless Henry's constant (7). Using equations 14–17 and the knowledge that  $C_{Gi} = H \cdot C_{Li}$  (ie, equilibrium exists at the interface because the interface offers no resistance to mass transfer), the various mass transfer coefficients can be shown to be related as follows (7):

$$\frac{1}{K_L} = \frac{1}{k_L} + \frac{1}{H k_G} \quad (18)$$

For a sparingly soluble gas, eg, oxygen,  $H$  is much greater than unity ( $H \approx 30$  for oxygen in water); furthermore, the coefficient  $k_G$  is typically larger than  $k_L$  because the gas-phase diffusivities are vastly greater than those in liquids (eg,

## 6 MASS TRANSFER

$D_{\text{oxygen/air}} = 10^4 D_{\text{oxygen/water}}$  at 20°C). Consequently, the second term on the right-hand-side of equation 18 is negligible relative to the first, and the equation becomes

$$\frac{1}{K_L} \approx \frac{1}{k_L} \quad (19)$$

This implies that essentially all resistance to interfacial mass transfer of a sparingly soluble gas is localized in the liquid film at the interface, that is, the mass transfer is liquid film controlled (7).

Because the transport flux  $J$  equals the rate of transfer per unit gas–liquid interfacial area, equation 16 may be expressed in terms of rate as follows

$$\frac{dC_L}{dt} = K_L a_L (C^* - C_L) \quad (20)$$

where  $C_L$  is the dissolved gas concentration at time  $t$  and  $a_L$  is the gas–liquid interfacial area per unit volume of the liquid.

**3.1. Volumetric Gas–Liquid Mass Transfer Coefficient,  $k_L a_L$ .** In view of the approximation in equation 19, the overall volumetric mass transfer coefficient  $K_L a_L$  for gas–liquid mass transfer is often expressed as  $k_L a_L$ . The overall volumetric gas–liquid mass transfer coefficient  $k_L a_L$  and the concentration driving force ( $C^* - C_L$ ) for mass transfer must be known if the rate of supply of a soluble gas is to be quantified (7). The mass transfer driving force, which is easily determined, depends on temperature and pressure. The coefficient  $k_L a_L$  depends on the properties of the fluid, the hydrodynamic regime, and the configuration of the gas–liquid contacting device. The factors influencing  $k_L a_L$  and mass transfer are summarized in Table 6. Prediction of  $k_L a_L$  is an important part of gas–liquid contactor design. The individual terms in  $k_L a_L$  are difficult to measure directly, but the product is relatively easily measured (7).

Usually, the overall volumetric gas–liquid mass transfer coefficient is expressed in terms of the liquid volume in the reactor or gas–liquid contactor; however, sometimes the basis of expression has been the gas–liquid dispersion volume (7). An identical basis is necessary for comparing mass transfer capabilities and the coefficient expressed in one form may be converted to the other if the overall gas holdup ( $\varepsilon_G$ ) is known:

$$k_L a_L = \frac{k_L a_D}{1 - \varepsilon_G} \quad (21)$$

The  $k_L a_L$  values for oxygen transfer in aqueous fluids can range from  $10^{-3}$  to  $10^{-1} \text{ s}^{-1}$ , depending primarily on the viscosity of the fluid.

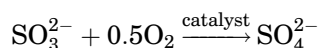
As noted earlier, the rate of diffusive transport of a component through a unit area perpendicular to the direction of transport can be expressed as mass flux or molar flux—kilogram or kilomole of component transferred per unit area per unit time. The flux  $J$  is proportional to a mass transfer driving force and a mass transfer coefficient  $K_L$ , or  $J = K_L \cdot (\text{driving force})$ . Mass transfer is dri-

ven by differences in chemical potential. A species diffuses from regions of high potential to those of low potential until the difference has been eliminated. In practice, the driving force for mass transfer may be expressed as a concentration difference, partial pressure difference, or mole fraction difference. For example, when oxygen-free water is brought in contact with air, oxygen diffuses from air to water until the water becomes saturated. At this point the oxygen concentrations in the two phases are in dynamic equilibrium, but there is no net transfer. Note that the concentrations of oxygen in water and air are not equal, but the chemical potentials are. Depending on how the mass flux  $J$  and the driving force are expressed, the mass transfer coefficient may have different numerical values and different units as noted in Table 7 for a few cases. A coefficient expressed in one form may be easily converted to a different one.

**Measurement of  $k_L a_L$ .** Several methods are available for measuring  $k_L a_L$  values (2, 7–9). Here, only a few of the more useful and common methods will be noted.

**Sulfite Oxidation Method.** The sulfite oxidation method has been extremely widely used, but it is suited to measurements only in physical systems (ie, those without live microorganisms), eg, water or some polymer solutions. The method is subject to many interferences (7,8). Also, because of a high ionic strength, the sulfite oxidation medium tends to be strongly noncoalescing and quite different from many of the gas–liquid systems of interest. Consequently, the sulfite oxidation measurements are not readily translated to relevant systems.

The sulfite oxidation method relies on oxidation of sulfite to sulfate using dissolved oxygen:



The reaction is catalyzed by copper(II), cobalt(II), as well as other metal ions. The rate of sulfite oxidation is a measure of the rate of oxygen transfer to the liquid. The overall reaction generates  $\text{H}^+$  and pH control is necessary because the reaction rate is pH dependent. Also, the temperature needs to be controlled carefully to assure constant reaction kinetics. Impurities, eg, iron, manganese and other transition metals in the parts per million range, affect the reaction.

For  $k_L a_L$  measurements the reaction conditions should be such that the reaction occurs in the bulk liquid and not at the gas–liquid interface. Thus, Cu(II) catalysis is used with a sufficiently high sulfite concentration that the oxidation rate is independent of the sulfite level. The rate of sulfite consumption is given by

$$-\frac{d[\text{SO}_3^{2-}]}{dt} = k_L a_L (C^* - C_L) \quad (22)$$

where  $C^*$  and  $C_L$  are the saturation concentration of dissolved oxygen and the actual instantaneous concentration at time  $t$ . The concentration  $C_L$  is usually close to zero. The sulfite consumption rate, which should remain constant, is

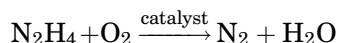
## 8 MASS TRANSFER

followed by quenching the samples taken at various times with excess iodine and back titration of the residual iodine with thiosulfate (7).

Another oxygen-consuming reaction is the oxidation of dithionite ( $\text{S}_2\text{O}_4^{2-}$ ) in alkaline solutions; however, in view of uncertain kinetics and other factors, the usefulness of that reaction for  $k_L a_L$  measurements remains questionable.

*Chemical Absorption of Carbon Dioxide.* This method is similar in principle to the sulfite oxidation procedure. Carbon dioxide is absorbed into a mildly alkaline or suitably buffered solution, where it is converted to other species. Chemical absorption of carbon dioxide into  $\text{Na}_2\text{CO}_3$ – $\text{NaHCO}_3$  solution is sufficiently slow for use in  $k_L a_L$  determination when the ratio of carbonate to bicarbonate concentrations is between 3 and 5 (7). Other reaction conditions need to be controlled to ensure that the reaction rate does not enhance mass transfer. The method has limitations similar to those of the sulfite oxidation technique.

*The Hydrazine Method.* The hydrazine method makes use of the reaction



hydrazine

The reaction is best carried out at pH 11–12 using copper sulfate catalyst (7). A steady flow of hydrazine into an aerated reactor is used to maintain a constant concentration of dissolved oxygen. The amount of hydrazine consumed per unit time equals the oxygen absorption rate. The reaction does not produce any ionic species; hence, the ionic strength of solution can be kept lower than with the sulfite oxidation or the carbon dioxide absorption methods.

*Oxygen Balance Method.* This technique depends on measurement of mass flow rates of aeration gas into and out of the oxygen consuming reactor. The mass fraction of oxygen in the inlet and exhaust gas streams must also be determined (mass spectrometer, paramagnetic oxygen analyzer), as well as the steady-state dissolved oxygen concentration in the fluid (dissolved oxygen electrode). The  $k_L a_L$  is obtained from the oxygen balance:

$$F(x_i - x_o) = V_L k_L a_L (C^* - C_L) \quad (23)$$

where  $F$  is the mass flow rate of gas,  $x_i$  and  $x_o$  are the mass fractions of oxygen in the gas ( $i$  = inlet,  $o$  = outlet), and  $V_L$  is the volume of the fluid in the reactor. Equation 23 assumes no evaporation and it does not correct for possible evolution of carbon dioxide; however, the necessary corrections can be easily incorporated. For a constant volume continuous flow reactor, equation 23 needs to be further modified to account for oxygen entering and leaving the reactor via the liquid streams.

The oxygen balance method requires accurate measurements of gas flow rates and oxygen concentrations. The oxygen mass fraction in the inlet and outlet gas must differ measurably (ie, the oxygen consumption rate in the reactor should be relatively large) for reliable  $k_L a_L$  measurements. Under suitable



conditions, the method is very reliable and it does not disturb the reactor by interrupting the air supply (9).

*Enzymatic Oxidation Method.* Oxygen transfer may be followed by the formation of gluconic acid via oxidation with oxygen in the presence of the enzyme glucose oxidase. The rate of absorption of oxygen is calculated from the rate of consumption of alkali that is needed to neutralize the acid. The liquid-phase oxygen concentration is determined with a dissolved oxygen electrode. The cost of the enzyme restricts the method to small-scale applications (7). The procedure applies only to physical systems.

*The Dynamic Gassing-in Method.* This method is particularly suited to use in microbial broths. In a fermentation at steady state, the oxygen supply rate exactly matches the rate of consumption by the microorganisms and the concentration of dissolved oxygen does not change, ie,

$$\frac{dC_L}{dt} = \underbrace{k_L a_L (C^* - C_L)}_{\text{oxygen supply or mass transfer term}} - \underbrace{q_{O_2} X}_{\text{consumption term}} = 0 \quad (24)$$

where  $q_{O_2}$  is the specific oxygen consumption rate and  $X$  is the concentration of viable biomass. If now the oxygen supply is interrupted, the mass transfer term in equation 24 becomes zero and, as shown in Fig. 2, the dissolved oxygen concentration declines linearly with time (9). The slope of the  $C_L$  versus  $t$  line during the unaerated period provides  $q_{O_2} \cdot X$ . After a short period, the oxygen supply must be resumed or the culture will be damaged. Now, the dissolved oxygen level rises (Fig. 2). During the rise period, the dissolved oxygen concentration as a function of time is given by

$$C_L = C^* - \frac{1}{k_L a_L} \left( q_{O_2} X + \frac{dC_L}{dt} \right) \quad (25)$$

which is a rearranged form of equation 24. Thus,  $k_L a_L$  can be calculated from the slope of a plot of  $C_L$  versus  $(q_{O_2} X + \frac{dC_L}{dt})$ . This procedure requires interrupting the oxygen flow to the fermenter and the dissolved oxygen electrode needs to be capable of a rapid response. Also, the dissolved oxygen concentration must not fall below a critical concentration so that  $q_{O_2}$  remains independent of the oxygen concentration.

The gassing-in method is commonly applied also to physical systems (7). In such cases, the dissolved oxygen in the liquid is first reduced to near zero by bubbling with nitrogen. The nitrogen flow is then stopped, the bubbles are allowed to leave the fluid, and the system is oxygenated by bubbling with air. The

## 10 MASS TRANSFER

concentration of the dissolved oxygen in the liquid is followed as a function of time, and the  $k_L a_L$  is calculated as the slope of the linear equation

$$\ln \left( \frac{C^* - C_{L0}}{C^* - C_L} \right) = k_L a_L t \quad (26)$$

where  $C^*$  is the saturation concentration of dissolved oxygen,  $C_{L0}$  is the initial dissolved oxygen concentration at time  $t_0$  when a hydrodynamic steady state has been reestablished upon commencement of aeration, and  $C_L$  is the dissolved oxygen concentration at any time  $t$  (7). Equation 26 is obtained by integration of equation 24, assuming a well-mixed liquid (ie, uniform  $C_L$ ), no change in gas-phase composition (ie, a constant  $C^*$ ), and an absence of oxygen consumption (ie,  $q_{O_2} = 0$ ) in the physical system.

Correct evaluation of  $k_L a_L$  by this method requires attention to several factors including the response dynamics of the dissolved oxygen electrode and the nature of mixing in the gas and the liquid phases. In large intensely mixed reactors, a well-mixed liquid phase may still be assumed, but the gas-phase composition changes significantly from the inlet to exhaust. The gas is generally in plug flow and, thus, a log mean concentration driving force  $(C^* - C_L)_{LM}$  should be used in equation 24. The driving force is

$$(C^* - C_L)_{LM} = \frac{C_{in}^* - C_{out}^*}{\ln \left( \frac{C_{in}^* - C_L}{C_{out}^* - C_L} \right)} \quad (27)$$

where  $C_{in}^*$  and  $C_{out}^*$  are the saturation concentrations in equilibrium with the gas-phase composition at the reactor inlet and outlet, respectively.

Generally, the nature of mixing in the gas phase is inconsequential in  $k_L a_L$  determinations so long as  $1/k_L a_L$  is less than the residence time of the gas phase in the liquid. The mean residence time  $t_R$  of the gas phase in bubble columns and stirred tanks can be estimated using (7)

$$t_R = \frac{h_L \varepsilon_G}{(1 - \varepsilon_G) U_G} \quad (28)$$

where  $\varepsilon_G$  is the overall gas holdup. Equation 28 may be applied also to risers of airlift reactors when there is little or no gas in the downcomer. In the latter case, the  $U_G$  should be replaced with  $U_{Gr}$ —the superficial gas velocity based on the riser cross-section—and the gas holdup should be replaced with  $\varepsilon_{Gr}$ . When there is gas in the downcomer, equation 28 may still be used because the downcomer gas holdup acts mostly as a dead volume.

The response characteristics of the dissolved oxygen electrode have little influence on the dynamic determination of  $k_L a_L$  if the response time (63% of full response) is less than or equal to  $1/k_L a_L$ . Consult Chisti (7) for additional details. Other variations of the gassing-in technique exist. For example, methods have been developed to simultaneously determine  $k_L a_L$  and oxygen consumption rate without having to interrupt the flow of gas (10). Such schemes are especially

useful for use in bubble columns and airlift bioreactors in which gas is the sole mechanism of achieving mixing.

**Estimation of  $k_L a_L$  for Gases Other Than Oxygen.** Most of the available data and correlations for  $k_L a_L$  were obtained for mass transfer of oxygen. The overall volumetric mass transfer coefficient for transfer of other gases can be estimated using the oxygen transfer data and the diffusion coefficients for oxygen and the other gas (7); thus,

$$(k_L a_L)_{\text{gas}} = \frac{D_{\text{gas}}}{D_{\text{oxygen}}} (k_L a_L)_{\text{oxygen}} \quad (29)$$

or

$$(k_L a_L)_{\text{gas}} = \sqrt{\frac{D_{\text{gas}}}{D_{\text{oxygen}}}} (k_L a_L)_{\text{oxygen}} \quad (30)$$

Equation 29 applies when the transfer can be ascribed to the film penetration mechanism of the two-film theory (7). Equation 30 is applicable when the surface renewal is the predominant mechanism of mass transfer (7). The difference between the two correction factors is small. The diffusivities used for the correction should be at the same temperature as the  $k_L a_L$  data. The correction is satisfactory only for transfer in identical fluids at identical hydrodynamic conditions. Data on carbon dioxide mass transfer have been reviewed by Ho and Shanahan (11).

**3.2. Solubility of Gases.** Information on solubility of oxygen is needed for estimating the concentration difference driving force for mass transfer. Calculation of the saturation concentration  $C^*$  of dissolved oxygen (equation 17) requires a knowledge of the Henry's law constant,  $H$ . The dimensionless  $H$  for oxygen in pure water may be calculated as a function of temperature  $T$  ( $^{\circ}\text{C}$ ) using the equation:

$$H = -9281.4 \times 10^{-3} + 4030.9 \times 10^{-3}T - 1403.5 \times 10^{-4}T^2 + 178.8 \times 10^{-5}T^3 \quad (31)$$

Equation 31 provides almost exact values of  $H$  over the range 20–30 $^{\circ}\text{C}$ . Oxygen solubility in water at a pressure of 1 atm can be calculated with the equation,

$$C^* = 2178.549 \times 10^{-3} - 549.304 \times 10^{-4}T - 848.781 \times 10^{-6}T^2 - 483.785 \times 10^{-8}T^3 \quad (32)$$

where the temperature  $T$  is in  $^{\circ}\text{C}$  and  $C^*$  is in mmol/L. Equation 32 applies over 0–40 $^{\circ}\text{C}$ .

In addition to temperature, other factors influence oxygen solubility and the  $H$  value. Solubility declines with increasing ionic strength of solution. Solubility depends also on the types of ions in solution. For example, for the same molar concentrations of sodium chloride and hydrochloric acid in different samples of

## 12 MASS TRANSFER

pure water, the oxygen solubility is lower in the salt solution. Solubility data for oxygen and other gases are available in handbooks. For comparison, aqueous solubilities of carbon dioxide, chlorine, and sulfur dioxide are 1.688, 7.16, and 112.9 kg/m<sup>3</sup> (at 20°C and 1-atm pressure), respectively.

### 4. Liquid–Liquid Mass Transfer

Transfer of a solute from an immiscible liquid dispersed into another liquid (the continuous phase) can be analyzed using the two-film approach discussed for gas–liquid mass transfer. Now, the overall mass transfer coefficient  $K_L$  and the film coefficients for the dispersed ( $k_{Ld}$ ) and the continuous ( $k_{Lc}$ ) phases are related as follows:

$$\frac{1}{K_L} = \frac{1}{k_{Lc}} + \frac{K_p}{k_{Ld}} \quad (33)$$

In equation 33,  $K_p$  is the partition coefficient of the solute between the two phases. The partition coefficient defines the equilibrium distribution of the solute between the phases; thus,

$$K_p = \frac{C_{Lc}}{C_{Ld}} \quad (34)$$

where  $C_{Lc}$  and  $C_{Ld}$  are the equilibrium concentrations of the solute in the continuous and the dispersed phases, respectively. Again, as for gas–liquid mass transfer, the interface between the phases is assumed to offer no resistance to mass transfer; hence, the equilibrium relationship determines the solute concentrations at the interface.

The overall volumetric mass transfer coefficient for liquid–liquid mass transfer is  $K_L a_{Lc}$  where the specific interfacial area ( $a_{Lc}$ ) is based on the volume ( $V_{Lc}$ ) of the continuous phase. The rate of mass transfer from the dispersed to the continuous phase is given by

$$\frac{dC_{Lc}}{dt} = K_L a_{Lc} (C^* - C_{Lc}) \quad (35)$$

where  $C^*$  is the saturation concentration of the solute in the continuous phase in equilibrium with the dispersed phase.

### 5. Solid–Liquid and Solid–Gas Mass Transfer

Mass transfer to or from suspended solids is important in many processing situations. Solid–liquid (or gas) mass transfer may be rate limiting in heterogeneous catalysis, during dissolution of solids, adsorption, as well as in other cases. The rate of mass transfer to or from the suspended particle depends on the

solid–liquid mass transfer coefficient ( $k_L$ ), the total solid–liquid interfacial area ( $A_s$ ), and the concentration driving force; thus,

$$V_L \frac{dC_L}{dt} = k_L A_s (C^* - C_L) \quad (36)$$

where  $C_L$  is the concentration of the transferring component in the liquid at time  $t$ ,  $C^*$  is the saturation concentration (or solubility) of the transferring component, and  $V_L$  is the volume of the suspending liquid. Equation 36 is written for transfer from the solid to the liquid. By analogy with the film model of mass transfer, the coefficient  $k_L$  conceptually equals the diffusivity of the solute divided by the thickness of the stagnant liquid film at the solid–liquid interface;  $k_L$  is needed for quantifying the rate of mass transfer. Methods for estimating the solid–liquid or solid–gas (also gas–liquid if liquid is adsorbed as a very thin film on the surface of the solid) mass transfer coefficient  $k_L$  in various situations are discussed in a later section of this article.

## 6. Mass Transfer Behavior

**6.1. General Aspects.** Mass transport by diffusion and forced convection are influenced by the following variables: the mass transfer coefficient  $k$ , the molecular diffusivity of the transferring component  $D$ , the fluid density  $\rho$  and viscosity  $\mu$ , a characteristic length  $d$ , and the velocity of flow  $U$ . Mass transfer by natural convection is influenced also by the gravitational acceleration  $g$  and the density difference  $\Delta\rho$  between phases. These variables can be grouped into the following principal dimensionless groups or numbers:

$$Re \text{ (Reynolds number)} = \frac{\text{inertial force}}{\text{viscous force}} = \frac{\rho_L U_L d}{\mu_L} \quad (37)$$

$$Sh \text{ (Sherwood number)} = \frac{\text{total mass transfer}}{\text{diffusive mass transfer}} = \frac{k_L d}{D_L} \quad (38)$$

$$Sc \text{ (Schmidt number)} = \frac{\text{momentum diffusivity}}{\text{mass diffusivity}} = \frac{\mu_L}{\rho_L D_L} \quad (39)$$

$$Gr \text{ (Grashof number)} = \frac{(\text{inertial force})(\text{bouyancy force})}{(\text{viscous force})^2} = \frac{d^3 \rho_L \Delta\rho g}{\mu_L^2} \quad (40)$$

$$Fr \text{ (Froude number)} = \frac{\text{inertial force}}{\text{gravitation force}} = \frac{U_L^2}{gd} \quad (41)$$

where the subscript  $L$  denotes the liquid-phase. Reynolds number, Sherwood number, and Schmidt number can be written for gas and liquid phases. The above noted dimensionless numbers represent ratios of various factors that may play a role in a given situation. Grashof number is important in situations where density difference driven natural convection affects mass transfer.

Reynolds number is employed in situations where forced convection is the predominant influence on transport processes. Froude number is useful in describing gravity-influenced flows. Schmidt number, ratio of momentum diffusivity to mass diffusivity, is a measure of relative effectiveness of mass and momentum transfer. Some of those dimensionless numbers may be expressed in other forms depending on the situation. A few possible alternatives are noted in Table 8. In addition to the dimensionless groups discussed above, other groups relevant to mass transfer and related fluid mechanics are encountered in the literature. Some of the more common ones and their physical significance are noted in Table 9.

Grouping the many variables that affect mass transfer into a few dimensionless numbers greatly simplifies the process development experimentation and data correlation for predicting the behavior of a system. For example, for fluids flowing in straight pipes, the flow pattern changes from laminar to turbulent at a  $Re$  number value of  $\sim 2300$ . This occurs irrespective of which specific fluid (air, water, hydrocarbon, or thick glucose syrup) is being used so long as the combination of the fluid density, viscosity, flow velocity, and pipe diameter yields a  $Re$  number value that  $> 2300$ . Equations for correlating the mass transfer behavior of systems are often expressed in terms of dimensionless groups.

**6.2. Behavior of Dispersions.** A dispersion consists of one or more phases dispersed in a continuous phase. The continuous phase may be a gas or liquid. The dispersed phase may be liquid droplets, solid particles, or gas bubbles. The magnitude of mass transfer coefficient inside and outside fluid particles depends on whether the particles behave as ridged spheres or they are mobile. Small drops and bubbles behave as noncirculating ridged spheres. Larger bubbles and drops have internal fluid circulation and mobile interfaces because of relative motion between the particle and the surrounding fluid. Bubbles are immobile if the dimensionless diameter  $d^* \leq 10$ . The interface is nearly always mobile if  $d^* > 50$ . Here the dimensionless diameter number is

$$d^* = d_B \left( \frac{\mu_L^2}{\rho_L g (\rho_L - \rho_G)} \right)^{-1/3} \quad (42)$$

as defined by Wesselingh (7). Using this criterion, in air–water, bubbles  $< 0.5$  mm will always be ridged, whereas bubbles larger than  $\sim 2.5$  mm will have mobile interfaces (7).

In certain cases, drops and bubbles may experience additional interfacial motions that are a consequence of mass transfer itself. Because the local mass transfer coefficient around a particle may be different at different locations, the local mass transfer rates may be different. In this situation, uneven transfer of a solute, eg, acetone or ethanol, will generate solutions of different local concentrations and surface tensions. Adjacent films of different surface tension lead to violent motions: regions of high surface tension contract and the film ruptures in regions of low surface tension. This effect is the well-known Marangoni effect and it can significantly enhance mass transfer especially in liquid–liquid extraction processes.

For suspended solids, increasing agitation beyond that needed to achieve complete suspension has little impact on mass transfer coefficient. The coefficient is influenced by relative velocity between the phases that is determined by density differences. In gas–liquid dispersions, too, the  $k_L$  is not substantially affected by increasing agitation, but the overall volumetric mass transfer coefficient ( $k_L a_L$ ) increases because of the increase in gas–liquid interfacial area.

For freely suspended particles and bubbles, mass transfer to or from the bubble or particle obeys the general relationship

$$Sh = f(Gr, Sc) \quad (43)$$

For just suspended small particles ( $d_p < 0.6$  mm) in stirred tanks, Calderbank and Moo-Young (12) recommended the equation:

$$k_L = \frac{2D_L}{d_p} + 0.31 Sc^{-2/3} \left( \frac{\Delta \rho_L \mu_L g}{\rho_L^2} \right)^{1/3} \quad (44)$$

which is suitable for suspensions as well as gas–liquid dispersions of non-circulating bubbles ( $d_p < 0.6$  mm). For larger circulating bubbles and liquid drops ( $d_p > 2.5$  mm) in just suspended state, the recommended equation is

$$k_L = 0.42 Sc^{-0.5} \left( \frac{\Delta \rho_L \mu_L g}{\rho_L^2} \right)^{1/3} \quad (45)$$

For bubbles in the 0.6–2.5-mm range, the  $k_L$  may be estimated as a linear function of bubble diameter.

Large spherical cap bubbles frequently occur in gas–liquid dispersions especially when the viscosity of liquid exceeds  $\sim 7 \times 10^{-2}$  Pa·s. Calderbank and Lochiel (13) correlated mass transfer from such bubbles using the equation

$$Sh = \frac{1.79(3R_b^2 + 4)^{2/3}}{R_b^2 + 4} (Re \cdot Sc)^{1/2} \quad (46)$$

where  $R_b$  is the ratio of bubble width to bubble height. For spherical caps,  $R_b$  is  $\sim 3.5$ ; hence, equation 46 becomes

$$Sh = 1.31(Re \cdot Sc)^{1/2} \quad (47)$$

Mass transfer to or from a particle suspended in a stagnant fluid occurs solely by diffusion. For a single spherical particle surrounded by a stagnant medium, the theoretical minimum value of the transfer coefficient is given by  $Sh = 2$ . For a single particle in the creeping flow regime ( $Re < 0.1$ ), the specific relationship is

$$Sh = 0.39(Gr \cdot Sc)^{1/3} \quad (48)$$

## 16 MASS TRANSFER

Equation 48 applies to particles with ridged interfaces and this includes noncirculating small bubbles ( $Re < 0.1$ ). Thus, compared to the case for a single noncirculating bubble (equation 48), the mass transfer coefficient in swarms of ridged bubbles (equation 44) is  $\sim 20\%$  lower.

For power inputs greater than needed for just suspension, Calderbank and Moo-Young (12) have established the following equation in stirred tanks

$$k_L = 0.13 \left( \frac{(P_G/V_L)\mu_L}{\rho_L^2} \right)^{1/4} Sc^{-2/3} \quad (49)$$

where  $P_G/V_L$  is the power input per unit volume.

Transfer coefficient correlations generally require a knowledge of liquid properties, eg, viscosity and density. This is usually not a problem when dealing with newtonian liquids, but difficulties arise with slurries and non-newtonian media. Many slurries can be treated as pseudohomogeneous fluids (7). Depending on the amount of suspended solids, slurries may behave as newtonian or non-newtonian power law fluids. For small amounts of spherical solid particles, newtonian behavior is commonly observed and in this case the viscosity of the slurry is independent of the shear rate. The newtonian viscosity may be estimated using equations of Einstein and Vand (9). Another suitable equation is that of Thomas:

$$\mu_{SL} = \mu_L (1 + 2.5 \phi_S + 10.05 \phi_S^2 + 0.00273 e^{-16.6 \phi_S}) \quad (50)$$

where  $\phi_S$  is the volume fraction of suspended solids and  $\mu_L$  is the viscosity of the suspending fluid.

When the slurry behaves as a non-newtonian power law fluid, the apparent viscosity depends on the shear rate; thus,

$$\mu_{ap} = K \gamma^{n-1} \quad (51)$$

where  $K$  is the consistency index or thickness of the fluid and  $n$  is its flow behavior index. The parameter  $\gamma$  is the shear rate. The shear rate is difficult to define in most realistic configurations of gas-liquid contactors under the usual operational conditions; nevertheless, following expressions are commonly employed in estimating shear rates:

### 1. Bubble Columns and Airlift Devices

$$\gamma = \alpha U_G \quad (52)$$

where the constant  $\alpha$  has been specified variously as 1000, 2800, 5000  $m^{-1}$ , etc (14). Equation 52 has been applied also to airlift reactors, but that use is incorrect: For airlift reactors, the superficial gas velocity based on the cross-sectional area of the riser should be used in expressions such as equation 52 as recommended by Chisti (7). Depending on the constant used, equation 52 provides



wildly different values of the supposed shear rate; hence, its use is not generally favored and it has been severely criticized (7,14,15). Another expression for shear rate in airlift reactors is

$$\gamma = 3.26 - 3.51 \times 10^2 U_{Gr} + 1.48 \times 10^4 U_{Gr}^2 \quad (53)$$

which was developed for  $0.004 < U_{Gr} \text{ (m/s)} < 0.06$  (16). Equation 53 also has significant problems as discussed elsewhere (15,17). Alternative approaches for estimating shear rates have been propounded by Grima and co-workers (15). Methods of estimating shear rates in other process devices have been discussed exhaustively, elsewhere (18–20). An excessive shear rate can be damaging to some fragile catalysts and large molecules (18–20).

## 2. Stirred Vessels

The mean shear rate in impeller agitated tanks is usually given as

$$\gamma = k_i N \quad (54)$$

where  $k_i$  is an impeller-dependent constant (9). Some typical  $k_i$  values are: 11–13 for 6-bladed turbines, 10–13 for paddles,  $\sim 10$  for propellers, and  $\sim 30$  for helical ribbon impellers. Again, as with pneumatically agitated reactors, much of the discrepancy among various predictive correlations that rely on a shear rate dependent apparent viscosity has been associated with the use of equations, eg, equation 54 (21).

The apparent viscosity of many slurries declines with increasing shear rate, ie,  $n < 1$  (equation 51), and these fluids are known as shear thinning or pseudoplastic. Because shear rate is not easily defined in typical reactors (5,7,14,15,21), correlations employing solids holdup directly are preferred to those relying on a poorly established apparent viscosity of the slurry (7). As with viscosity, the density of a pseudohomogeneous slurry may be related to phase holdups as follows:

$$\rho_{SL} = \rho_L(1 - \phi_S) + \rho_S \phi_S \quad (55)$$

In some viscous fluids, the principal resistance to gas–liquid mass transfer may be in the bulk fluid or at the solid–liquid interface and not in the liquid film at the gas–liquid interface. In such cases, dilution of the fluid with water and increased agitation can improve the transfer rate a little. In slurries, the morphology of the suspended solids can be modified sometimes, to substantially reduce the slurry viscosity and improve mass transfer. Additional details on transport fundamentals of dispersions have been noted by Moo-Young and Blanch (22) and Knudsen and co-workers. (1). Similar discussions with a focus on gas–liquid mass transfer in non-newtonian media are due to Oolman and Blanch (23). Carbon dioxide mass transfer in bioreactors has been treated in depth by Ho and Shanahan (11). Mass transfer in gas–liquid dispersions and slurries can be substantially enhanced by the use of ultrasound, as reviewed by Chisti (24).

**6.3. Gas–Liquid Mass Transfer.** In small reactors, absorption of a gas through the surface of the fluid may be sufficient to provide the necessary transfer of the gas from the headspace to the fluid. In other cases, the gas will need to be bubbled or sparged through the body of the fluid, to attain sufficient rates of mass transfer. These schemes are discussed separately below.

**Surface Aeration.** In small reactors and for a slow consumption of the gas by the reaction, gas absorption through the surface of the pool of fluid can be sufficient to meet demand of the reaction (25). Surface aeration is used especially commonly in the early stages of microbial culture to provide oxygen in shake flasks and small scale culture devices. Understanding and characterization of surface aeration in small devices is essential for process scaleup that minimally attempts to reproduce on the larger scale the process performance attained in the laboratory. Surface aeration is employed also in relatively small production bioreactors for growing cultures with extremely low oxygen requirements. Surface aeration in the principal types of laboratory and production devices is detailed in the following sections.

**Laboratory Devices. Shake Flasks.** In 500-mL Erlenmeyer flasks placed on reciprocating and rotary shaker platforms, Yamada and co-workers, (26) measured volumetric rates of oxygen transfer in sulfite solutions and in *Acetobacter suboxydans* fermentations for converting sorbitol to sorbose. The rates were expressed in terms of the volumetric oxygen transfer coefficients through the flask closure ( $K_P$ ) and across the gas–liquid interface ( $K_S$ ):

$$\text{Volumetric rate of oxygen transfer (mol O}_2\text{/mL} \cdot \text{h)} = \frac{1}{(\frac{1}{K_P} + \frac{1}{K_S})} \frac{1}{V_L} (p_{\text{atm}} - p_L) \quad (56)$$

In equation 56,  $V_L$  (mL) is the volume of liquid in the flask;  $p_{\text{atm}}$  (atm) and  $p_L$  (atm) are the partial pressures of oxygen in the atmosphere outside the flask and in the liquid in the flask, respectively. The units of  $K_P$  and  $K_S$  are  $\text{mol} \cdot \text{O}_2 \cdot \text{atm}^{-1} \cdot \text{h}^{-1}$ . The mass transfer coefficient  $K_P$  through the closure declined with increasing weight (3–7 g) of cotton used to form the plug. The mean  $K_P$  value for cotton plugs was  $2.87 \times 10^{-2} \text{ mol} \cdot \text{O}_2 \cdot \text{atm}^{-1} \cdot \text{h}^{-1}$ . Values for polyurethane foam and silicone foam plugs were a little lower. Compared to open flasks, cotton plugs restricted oxygen transfer. The  $K_S$  values in sulfite oxidation solutions agitated at 110–140 rpm ranged over  $2.04\text{--}4.63 \times 10^{-2} \text{ mol} \cdot \text{O}_2 \cdot \text{atm}^{-1} \cdot \text{h}^{-1}$ . Under similar conditions in *Acetobacter suboxydans* fermentations, the  $K_S$  values were lower—only 50–60% of those obtained with sulfite oxidation. Various types of baffles and indentation in the flasks enhanced  $K_S$  by  $\sim 50\%$  relative to the base case.

For mass transfer from liquid surface in unbaffled Erlenmeyer shake flasks the following equation has been recommended:

$$k_L a_L \left( \frac{\mu_L}{\rho_L g^2} \right)^{1/3} = 0.5 \left( \frac{\mu_L}{\rho_L D_L} \right)^{-1/2} \left( \frac{d_F}{V_L} \right)^{8/9} \left( \frac{\mu_L^2}{\rho_L^2 d_F^3 g} \right)^{8/27} \left( \frac{N^2 \sqrt{e} d_F}{g} \right)^{0.5} \quad (57)$$

where  $d_F$  is the maximum diameter of the flask,  $N$  is the speed of rotation, and  $\hat{e}$  is the eccentricity of the shaker platform (27). Equation 57 applies to animal cell culture media when the liquid volume in the flask is 50–200 mL.

Open unbaffled shake flasks of 250-mL capacity filled to 100 mL with water at 37°C have been reported to have a  $k_L a_L$  value of  $30.8 \pm 6.7 \text{ h}^{-1}$  when agitated at 250 rpm on an orbital shaker (28). For otherwise identical conditions the measured  $k_L a_L$  value in baffled flasks was  $59.2 \pm 7.4 \text{ h}^{-1}$  (28). Mass transfer data in shake flasks operated with other combinations of fill levels, agitation speeds and liquid viscosities have been published (29).

**Spinner Flasks.** Spinner flasks (Fig. 3) are commonly used for small scale culture of animal cells. Aunins and co-workers (30) reported  $k_L a_L$  measurements (surface aeration) in 500 mL Corning spinner flasks (Fig. 3) filled to a depth of 0.08 m with Dulbecco's Modified Eagle's Medium (DMEM) supplemented with 5% (vol/vol) fetal calf serum and 1 kg/m<sup>3</sup> ethylenediaminetetraacetic acid (EDTA). The data were obtained at 37°C and followed the equation

$$Sh = 1.08 Re^{0.78} \quad (58)$$

where the Sherwood number is based on the vessel diameter and the  $Re$  number is based on the impeller diameter. The measurements spanned the impeller speed range 25–150 rpm, impeller diameters of 0.0525 and 0.078 m, and impeller  $Re$  number of 1500–20,000. Locating the impeller < 0.01 m below the liquid surface dramatically enhanced the  $k_L a_L$ . At 50 rpm, with 0.078-m diameter paddle impeller placed at the liquid surface, the  $k_L a_L$  value was  $\sim 9.72 \times 10^{-4} \text{ s}^{-1}$ . Moving the impeller to 0.01 m below the surface provided a  $k_L a_L$  value of  $\sim 4.17 \times 10^{-4} \text{ s}^{-1}$ . Lowering the impeller further into the fluid did not affect the  $k_L a_L$  significantly.

**Stirred Vessels.** Lavery and Nienow (31) reported  $k_L a_L$  measurements in water, RPMI 1640 basal cell culture medium, and the medium supplemented with 5% (vol/vol) fetal calf serum in a small, unbaffled, spherical cell culture vessel (1.5 L, static surface area of liquid =  $2.23 \times 10^{-2} \text{ m}^2$ ) stirred with one or two 3-bladed propellers ( $d_i = 0.060 \text{ m}$ , located 0.035 m apart). The lower impeller was positioned 0.003 m from the bottom of the vessel flask and the upper was 0.002 m below the surface of the liquid. The agitation speeds were 1.6–5.8 s<sup>-1</sup> (100–350 rpm). Air was sparged (100 mL/min) either in the liquid under the lower propeller or only through the headspace (ie, surface aeration). The submerged aeration  $k_L a_L$  values generally agreed with predictions of Van't Riet's correlation for non-ionic solutions (ie, equation 78). Relative to measurements in water, the serum and the basal medium had little effect on  $k_L a_L$  values. The  $k_L$  for surface aeration was little affected by the number of impellers (whether 1 or 2). The  $k_L a_L$  values for surface aeration were  $\sim 75\%$  of those for submerged aeration in the reactor used. Addition of silicone antifoam (6 ppm) reduced the  $k_L a_L$  values by  $\sim 50\%$ . In the basal medium with serum and the antifoam, the  $k_L$  values for surface aeration (no vortex) were  $(1.18\text{--}3.54) \times 10^{-5} \text{ m/s}$ . The  $k_L a_L$  values for submerged aeration were  $(2.8\text{--}8.5) \times 10^{-4} \text{ s}^{-1}$ .

## 20 MASS TRANSFER

*Other Devices.* For absorption of oxygen at free surface of sodium sulfite solution in cylindrical containers placed on an orbital shaker platform, the volumetric mass transfer coefficient has been correlated (32) as follows:

$$k_L a_L = 6 \times 10^{-5} (P/V_L)^{0.4} d_T^{-0.25} h_L^{-0.6} \quad (59)$$

Equation 59 is independent of gas flow rate in the headspace; it was determined for  $20 \leq P/V_L \text{ (W/m}^3\text{)} \leq 500$  and  $0.5 \leq h_L/d_T \leq 1.5$  ( $d_T = 0.12$  or  $0.15$  m). The agitation speed of the shaker platform varied over  $1.2\text{--}3.3 \text{ s}^{-1}$ , and the moving vessel described a diameter of  $0.01\text{--}0.04$  m.

*Larger Systems.* Stirred Tanks. Multibladed disk turbines located at the surface provide superior surface aeration relative to other types of impellers (33). To prevent entrainment of bubbles, the turbines must be operated such that (33)

$$Nd_i \leq 0.11(d_i/d_T)^{-0.2} \quad (60)$$

As the tank diameter increases, the ability of a given impeller to agitate the entire liquid surface declines if the agitation speed is to remain below the bubble entrainment limit. The optimum impeller size for surface aeration is given by (33)

$$\frac{d_i}{d_T} \approx 0.5 \quad (61)$$

Surface aeration is suited only to small reactors because  $k_L a_L$  declines rapidly with increasing tank volume of surface aerated reactors. For subsurface impellers operated such that there is no entrainment of gas, the mass transfer coefficient  $k_L$  has been correlated with the impeller  $Re$  number as follows (27):

$$Sh = 1.4 Re_i^{0.76} \quad (62)$$

which applies to water-like media.

The contribution of the free surface to aeration in conventionally stirred, baffled tanks declines as the scale of operation increases. The liquid-phase mass transfer coefficient at the free surface (no vortex) in such tanks can be estimated using the correlations summarized in Table 10 (34–37). A preferred correlation (35) is

$$k_L = 0.138 Sc^{-2/3} \left( \frac{4\mu_L Po N^3 d_i^5}{\pi d_T^2 h_L \rho_L} \right)^{1/4} \quad (63)$$

where  $Po$  is the power number ( $Po = P/(\rho_L N^3 d_i^5)$ ),  $d_T$  and  $d_i$  are the diameters of the tank and the impeller, respectively,  $h_L$  is the height of liquid in the tank,  $N$  is the impeller rotational speed, and  $P$  is the power input. Equation 63 applies to

newtonian media without antifoams or surfactants present. Added surfactants, fatty acids and proteins reduce  $k_L$  relative to values in clean liquids.

For a large ( $1.46 \text{ m}^3$ ) concentric draft-tube reactor with downward pumping 5-bladed hydrofoil impellers located in the draft-tube, Chisti and Jauregui-Haza (38) correlated the  $k_L a_L$  for surface aeration (air-water) with the impeller speed ( $N$ ), as follows:

$$k_L a_L = 8.043 \times 10^{-6} e^{1.197N} \quad (64)$$

At the lowest aeration rate used (0.0156 m/s superficial aeration velocity in the annular zone) in the sparged mode of operation, the contribution of surface aeration to the total mass transfer varied from 1.5 to 11.6%, depending on the speed of the impeller (38).

**Vortex Aeration.** In unbaffled stirred tanks, agitation with a centrally located impeller creates a vortex that draws closer to the impeller as the rate of agitation increases (Fig. 4). In a vortex aerated industrial reactor (240 L) used in producing diphtheria vaccine, the following equation has been reported (25):

$$k_L a_L = 7.33 \times 10^{-4} + 1.36 \times 10^{-4} Q_G \quad (65)$$

where  $Q_G$  is the surface aeration rate (10–45 normal L/min). The equation was developed in aqueous sodium chloride ( $2.5 \text{ kg/m}^3$ ) and in the medium used in culturing the diphtheria bacterium. The tank was agitated with a 6-bladed Rushton-type turbine (without disk) and the agitation rate was 300–800 rpm. The working aspect ratio was 0.74, which is substantially lower than values that are typically used in gas sparged reactors. Over the entire range of agitation rates used, the vortex was fully developed and reached the eye of the impeller (25). The conditions used in establishing equation 65 were identical to those employed in commercial processes for producing the vaccine (25).

**Wetted-Wall Columns.** Processing situations often involve adsorption of a sparingly soluble gas in a liquid film trickling down the surface of an inert support matrix. For a film falling down a flat or curved surface, the mass transfer coefficient  $k_L$  can be shown to typically follow the relationship:

$$Sh_x = \frac{k_L x}{D} = \frac{2}{\sqrt{\pi}} Re_x^{1/2} Sc^{1/2} \quad (66)$$

where  $x$  is the length of the film. The  $Re$  number in equation 66 is calculated as follows:

$$Re_x = \frac{\rho_L U_{\max} x}{\mu_L} \quad (67)$$

## 22 MASS TRANSFER

where  $U_{\max}$  is the liquid flow velocity at the gas–liquid interface. Equation 66 derives from fundamental principles and it applies when there is no chemical reaction and the penetration distances are short (or the contact period is brief).

When the diffusing component is consumed by a chemical reaction in the liquid film, the mass transfer coefficient is always enhanced relative to the non-reacting case. The relationship 66 also applies to falling film absorption with chemical reaction, but the coefficient (ie,  $2/\sqrt{\pi}$ ) depends on the rate constant of the reaction. Absorption with reaction is commonly used to remove trace solutes from a gas stream.

Many empirical correlations have been reported for mass transfer coefficient in liquid films in wetted-wall falling film columns. One of the recommended (3) equations is

$$k_L = 9.0 Re^{-0.40} Sc^{-0.67} U_L \quad (68)$$

where the  $Sc$  and  $Re$  are based on properties of the liquid. Depth of the film and the mean film velocity ( $U_L$ ) are used to calculate the  $Re$  number. Equation 68 is appropriate for  $Re < 2000$  and  $Sc < 100$ . Another useful equation is

$$Sh = 0.023 Re^{0.8} Sc^{1/3} \quad (69)$$

The gas and liquid film coefficients in highly turbulent films ( $Re > 4000$ ) in cocurrent wetted-wall columns can be estimated using the following equations (39):

$$Sh_L = 0.01613 Re_G^{0.664} Re_L^{0.426} Sc_L^{0.5} \quad (70)$$

$$Sh_G = 3.1 \times 10^{-4} Re_G^{1.05} Re_L^{0.207} Sc_G^{0.5} \quad (71)$$

These equations apply when  $4000 \leq Re_L \leq 12,000$  and  $7500 \leq Re_G \leq 18,300$ . Other correlations for mass transfer in wetted-wall columns have been summarized by Spedding and Jones (40).

**Packed and Tray Columns.** In packed absorption towers, the interfacial area for mass transfer generally decreases with a decrease in the liquid flow rate and with increasing surface tension. (A high surface tension reduces wetting of the packing and causes the liquid to flow in rivulets.) For columns packed with Rashig rings and Berl saddles, the gas and liquid film coefficient can be estimated with the following equations:

$$\left(\frac{k_G M_G}{G}\right) \left(\frac{\mu_G}{\rho_G D_G}\right)^{2/3} = 1.195 \left(\frac{Gd}{\mu_G (1 - \phi)}\right)^{-0.36} \quad (72)$$

and

$$\left(\frac{k_L M_L}{L_m}\right) = 25.1 \left(\frac{\mu_L}{\rho_L D_L}\right)^{0.5} \left(\frac{L_m d}{\mu_L}\right)^{0.45} \quad (73)$$

In these equations,  $G$  is the mass flux of gas in the column,  $\phi$  is the void fraction of the packing,  $d$  is the diameter of a sphere with the same surface area as a piece of the packing,  $M_G$  is the molar mass (kg/kmol) of the gas,  $M_L$  is the molar mass (kg/kmol) of the liquid, and  $L_m$  is the mass flux ( $\text{kg}\cdot\text{s}^{-1}\text{ m}^{-2}$ ) of the liquid in the column. The  $k_L$  and  $k_G$  values in equation 72 and equation 73 are in  $\text{kmol}\cdot\text{s}^{-1}\text{ m}^{-2}$ .

For mass transfer in a bubble-cap tray column, the gas film coefficient can be estimated using the equation

$$k_g = 7 \left( \frac{u^{0.5} D_G}{h_T} \right)^{0.5} \quad (74)$$

where  $k_g$  is in cm/s,  $u$  is the gas velocity in cm/s, the diffusivity  $D_G$  is in  $\text{cm}^2/\text{s}$ , and  $h_T$  (cm) is the liquid level on the tray. The coefficient  $k_g$  (cm/s) is related with  $k_G$  ( $\text{kmol}\cdot\text{s}^{-1}\text{ m}^{-2}$ ) as follows:

$$k_G = \frac{k_g}{100V_G} \quad (75)$$

where  $V_G$  is the molar volume of the gas ( $\text{m}^3/\text{kmol}$ ).

In dealing with absorption columns and distillation towers, the mass transfer performance is often expressed in terms of the height of an overall transfer unit,  $HTU$ . The  $HTU$  values can be different for mass transfer in the gas and liquid-phases. The  $HTU$  is related with the overall volumetric mass transfer coefficient; thus

$$HTU_G = \frac{G_g}{K_G a \cdot P_g} \quad (76)$$

$$HTU_L = \frac{L_L}{K_L a \cdot \rho_L} \quad (77)$$

for the gas and liquid-phases, respectively. In these equations,  $P_g$  is the average column pressure (Pa),  $G_g$  and  $L_L$  are the molar fluxes ( $\text{kmol}\cdot\text{s}^{-1}\text{ m}^{-2}$ ) of the gas and liquid in the column, and the overall mass transfer coefficients  $K_G a$  and  $K_L a$  have the units of  $\text{kmol}\cdot\text{s}^{-1}\text{ m}^{-1}\cdot\text{Pa}^{-1}$  and  $\text{kmol}\cdot\text{kg}^{-1}\text{ s}^{-1}$ , respectively.

**Submerged Aeration.** Submerged aeration in which air, oxygen, or other gas is sparged or bubbled through the fluid is the norm in large-scale gas–liquid reactors. Typically, submerged gassing is carried out in stirred tanks, bubble columns, and airlift reactors. Stirred vessels and bubble columns are the most common types of gas–liquid reactors in the chemical industry. Typically, sparged aerated bubble columns and stirred tanks have aspect ratios between three and four. Airlift devices generally have higher aspect ratios, usually greater than six. Superficial aeration velocities of up to  $0.1\text{ m}\cdot\text{s}^{-1}$  are used in airlift vessels but lower maximum values are the norm in bubble columns. Aeration rates are substantially lower in stirred tanks to prevent flooding of the impeller. A flooded impeller is a poor mixer and gas disperser.

*Stirred Tank Reactors.* The gas–liquid volumetric mass transfer coefficient in stirred vessels has generally shown good correlation with agitation power input and the superficial gas velocity; thus,

$$k_L a_L = \alpha (P_G/V_L)^\beta U_G^\gamma \quad (78)$$

where  $P_G/V_L$  ( $\text{W/m}^3$ ) is the gassed power input and  $U_G$  ( $\text{m/s}$ ) is the superficial aeration velocity. Generally,  $0.4 < \beta < 1$  and  $0 < \gamma < 0.7$  (8). For pure water,  $\alpha$ ,  $\beta$ , and  $\gamma$  values are  $2.6 \times 10^{-2} (\text{s}^{\beta+\gamma-1} \text{m}^{3\beta-\gamma} \text{J}^{-\beta})$ , 0.4, and 0.5, respectively, when  $500 < P_G/V_L (\text{W/m}^3) < 10,000$  (8). These values have been shown to apply over a wide scale:  $0.002 \leq V_L (\text{m}^3) \leq 2.6$ . In strongly ionic aqueous solutions, the  $\alpha$ ,  $\beta$ , and  $\gamma$  values become  $2.0 \times 10^{-3} (\text{s}^{\beta+\gamma-1} \text{m}^{3\beta-\gamma} \text{J}^{-\beta})$ , 0.7, and 0.2, respectively, when  $500 < P_G/V_L (\text{W/m}^3) < 10,000$  and  $0.002 \leq V_L (\text{m}^3) \leq 4.4$  (8). In pure water and ionic aqueous media, the volumetric mass transfer coefficient depends only on the specific power input irrespective of the type of stirrer—whether turbines, propellers, paddles, or self-sucking agitators—used for agitation. The number of impellers does not matter and neither does the location so long as it is within the usual ranges. Similarly, the height of liquid and the type of sparger have negligible influence under representative operating conditions (8). The parameters values noted above assume an absence of flooding. Maximum aeration rates that still assure unflooded operation depend on the geometry of the impeller as discussed by Nienow (41).

For single impeller stirred air–water system, Bakker and co-workers (42) recommended the following values of the constants in equation 78:  $\beta = \gamma = 0.6$ , and  $\alpha = 0.015 \pm 0.005$ . The parameters noted apply only to the nonflooded state. At high gas flow rates, concave-bladed gas dispersion impellers (Fig. 5) yield at least 20% higher  $k_L a_L$  than obtainable with Rushton turbines under the same conditions (42). The constants in equation 78 can be strongly affected by fluid properties, presence of surfactants and insoluble oils. For fluids other than water and for multi-impeller systems, Bakker and co-workers (42) recommended measuring  $\alpha$ ,  $\beta$ , and  $\gamma$  in a geometrically similar small-scale stirred reactor. This data can be used in equation 78 for scaleup.

For fermentations of *Endomyces* sp. in stirred fermenters,  $\alpha$ ,  $\beta$ , and  $\gamma$  values in equation 78 have been reported to be  $4.015 \times 10^{-2} (\text{s}^{\beta+\gamma-1} \text{m}^{3\beta-\gamma} \text{J}^{-\beta})$ , 0.33, and 0.56, respectively, over a broad scale [ $0.03 \leq V_L (\text{m}^3) \leq 50$ ]. In a 5-L stirred fermenter operated with high density culture of a recombinant *Escherichia coli*, Shin and co-workers (43) reported the following equation for  $k_L a_L$ :

$$k_L a_L = 0.0195 (P_G/V_L)^{0.55} U_G^{0.64} (1 + 2.12X + 0.20X^2)^{-0.25} \quad (79)$$

where  $X$  ( $\text{g/L}$ ) is the biomass concentration. The  $X$  values ranged over 0–75  $\text{g/L}$  and the  $k_L a_L$  values during culture varied over  $(10\text{--}25) \times 10^{-3} \text{ s}^{-1}$ .

In stirred tank bioreactors for animal cell culture, the type of impeller used does not affect  $k_L a_L$  so long as mixing is sufficient. For power inputs that are typical ( $\leq 25 \text{ W/m}^3$ ), better mixing is attained with relatively large ( $d_i/d_T \sim 0.5\text{--}0.6$ ), slow moving, axial flow impellers. For typically used conditions, the  $k_L a_L$  should be calculated as for bubble columns (equation 81) because for



impeller power inputs less than about  $40 \text{ W/m}^3$ , the impeller has little effect on  $k_L a_L$ . Stirred tank design considerations for animal cell culture have been discussed by Chisti (44) and others (33).

Some of the main correlations for estimating gas–liquid volumetric mass transfer coefficient in stirred reactors are summarized in Table 11, which includes equations suitable for relatively viscous power law fluids (21, 45–48). Methods for estimating the power input in mechanically agitated reactors have been detailed by Chisti and Moo-Young (9), Nienow (41), and Ascanio and co-workers (49).

**Bubble Columns.** For a given fluid in bubble columns the  $k_L a_L$  is affected mainly by the superficial gas velocity which also determines the specific power input (7). The specific power input can be calculated using the equation

$$\frac{P_G}{V_L} = \rho_L g U_G \quad (80)$$

where  $V_L$  is the volume of the liquid or slurry and  $\rho_L$  is its density. Properties of the fluid also affect  $k_L a_L$ . In water-like fluids, the aspect ratio of bubble columns does not affect  $k_L a_L$  so long as the column diameter exceeds  $\sim 0.1 \text{ m}$  (7). Similarly, liquid superficial velocities do not affect  $k_L a_L$  provided  $U_L \leq 0.1 \text{ m/s}$ .

For power inputs that are typically used in reactors, the  $k_L a_L$  in relatively coalescing media is little influenced by the design of the sparger because the turbulence in the fluid controls the bubble size. In strongly ionic low viscosity media, bubbles do not coalesce easily and the bubble size depends on the characteristics of the gas sparger. Porous plate spargers and those with smaller holes produce smaller bubbles and higher  $k_L a_L$  values. Small bubbles are produced also under highly turbulent conditions irrespective of the sparger hole size. Such bubble are especially persistent in viscous media because the viscous drag prevents them from leaving the fluid. Persistent microbubbles are seen in solutions of polymers.

In coalescence inhibiting media, the  $k_L a_L$  in bubble columns at very low superficial gas velocities depends on the sparger hole diameter: the  $k_L a_L$  declines as the sparger hole diameter increases over the range  $0.01\text{--}2 \text{ mm}$  (33). Relative to values in clean fluids, presence of surfactants reduces  $k_L a_L$ , but the reduction is greater in finer dispersions (ie, in small, ridged bubbles) generated by small hole spargers than in dispersions of larger, circulating bubbles. For quite low aeration rates, the  $k_L a_L$  for air–water system may be calculated with the equation (33)

$$\frac{k_L a_L}{U_G} \left( \frac{\mu_L^2}{\rho_L^2 g} \right)^{1/3} = \alpha \left[ (\mu_L g / \rho_L)^{-1/3} U_G \right]^{-\beta} \quad (81)$$

The values of  $\alpha$  and  $\beta$  for use with various sparger hole sizes are noted in Table 12 (33). Equation 81 was developed in bubble columns with aspect ratios  $1 \leq (h_L/d_T) \leq 3$  when the specific power inputs were  $3 \leq P_G/V_L \text{ (W/m}^3\text{)} \leq 38$ .

Although the overall  $k_L a_L$  in tall reactors may be little affected by the height, the overall mass transfer rates tend to be greater in taller systems because the mass transfer driving force increases with increasing hydrostatic

pressure. Mass transfer in bubble columns is discussed further by Shah and co-workers (50), Chisti (7,17), Deckwer (51), and Deckwer and Schumpe (52). The various correlations available for estimating  $k_L a_L$  or  $k_L$  in bubble columns are summarized in Table 13 (7, 53–62). Those correlations apply to the relatively high gas flow rates that are typical of chemical reactors. The correlation of Akita and Yoshida (55) is recommended for viscosities less than  $21 \times 10^{-3}$  Pa·s. The correlation of Kawase and co-workers (59) (Table 13) has also agreed well with independent measurements (63).

*Airlift Reactors.* Because of good oxygen transfer performance airlift devices have been used commonly as bioreactors for culturing yeasts, bacteria, and filamentous fungi (7,17). Compared to mechanically agitated vessels, airlift reactors require less power for attaining a given rate of gas–liquid mass transfer. Airlift devices outperform bubble columns in suspending solids. Relative to bubble columns, the airlift reactors have a better defined flow pattern; airlift systems are better than bubble columns in heat transfer capabilities (17). The operational range of airlift reactors tends to be generally broader than for similar bubble columns. Unlike in bubble columns, the overall height  $h_L$  of liquid in airlift reactors affects  $k_L a_L$  because the height strongly influences the liquid circulation velocity and, hence, the gas holdup (17).

Many equations have been developed to relate the apparent viscosity of non-newtonian media to the  $k_L a_L$  in airlift reactors. Most authors agree that  $k_L a_L$  generally declines with increasing apparent viscosity; however, there is great discrepancy on the precise magnitude of the viscosity effect (7,17). The exponent on the apparent viscosity term has been given variously as  $-0.255$  (64),  $-0.66$ ,  $-0.89$ , and other values (7). Such discrepancies are associated in part with the questionable practice of defining shear rate as an arbitrary linear function of the gas velocity (7,14). The viscosity associated decline in  $k_L a_L$  is especially pronounced for viscosities exceeding  $\sim 2.5 \times 10^{-2}$  Pa·s. In highly viscous non-newtonian fluids, the use of a supplementary axial flow impeller in the draft-tube of airlift reactors is known to enhance mass transfer and mixing performance (38).

Table 14 lists the correlations available for estimating the gas–liquid mass transfer coefficient in airlift reactors (64–69). Other correlations have been reviewed by Petersen and Margaritis (70) and Kilonzo and co-workers (71). These correlations are suitable only for initial estimates because the hydrodynamic and transport behavior of airlift devices is quite sensitive to the type of fluid, the reactor geometry, the distribution of gas holdup in the various zones, and the induced liquid circulation rate. Because of the numerous influences, a superior approach to prediction of mass transport for a more reliable design and scaleup relies on data measured at small scale. This method is discussed below.

*A General Method of Predicting  $k_L a_L$  for Scaleup.* Although various correlations can be used to directly estimate  $k_L a_L$ , the reliability of such estimates is often quite poor. A more reliable prediction of  $k_L a_L$  for process scaleup is based on methodology that combines fundamental principles with small-scale experimentation. This proven approach is especially suited to prediction of  $k_L a_L$  in complex media. Thus, based on purely analytical reasoning, the volumetric mass transfer

coefficient ( $k_L a_L$ ), gas holdup ( $\varepsilon_G$ ), the Sauter mean bubble diameter ( $d_B$ ), and the true mass transfer coefficient ( $k_L$ ), have been related as follows (7)

$$\frac{k_L}{d_B} = \frac{k_L a_L (1 - \varepsilon_G)}{6 \varepsilon_G} \quad (82)$$

Calculations of the  $k_L/d_B$  ratio from the measured  $k_L a_L$  and gas holdup have shown that in bubble columns and airlift devices this ratio is constant for a given fluid irrespective of the aeration rate (7,72). The value of  $k_L/d_B$  depends on the properties of the fluid. Thus, in slurries of cellulose pulp,  $k_L/d_B$  is affected by the concentration of solids (Fig. 6). For aqueous salt solution (0.15 M NaCl) with or without suspended cellulose fiber, the  $k_L/d_B$  ratio has been expressed as

$$\frac{k_L}{d_B} = 5.63 \times 10^{-5} \left( \frac{g \rho_L^2 \sigma_L D_L}{\mu_L^3} \right)^{\frac{1}{2}} e^{-0.131 C_s^2} \quad (83)$$

where  $C_s$  is the concentration of solids (% wt/vol). Equation 83 applies to airlifts as well as bubble columns (7). Chisti's (7) observations of constant  $k_L/d_B$  ratio in pneumatically agitated reactors have also been confirmed by others (17).

The observed constancy of  $k_L/d_B$  provides a reliable method for predicting  $k_L a_L$  in large-scale reactors from data easily measured in a small-scale model unit (7). This proven technique consists of the following steps:

1. Measure the gas holdup and the  $k_L a_L$  in a small model reactor with the fluid of interest over the range of gas flow rates that are of interest.
2. Use the data from step 1 to calculate the constant  $k_L/d_B$  ratio (equation 82).
3. Measure or calculate the riser gas holdup ( $\varepsilon_{Gr}$ ) in the full-scale reactor. (7, 17).
4. Calculate the  $k_L a_L$ -value for the large reactor:
  - (a.) for bubble columns

$$k_L a_L = \frac{k_L}{d_B} \frac{\varepsilon_G}{(1 - \varepsilon_G)} \quad (84)$$

- (b.) for airlift reactors

$$k_L a_L = \frac{k_L}{d_B} \frac{\varepsilon_{Gr}}{(1 - \varepsilon_{Gr})} \frac{A_r}{A_r + A_d} \quad (85)$$

In equations 84 and 85, the gas holdup and the geometric parameters  $A_r$  and  $A_d$  are for the large reactor; the  $k_L/d_B$ -value is from step 2. The rationale for equations 84 and 85 has been discussed by Chisti (7).

Figure 7 compares the measured  $k_L a_L$ -values with prediction of the foregoing procedure for 11 reactors including bubble columns and external and internal-loop airlift devices (7). The comparison spans water-like media, as well as pseudoplastic slurries of cellulose fiber. In all cases, the predictions agree remarkably well with the measurements (Fig. 7). Note that the Solka Floc cellulose fiber slurries in aqueous salt solutions, as used in Fig. 6 and 7, are generally pseudoplastic (7,61).

The various aspects of design of airlift reactors have been exhaustively treated in the literature (7,17). A few specifics are discussed in the following sections. *Axial Dissolved Oxygen Profiles.* As clearly demonstrated (7), the steady-state dissolved oxygen concentration varies axially in tall bubble columns and airlift reactors even in the absence of an oxygen consuming reaction. The exact nature of the concentration profile depends on the state of mixing in the reactor. During the culture of baker's yeast in a draft-tube sparged concentric tube internal-loop airlift reactor, Russell and co-workers (73) observed that the steady state dissolved oxygen concentration in the riser and the downcomer increased with increasing aeration rate. The dissolved oxygen levels were always several-fold higher in the downcomer than in the riser (73). In the riser, the dissolved oxygen levels tended to be  $\leq 30\%$  of air saturation. The oxygen concentration did not vary radially either in the riser or in the downcomer. Similarly, no significant variations were observed axially in the downcomer (73).

Local variations in dissolved gas concentration in tall reactors can affect the overall rate of reaction and the productivity of the reactor. Methods are now available for predicting the axial variations in dissolved gas concentration in bubble columns and airlift reactors (74,75). The ability for predicting the local gas concentration has important implications for scaleup of gas-liquid reactors. *Contributions of Various Zones to Overall  $k_L a_L$ .* Many airlift reactors consist of two hydrodynamically distinct zones—the riser and the downcomer—that contribute differently to the observed mass transfer (7). Sometimes a third zone—the gas-liquid separator (76)—may also exist with its own contribution toward mass transfer.

In airlift reactors that do not have gas-liquid separators, the measured  $k_L a_L$  consists of contributions from the riser and the downcomer zones; thus,

$$(k_L a_L)_{\text{measured}} = \frac{A_r (k_L a_L)_r + A_d (k_L a_L)_d}{A_r + A_d} \quad (86)$$

Equation 86 is an analytical expression that relates the measured  $k_L a_L$  to the separate, hypothetical, contributions of the riser and the downcomer (7). Equation 86 leads to the general conclusion that for any airlift device in which gas-liquid mass transfer is confined to the riser (ie, no gas in the downcomer), the actual volumetric mass transfer coefficient in the riser would be larger than the apparent measured value; the difference being dependent on the  $A_r/A_d$  ratio. Equation 86 applies to reactors in which the riser and the downcomer have approximately equal heights. In cases in which a significant portion of the liquid resides in the head zone, equation 86 should be modified to account for that volume (17). Generally,  $(k_L a_L)_d < (k_L a_L)_r$ .

Based on data obtained in several concentric draft-tube airlift reactors that were sparged either in the draft-tube or the annulus (aspect ratios = 6–11;  $U_G = 0.019$ – $0.12$  m/s), Koide and co-workers (77) suggested that in air-water systems the contribution of the downcomer zone to gas-liquid mass transfer was “relatively large.” Furthermore, in liquids, eg, aqueous salt solutions in which the bubbles are smaller than in water, the riser and the downcomer were claimed to contribute to the total mass transfer in proportion to the fraction of the

total volume that those zones occupied (77). These observations in relatively small reactors are not entirely consistent with other findings (7,17).

*Mass Transfer Enhancement by Static Mixers.* Installation of static mixer elements in airlift and bubble column reactors is known to enhance the gas–liquid mass transfer coefficient relative to mixer-free operation (17,78). The enhancement is mostly due to an increase in the gas–liquid interfacial area that is brought about by the bubble breaking action of the mixer elements. Installation of static mixers has improved productivity of certain oxygen-limited processes in airlift reactors (79).

The mass transfer enhancing effect of static mixers is most pronounced in viscous fluids that give rise to large spherical cap bubbles (78); less dramatic, but still large improvements, are observed with water-like media. Generally, for a given fluid, the mass transfer coefficient and the gas velocity in the riser of a given airlift reactor may be correlated in the form

$$k_L a_L = \alpha U_{Gr}^\beta \quad (87)$$

For a given fluid, the exponent  $\beta$  in equation 87 is not affected by the presence of static mixers in the reactor; however, the mixers significantly enhance the value of  $\alpha$  (78). The improvement in  $\alpha$  depends mainly on the consistency index ( $K$ ) or the ‘thickness’ of the fluid: generally, the thicker the fluid, the greater the effect of static mixers (78). The approximate relationship among  $\alpha$ ,  $\alpha_M$  (the  $\alpha$ -value in presence of static mixers) and  $K$  has been established to be

$$\frac{\alpha_M}{\alpha} = 4.43K^{0.12} \quad (88)$$

Equation 87 was determined for  $\sim 10^4$ -fold variation in  $K$ . The flow behavior index  $n$  (varied between 0.5 and 1.0) had no direct impact on enhancement of  $k_L a_L$  by the mixers (78). Depending on the fluid, the static mixers were found to enhance  $k_L a_L$  by 30–500% relative to mixer-free operation (78). The constants in equation 87 are expected to depend on the type of static mixer used.

Installation of mixing elements in airlift reactors slows down the circulation of fluid; hence, fewest possible mixing elements should be used to satisfy the mass transfer needs while limiting the loss of liquid circulation. The optimal interval between elements depends on the type of fluid. The more coalescing the fluid, the closer must the mixers be positioned for maximum performance. There is an upper limit to the viscosity that may be used in airlift reactors with static mixers (78). In excessively viscous media, just a few mixing elements can slow down the liquid so much so that the reactor stagnates.

*Reciprocating Jet Gas–Liquid Contactor.* A reciprocating plate or reciprocating jet gas–liquid contactor has been employed in some laboratory studies. The device is similar to a pulsed extraction column. It consists of a cylindrical tank containing a central shaft that supports a frame of evenly spaced perforated plates or disks. The plates are mounted horizontally relative to the axis of the shaft. The plates or baffles remain clear of the vessel walls; the inter-disk space and the diameter of perforation varies. Typically, disks are

placed 0.07–0.10-m apart and the perforations, 0.06–0.08 m in diameter, occupy a large proportion of the disk surface. The stack of disks oscillates up and down through the fluid. The liquid moves through the perforations as jets that change direction as the movement of stack reverses. The frequency of oscillation is usually a few cycles per second and the vertical movement is small. Brauer reported on these devices in the early 1980s and more gas–liquid mass transfer data have since appeared (80–82). The  $k_L a_L$  in reciprocating jet reactors increases with increasing frequency and amplitude of oscillation of the baffles. The power input also increases. The  $k_L a_L$  generally follows the equation

$$k_L a_L = \alpha (P/V_L)^\beta U_G^\gamma \quad (89)$$

where  $\alpha$ ,  $\beta$ , and  $\gamma$  depend on the reactor geometry, fluid properties, and the power input range. Some typical values for those parameters are noted in Table 15. Commercial utility of reciprocating plate reactors remains to be proven.

**Tubular Loop Reactors.** Tubular loop reactors employ cocurrent flow of gas and liquid in a pipe. The liquid is recirculated by a pump. This design is not practical except for low volume processes or unusual situations, eg, seen in the tubular solar receivers of photobioreactors used in culturing microalgae (83–85). For a tubular loop (0.025 m tube diameter, 22 m length), Ziegler and co-workers (86) recommended the equation

$$k_L a_L = 5.321 \times 10^{-5} (P_G/V_L)^{0.9} U_G^{0.2} + 8.333 \times 10^{-3} \quad (90)$$

Equation 90 was obtained using the sulfite oxidation system. Gas–liquid mass transfer in loop reactors is further discussed by VandenHeuvel and co-workers (87).

**Fluidized Beds.** Gas–liquid–solid fluidized-bed reactors are seen in wastewater treatment, some chemical processes, and immobilized cell culture. These reactors usually consist of a cylindrical vessel containing a suspension of the catalyst. The relatively heavy solids are kept in suspension by continuous flow of a liquid and gas. A solid–liquid separator, usually a sedimentation device, located near the top of the reactor prevents washout of solids. Essential design features of gas–liquid–solid fluidized-bed reactors are discussed by Muroyama and Fan (88). The gas–liquid mass transfer coefficients in three-phase fluidized beds may be estimated using the correlation:

$$\frac{k_L a_L d_p^2}{D_L} = \alpha \left( \frac{d_p U_t \rho_L}{\mu_L} \right)^{3.3} \left( \frac{\mu_L U_G}{\sigma_L} \right)^{0.7} \quad (91)$$

( $\alpha = 2.33 \times 10^{-5}$  when  $Re_t < 2000$ ;  $\alpha = 3.946 \times 10^{-7}$  when  $Re_t > 2000$ )

where  $U_t$  is the terminal settling velocity of the particle and  $Re_t$  is the  $Re$  number based on the terminal settling velocity. Equation 91 was developed for carbon dioxide absorption in water containing porcelain beads, sand, lead shot, or iron shot. The terminal settling velocity of the solids ranged over 0.12–0.815 m/s. Other parameters were:  $0 \leq U_G$  (m/s)  $\leq 0.1$ ;  $0.05 \leq U_L$  (m/s)  $\leq 0.172$ ;  $1.06 \leq d_p$  (mm)  $\leq 6.84$ ; and  $2400 \leq \rho_S$  (kg/m<sup>3</sup>)  $\leq 11,180$ .

Another correlation for gas–liquid mass transfer in fluidized beds is due to Nguyen-Tien and co-workers (89):

$$k_L a_L = 0.394 \left(1 - \frac{\varepsilon_S}{0.58}\right) U_G^{0.67} \quad (92)$$

where  $\varepsilon_S$  is the volume fraction of solids. For three-phase circulating bed reactors, Loh and co-workers (90) have recommended the following equation

$$k_L a_L = 1.4 \times 10^{-4} \left(\frac{P}{V_L}\right)^{0.91} \frac{(1 - 2.5\varepsilon_S)^{0.95}}{(1 - \varepsilon_S)^{4.3}} \quad (93)$$

Because  $k_L a_L$  is generally not too sensitive to the liquid flow rate, the equations developed for slurry bubble columns may also be applied to fluidized beds. Consult Muroyama and Fan (88) for further details on gas–liquid mass transfer in fluidized beds.

**Other Factors Affecting  $k_L a_L$ .** *Surfactants and Antifoam Agents* Relative to clean systems, addition of surfactants may reduce or enhance  $k_L a_L$ . The specific effect and its magnitude depend on the type of surfactant, its concentration, and the nature of the fluid. The coalescence promotion effect of some surfactants reduces the specific interfacial area  $a_L$  and the  $k_L a_L$ . Addition of surface active agents, eg, ethanol to water, generally increases  $a_L$  and  $k_L a_L$ . Surfactants, eg, sodium dodecyl sulfate (SDS), or sodium lauryl sulfate (SLS), accumulate at the gas–liquid interface and usually cause a reduction in  $k_L$ .

**Temperature.** The overall volumetric gas–liquid mass transfer coefficient  $k_L a_L$  generally increases with increasing temperature. This is mainly because the diffusion coefficient increases with temperature. Also, the viscosity of the liquid declines with increasing temperature; hence, for a given energy input, the film thickness declines and the interfacial area may increase slightly. The  $k_L a_L$  value at any temperature  $T$  ( $^{\circ}\text{C}$ ) may be calculated from the  $k_L a_L$  at  $20^{\circ}\text{C}$  using the equation:

$$(k_L a_L)_T = (k_L a_L)_{20^{\circ}\text{C}} \theta^{(T-20)^{\circ}\text{C}} \quad (94)$$

where  $\theta$  is 1.200–1.024.

**Suspended Solids** How and how much suspended solids affect  $k_L a_L$  depends on several factors including concentration of solids, the density difference between the solid and the suspending fluid, the particle diameter, the operating conditions of the reactor (ie, the power input), and the hydrophobicity of the solids. Up to 15% (wt/wt) of particles smaller than  $\sim 50\mu\text{m}$  have little effect on  $k_L a_L$ ; however, much smaller amounts of larger particles can reduce  $k_L a_L$  significantly. Very small concentrations of relatively high density solids may actually enhance  $k_L a_L$  a little. Increasing amounts of low density fibers (eg, paper pulp) rapidly increase the apparent viscosity of the slurry and the  $k_L a_L$  may decline sharply (7). Effect of such solids on  $k_L a_L$  is illustrated in Fig. 8 which is for paper pulp fibers.

In a draft-tube sparged concentric draft-tube airlift reactor for potential application to microbial desulfurization of coal, the mass transfer coefficient data in a simulated basal salt medium were reported by Smith and Skidmore (91). The medium contained a total  $1.9 \text{ kg/m}^3$  of various salts in distilled water. Pulverized coal particles ( $74 \times 10^{-6} \text{ m}$  particle diameter; density =  $1415 \text{ kg/m}^3$ ) were suspended in the fluid to a concentration of 0–40% wt (equivalent to 0–0.315 volume fraction of solids in gas-free medium). Over the temperature range 303–345 K, the  $k_L a_L$ -values were strongly enhanced by increasing temperature. Increasing concentration of solids over 0–5% wt (equivalent to  $\phi_S$  of 0–0.035) increased the  $k_L a_L$ -values slightly, but further increase in solids loading strongly lowered the mass transfer coefficient (91). This phenomena was explained as being due to penetration of fine solid particles in the stagnant liquid film around gas-bubbles, reducing the effective diffusion length (91). However, as the concentration of solids increased beyond 5% wt, the solids caused a blocking effect that reduced the effective mass transfer area (7,91). In the region of enhanced mass transfer ( $0 \leq \phi_S < 0.035$ ), the  $k_L a_L$  was correlated with

$$k_L a_L = (5.7 - 144.8\phi_S + 5048.3\phi_S^2) \times 10^4 U_{Gr}^{1.55} e^{-2990/T} \quad (95)$$

whereas in the blocking region ( $0.035 \leq \phi_S \leq 0.315$ ), the following equation was obtained (91)

$$k_L a_L = (2.6 - 16.8\phi_S + 29.4\phi_S^2) \times 10^6 U_{Gr}^{1.45} e^{-4130/T} \quad (96)$$

Equations 95 and 96 agreed with the data to within  $\sim \pm 20\%$ . These equations applied over the  $U_{Gr}$  range  $(0.154 - 1.39) \times 10^{-1} \text{ m/s}$ , when the  $A_r/A_d$  and the aspect ratios were 1.3 and  $\sim 5$ , respectively.

Mass transfer measurements in suspensions of agar-filled soft polyurethane foam particles ( $d_p = 3 \text{ mm}$ ;  $\rho_p = 1030 \text{ kg/m}^3$ ,  $\mu_L = 1.9 \times 10^{-1} \text{ Pa}\cdot\text{s}$ ) in draft-tube sparged concentric tube airlift reactors have been reported (92). Increasing volume fraction of solids over the 0–0.1 range, enhanced the volumetric mass transfer coefficient by 15–20% over solids-free operation (92). Further increase in solids loading to 40% (vol/vol) caused a decline in  $k_L a_L$  values. The mass transfer coefficient values in airlift reactors were up to three fold higher than in comparable fluidized beds.

In suspensions of relatively low density calcium alginate beads in water and other newtonian fluids, (0–20% vol/vol solids, 1.88–3.98-mm bead diameter) in draft-tube sparged concentric-tube airlift reactors, Koide and co-workers (69) noted that the mass transfer coefficient declined with increasing concentration of solids, but was not affected by the size of the particles.

**Oxygen Transfer in Wastewater Treatment Processes.** The typically used bioreactor in activated sludge treatment of wastewater consists of a relatively shallow ( $\sim 4 \text{ m}$  deep) rectangular basin aerated by sparging through perforated pipes or diffusers located at the bottom of the tank. The oxygen transfer capability of such systems is quite limited; hence, biodegradation is slow. Usually only  $\sim 0.5$ – $2 \text{ kg}$  oxygen can be transferred per kilowatt-hour of energy spent. The



oxygen transfer capabilities of other conventional aeration systems have been detailed by Winkler (93).

Faster degradation of pollutants can be achieved with low volume high rate oxygen transfer systems. One such technology is the deep shaft reactor based on the airlift principle. This advanced activated sludge process relies on high hydrostatic pressure in a deep airlift column to significantly enhance oxygen transfer. In comparison with conventional processes, oxygen transfer rates are up to 10-fold greater (93). The transfer rate at peak load is  $\sim 1\text{-kg oxygen} \cdot \text{m}^{-3} \cdot \text{h}^{-1}$  (17). Several factors combine to yield this high level of performance, including long gas-liquid contact times and intense turbulence in the circulating fluid with  $Re$  numbers of the order of  $10^5$  or higher (93). The shaft is 30–220 m deep (93), 0.5–10 m in diameter, and partitioned vertically into a riser and a downcomer. Air is injected into the downcomer,  $\sim 20\text{--}40$  m below the surface (93), except during start-up when the riser is aerated (Fig. 9). To ensure that air bubbles move down the downcomer, a superficial liquid velocity of 1–2 m/s must be generated in the downcomer zone. Because the gas is not recirculated, the downcomer region above the sparger is free of bubbles. Oxygen transfer efficiencies of 3–5.5 kg oxygen/kWh can be attained (93). Up to 90% of the oxygen in the air is used up.

For deep shaft plants, Winkler (93) cites a biochemical oxygen demand (BOD) loading of 0.9-kg BOD/kg sludge solids per day. A retention time of about 1.5 has been mentioned for 92% BOD removal (93). Volumetric BOD removal is of the order of  $3.7\text{--}6.6\text{-kg BOD} \cdot \text{m}^3 \cdot \text{day}^{-1}$  which is generally associated with high rate treatment processes. Sewage is treated without primary sedimentation; only preliminary de-gritting is needed (93). Sedimentation of grit at the bottom of the shaft is prevented by ensuring that the flow velocity at the bottom exceeds 1 m/s. See Chisti (17) for additional details.

In addition to the deep shaft, a biotower configuration is increasingly being used in wastewater treatment. The biotower units consist of a relatively shallow (18–20 m) above-ground pool of liquid with or without multiple draft-tubes (downcomers). The towers handle streams with  $2\text{--}12\text{ kg/m}^3$  chemical oxygen demand. The oxygen transfer efficiency ranges over 1.2–3.8 kg oxygen/kWh (94). The biomass sludge produced rises to the top with the bubbles and is separated in an integral settling zone. Chisti (17) provides further details.

**6.4. Liquid-Liquid Mass Transfer.** Liquid-liquid dispersions are encountered in solvent extraction, emulsion polymerization, and fermentations of hydrocarbons and other water-immiscible liquids. Also, oxygen supply using water-immiscible perfluorocarbons and other fluids utilizes liquid-liquid mass transfer. Whereas in gas-liquid dispersions only the liquid film around the bubble is the principal resistance to mass transfer, in liquid-liquid dispersions the film inside the dispersed drops also affects the transport rate. Tables 16 and 17 (3,95) list the correlations that are useful in calculating the mass transfer coefficients in the dispersed and continuous phases. Noncirculating small drops can be treated as ridged particles and solid-liquid mass transfer correlations (see later sections) developed for suspended spherical solids can be used. Presence of surfactants often renders drops nonmobile and again solid-sphere correlations apply. For larger, mobile, or oscillating droplets, both the continuous phase

and the dispersed phase mass transfer coefficients are greater than for solid spheres.

**Perfluorocarbons and Oxygen Vectors.** Perfluorocarbons are water immiscible liquids that dissolve 10–20 times more oxygen than does water. These fluids can be used for bubble-free oxygenation and removal of carbon dioxide in certain processes. Another potential application is stripping of inhibitory oxygen produced via photosynthesis in cultures of microalgae. Perfluorocarbons are biologically inert and suitably selected ones are nontoxic to animal cells and microorganisms. Indeed, emulsified perfluorocarbons have been used to supplement blood to improve oxygen supply to human patients. In microbial culture, perfluorocarbon concentrations as low as 10% vol/vol have significantly enhanced culture performance.

One scheme for bubble-free oxygenation using perfluorocarbons is illustrated in Fig. 10. A separate vessel is used to aerate the organic phase and strip the carbon dioxide. The oxygen enriched liquid is pumped to the fermenter and sprayed into the culture medium. As the droplets settle to the bottom in the relatively quiescent environment of the reactor, the oxygen transfers to the aqueous phase. The oxygen depleted perfluorocarbon from the bottom of the reactor is recycled to the external aerator. Perfluorocarbons and other oxygen vectors enhance oxygen-transfer performance also when added to an aerated reactor. The oils extract more oxygen from the gas phase and effectively increase oxygen–culture contact time. In agitated continuous culture of *E. coli* operated at a dilution rate of  $0.275 \text{ h}^{-1}$  and  $35.5^\circ\text{C}$ , an emulsified perfluorocarbon added to the feed at 50% volume fraction could provide  $0.17 \text{ kg O}_2 \text{ m}^{-3}\text{h}^{-1}$  when the biomass concentration was  $0.74 \text{ kg/m}^3$  (96). The same system removed  $0.23 \text{ kg}\cdot\text{m}^{-3}\text{h}^{-1}$  of carbon dioxide.

Other oxygen carriers have been tested, including hemoglobin solutions and erythrocytes, hydrocarbons, eg, *n*-hexadecane and *n*-dodecane, silicone oil emulsions, and soybean oil. Relevant properties of two types of oxygen vectors are noted in Table 18. Gas–liquid mass transfer enhancement due to presence of water-immiscible oxygen vectors in aerated aqueous dispersions has been reviewed by Dumont and Delmas (97).

**Aqueous Two-Phase Extractions.** Aqueous two-phase extraction is used in bioprocessing to recover and purify bioactive proteins that are susceptible to denaturation during traditional solvent extraction that employs hydrophobic solvents. Save and co-workers (98) measured mass transfer coefficients of cytochrome *c*, amyloglucosidase, and  $\beta$ -galactosidase in aqueous two-phase systems in a stirred cell with a flat interface between phases. In the poly(ethylene glycol)–dextran system the controlling resistance to mass transfer occurred in the heavy phase (the dextran-rich phase). This was correlated as

$$k_L = 3.9 \times 10^{17} D_L^{1.8} E^{0.42} \mu_L^{0.78} \quad (97)$$

For poly(ethylene glycol)–sodium sulfate systems the controlling resistance lay in the light phase (PEG-rich phase) and the mass transfer coefficient was correlated as (98):

$$k_L = 0.17D_L^{0.33}E^{0.38} \quad (98)$$

In equations 97 and 98,  $\mu_L$  is the viscosity of the phase and  $D_L$  is the estimated diffusivity of the protein in that phase. The agitation power input per unit phase mass is represented by  $E$ . The  $E$  values ranged over  $\sim(2-32) \times 10^{-4}$  W/kg.

**6.5. Solid-Liquid and Gas-Solid Mass Transfer.** Dissolution or vaporization of a solid phase into a fluid, or crystallization from a liquid are problems of solid-fluid mass transfer. Other similar situations occur in adsorption/desorption of material and during reaction catalyzed by a solid-phase catalyst. Common examples of gas-solid mass transfer are seen in various kinds of drying operations. Mass transfer may occur to or from a fluid flowing past a stationary solid, or the solid may be suspended in the fluid. These cases are treated separately below.

*Flow Past a Solid Surface.* Material transport to or from a fluid moving past a stationary solid is encountered in packed beds of catalysts, chromatographic media, and solid adsorbents, eg, activated carbon. Other occurrences are in membrane processes, solid-state state fermentations (99), capillaries containing surface-supported catalysts, and fluidized beds. The rate of mass transfer in flow past a solid is controlled by the flow rate of the fluid, the geometry of the solid surface, the diffusivity of the solute, and the physical properties of the flowing fluid. Suitable correlations for estimating the mass transfer coefficient for flow past solids of various geometries—flat plate, sphere, pipe, etc—are listed in Table 19 (2,100). The correlations given are for smooth surfaces. Predictive equations, eg, those in Table 19 and others in this monograph, are usually accurate to only  $\sim\pm 50\%$  of the actual value. Some more important process-relevant cases of mass transfer in flow past stationary solids are discussed in greater depth in the following sections.

*Packed Beds.* External mass transfer to or from spherical solid particles in packed beds has been correlated with the following equations

$$Sh = \frac{0.4584}{\phi} Re^{0.5931} Sc^{1/3} \quad (99)$$

for gases when  $10 \leq Re \leq 10,000$  (101);

$$Sh = \frac{1.09}{\phi} Re^{1/3} Sc^{1/3} \quad (100)$$

for liquids when  $0.0016 \leq Re \leq 55$  and  $165 \leq Sc \leq 70,600$  (2); and

$$Sh = \frac{0.250}{\phi} Re^{0.69} Sc^{1/3} \quad (101)$$

for liquids when  $55 \leq Re \leq 15,000$  and  $165 \leq Sc \leq 10,690$  (2). The  $Re$  number in these equations is based on the particle diameter; the superficial fluid velocity is based on the total cross-section of the bed, and  $\phi$  is the voidage of the packed bed. For nonspherical particles, these equations should be corrected: the  $Re$  number

should be calculated using the diameter of a sphere having the same surface area as the particle. Mass transfer in packed beds has been reviewed by Larachi and co-workers (102) and Wang and co-workers (103).

Chromatography columns are a form of packed bed. Mass transfer in chromatographic columns has been discussed by Li and co-workers (104). Mass transport aspects of high performance liquid chromatography (HPLC) have been reviewed by Miyabe and Guiochon (105). Mass transfer of proteins in ion exchange media, eg, those used in many chromatographic separations, has been discussed by Carta and co-workers (106). During chromatography of macromolecules, eg, proteins, the combination of molecular diffusivities, particle size of the stationary phase and elution velocity are such that separation is invariably controlled by mass transfer of solute to the stationary phase.

*Aeration Through Polymer Tubing.* Bubble-free gas exchange through polymer tubing has been employed in animal cell culture and culture of microalgae. In the latter case, the gas inside the tube is carbon dioxide that is used by photosynthetic cultures to generate carbohydrates and cell mass. For animal cell culture, the tube may be supplied with air, pure oxygen, or an atmosphere containing 5% (vol/vol) carbon dioxide for pH control.

Either microporous or nonporous tubing may be used for oxygenation of cultures having low oxygen demands. Microporous tubing is made of polytetrafluoroethylene or polypropylene both of which are strongly hydrophobic. Micropores, 0.03–3.5  $\mu\text{m}$  in diameter, occupy between 30 and 75 % of the surface of the tube. The tubing is fairly ridged, with typical outer diameters of 2.5–4 mm and a wall thickness of  $\sim 0.5$  mm. The pressure inside the tubing cannot exceed the bubble point pressure or the gas will issue through the pores as bubbles. The bubble point pressure tends to be low, of the order of 10 mbar. So long as the pores are gas filled, they do not pose a significant resistance to mass transfer (27) that occurs only through the liquid film held outside the pores. Microporous tubing generally provides a better mass transfer performance than the nonporous silicone tubing if the pores remain unwetted. Pore wetting can be a problem especially during prolonged use.

In homogeneous nonporous silicone tubing, also known as solution-diffusion tubing, the oxygen from inside the tube transfers to the outside by diffusion through the silicone tube wall; the transfer rate is quite slow compared to unwetted microporous tubing. The typical dimensions of silicone tubing are inside diameter = 1.8 mm and outside diameter = 3.2 mm, or inside diameter = 3 mm and outside diameter = 4.6 mm. Silicone tubing may be internally pressurized. Because of stretching and internal gas pressure, the surface area of the installed tubing differs from that in the relaxed state. The entire surface of the tubing is effective in mass transfer, except when the tubing has been reinforced. Solubilities and diffusivities of different gases are different in silicone; hence, transport is selective (27).

The mass transfer coefficient  $k_L$  outside the microporous tubing in agitated tanks has been correlated as (33)

$$Sh = (7.8 + 0.0021 Re^{1.2}) Sc^{1/6} \quad (102)$$

for  $250 < Re < 6000$  and  $200 < Sc < 500$ . The  $Re$  number in equation 102 is based on the impeller tip speed and the outer diameter  $d_o$  of the tube; thus,

$$Re = \frac{\pi N \rho_L d_i d_o}{\mu_L} \quad (103)$$

The  $Sh$  number is based on  $d_o$  and oxygen diffusivity in the liquid. The  $d_i$  in equation 103 is the impeller diameter. Equation 102 was developed in a cell culture vessel having the polymer tubing coiled into a cylindrical draft-tube configuration (Fig. 11). A 2-bladed anchor impeller located inside the draft-tube was used for agitation. For any given  $Re$  number, the anchor impeller yielded higher values of  $Sh$  number relative to propellers and screw impellers. Equation 102 is for protein-free medium. For microporous tubes, the  $k_L$  values in protein containing media are  $\sim 20\%$  lower than in water. Presence of protein does not seem to affect the mass transfer coefficient of nonporous tubing (33). Equation 102 may be used also for homogeneous silicone tubing.

Depending on the porosity of tubing and its diameter, 1.8–3.0 m of polymer tubing is needed per liter of culture volume to meet the  $k_L a_L$  demands (33). This length of tubing is close to technical limits of accommodation in a given volume; therefore, aeration through polymer tubes is useful only for specific cases. The tubing is susceptible to fouling and requires periodic replacement. Anchorage dependent cells sometimes attach to the surface of silicone tubing; hence, oxygen transfer to bulk fluid is prevented.

For transfer of carbon dioxide through nonporous silicone membranes and tubes (wall thickness 1.5–2.0 mm) the diffusion coefficient ( $D$ ) has been reported to be  $1.92 \pm 0.14 \text{ m}^2/\text{min}$  at  $25^\circ\text{C}$  (107). For mass transfer through such a tube to a highly agitated culture volume  $V_L$ , the transfer rate can be written as

$$\frac{dC_L}{dt} = \frac{AD(C^* - C_L)}{V_L \delta_w} \quad (104)$$

where  $A$  is the surface area of the tube,  $\delta_w$  is its wall thickness,  $C_L$  is the instantaneous concentration of the diffusing gas in the liquid-phase, and  $C^*$  is the saturation concentration of the diffusing component in a liquid sample that is in equilibrium with a gas phase having the same composition as in the silicone tube;  $C^*$  may be calculated using Henry's law. Note that equation 104 assumes a constant composition of the gas within the tube (ie, no diffusion of other dissolved gases from the liquid into the tube). This assumption may be valid for relatively short tubes and high flow rates within the tubes. Aeration through polymer tubing is discussed further by Aunins and Henzler (27).

**Mass Transfer Effects in Membrane Processes.** Membrane filtrations particularly microfiltration and ultrafiltration are increasingly used in processing of chemicals to separate particles and concentrate macromolecules. Generally, a crossflow scheme is used in which the fluid being filtered flows parallel to the membrane, but perpendicular to the direction of the permeate flux. The turbulence generated by the flow improves mass transfer at the membrane surface; consequently, the buildup of a solute layer or gel layer on the surface of the

### 38 MASS TRANSFER

membrane is reduced to assure relatively high permeate or filtrate flux through the membrane. At steady state, a solute concentration profile develops on the upstream side of the membrane as shown in Fig. 12. The permeate flux  $J$  is related to the concentration  $C_{Ge}$  of the solute in the gel layer, the concentration  $C_B$  in the bulk fluid, and the mass transfer coefficient  $k_L$  as follows:

$$J = k_L \ln \frac{C_{Ge}}{C_B} \quad (105)$$

The mass transfer coefficient depends on the  $Re$  number on the slurry side of the membrane as follows

$$Sh = \alpha Re^\beta Sc^{1/3} \quad (106)$$

where the  $Sh$  and  $Re$  are based on the hydraulic diameter  $d_h$  of the flow channel. During ultrafiltration  $\beta$  is 0.5 in laminar flow and  $\sim 1.0$  in turbulent flow. In cross-flow microfiltration of particles,  $\beta$  equals 0.8 in laminar flow, but increases to  $\sim 1.3$  in turbulent flow (108). The  $\alpha$  value is 0.023 in turbulent flow. Other expressions for  $Sh$  number are

$$Sh = 1.62 \left( Re \cdot Sc \frac{d_h}{L} \right)^{0.33} \quad (107)$$

$$Sh = 1.86 \left( Re \cdot Sc \frac{d_h}{L} \right)^{0.33} \quad (108)$$

and

$$Sh = 0.023 Re^{0.875} Sc^{0.25} \quad (109)$$

Equations 107 and 108 are for laminar flow in tubes and channels, respectively; equation 109 is for turbulent flow. For fully developed laminar flow in ultrafiltration  $k_L$  may be related to shear rate  $\gamma$  by the Porter equation:

$$k_L = 0.816 \gamma^{0.33} D_L^{0.67} L^{-0.33} \quad (110)$$

where  $L$  is the length of the flow channel and the shear rate depends on the channel geometry:  $\gamma = 8U_L/d$  for tubes with diameter  $d$ , and  $\gamma = 6U_L/h$  for rectangular channels of height  $h$ .

The cross-flow velocity is the principal operating variable for enhancing the performance of a given filtration membrane module. The optimal cross-flow velocity depends on the product and the configuration of the filtration module. For tubular microfiltration membranes with  $\sim 5.5$ -mm inner diameter, the optimal crossflow velocity is  $\sim 2.5$ – $5$  m/s (109). The inner diameter of membrane tubes

is usually 4–20 mm. Hollow fibers have much smaller diameters at 0.5–2 mm. Membranes are often deployed as flat sheets in a plate-and-frame configuration in which the height of the flow channel is 0.5–1.5 mm (109). Although cross-flow induced turbulence can reduce concentration polarization, some suspended solids can be damaged by excessive turbulence (18,20).

Other methods for improving mass transfer in membrane processes include operation at higher temperature (ie, higher diffusivity and lower viscosity), addition of large inert particles to the feed to agitate the gel layer, and use of pulsating flow. Module design may also be modified to enhance turbulence in the flow channel; hence, turbulence promoters such as static mixers (eg, wire screens) may be used in tubes and channels, or membranes may be formed into a corrugated configuration. Another method of mass transfer enhancement is the use of dynamic filtration systems with rotating membranes, or agitators placed in close proximity to the membrane (9).

In both ultrafiltration and microfiltration the mass transfer coefficient tends to be quite small because of the small diffusivities of the particles and macromolecules. Formation of the gel layer, also known as concentration polarization, reduces the permeate flux in microfiltration to only ~5% of the pure water flux. Unlike microfiltration and ultrafiltration, pervaporation processes use nonporous homogeneous membranes. Typically, the solute flux is low and the mass transfer coefficient  $k_L$  is relatively large in view of the higher diffusivities of small solutes, eg, ethanol. For additional information on mass transfer in membrane processes see Mulder (110), Ho and Sirkar (111), and Brindle and Stephenson (112).

**Mass Transfer at Rough Surfaces.** Compared to smooth surfaces, mass transfer from a geometrically similar rough surface is generally higher for otherwise identical conditions. Roughness induces an earlier transition to turbulence in flow past a surface. The effect of surface roughness on mass transfer coefficients in newtonian fluids has been correlated by Kawase and co-workers (113) using the equation

$$Sh = 0.0093 (e/d)^{0.15} Re \cdot Sc^{0.5} (1.11 + 0.44 Sc^{-1/3} - 0.70 Sc^{-1/6}) \quad (111)$$

where  $e$  is the absolute roughness (mean height of projections from the surface) and  $d$  is pipe or channel diameter. The ratio  $e/d$  is known as relative roughness. Equation 111 is for the ranges:  $5 \times 10^3 < Re < 5 \times 10^5$ ,  $5 < Sc < 400$ , and  $0.003 \leq e/d \leq 0.056$ .

Mass transfer in biofilms under oscillatory flow conditions has been discussed by Nagaoka (114).

**Fluid–Solid Slurries.** For mass transfer to or from suspended solids, energy dissipation in the vicinity of the particles is generally assumed to control mass transfer in an isotropically turbulent field. Under such conditions, the small energy dissipating eddies are independent of the nature of the bulk flow; the properties of those eddies depend only on energy dissipation rate per unit mass of fluid,  $E$ . In general, the liquid-film mass transfer coefficient  $k_L$  at the solid–liquid interface is expressed in terms of  $E$  as follows (115):

$$Sh = \frac{k_L d_p}{D_L} = 2 + c \left( \frac{E^{1/3} \rho_L d_p^{4/3}}{\mu_L} \right)^a Sc^b \quad (112)$$

where  $(E^{1/3} \rho_L d_p^{4/3} / \mu_L)$  may be regarded as the energy dissipation  $Re$  number (116). Notice that in a quiescent environment, purely diffusive mass transfer occurs and equation 112 reverts to  $Sh = 2$  as expected from theoretical considerations. Irrespective of the reactor configuration, solid–liquid mass transfer in slurries is not significantly influenced by presence of gas bubbles. Solid–liquid mass transfer cases for the principal types of reactors are discussed in the following sections.

*Stirred Tanks.* Use the Calderbank and Moo-Young (12) equation 44 noted earlier, or the Liepe and Möckel equations recommended by Hempel (117):

$$Sh = 2 + 0.67 \left( \frac{P}{V_L} \frac{\rho_L^2 d_p^4}{\mu_L^3} \right)^{1/8} Sc^{1/3} \quad (113)$$

which is valid when

$$d_p < 5.2 \left( \frac{\Delta \rho}{\rho_L} \right)^{-5/6} \left( \frac{\mu_L^3 V_L}{P \rho_L^2} \right)^{1/4} \quad (114)$$

When the particle diameter exceeds that given by inequality 114, the recommended equation is

$$Sh = 2 + 0.35 \left( \frac{\Delta \rho}{\rho_L} \right)^{1/3} \left( \frac{P}{V_L} \frac{\rho_L^2 d_p^4}{\mu_L^3} \right)^{2/3} Sc^{1/3} \quad (115)$$

Solid–liquid mass transfer coefficients in solid–liquid and gas–liquid–solid systems in stirred tanks have been reviewed by Pangarkar and co-workers (118).

*Bubble Columns.* The recommended correlation is

$$\frac{k_L d_p}{D_L} = 2 + 0.545 Sc^{1/3} \left( \frac{g d_p^4 \rho_L^3 U_G}{\mu_L^3} \right)^{0.264} \quad (116)$$

which is due to Sanger and Deckwer (119). It is suitable for  $137 \leq Sc \leq 50,000$ .

*Airlift Reactors.* For typical operating conditions, solid–liquid mass transfer coefficient in airlift reactors is insensitive to the gas flow rate until such a point when increasing the superficial gas velocity ceases to produce much increase in circulation of the slurry. If aeration rate is increased further, the  $k_L$  increases rapidly (17,115). Pneumatic energy imparted to the slurry initially produces bulk circulation of fluid; only when circulation no longer improves, the energy is dissipated in microeddies that penetrate to the vicinity of the solid–liquid interface and enhance  $k_L$ . Slight variations in solids concentration (eg, 0.2–4% wt/wt) do not affect  $k_L$  in airlift reactors (115,120).

Under similar conditions, solid–liquid mass transfer in external-loop airlift reactors exceeds that in stirred tanks and bubble columns; airlifts perform



marginally better than fluidized beds (17). Performance of draft-tube internal-loop airlift devices also exceeds that of bubble columns. The solid–liquid mass transfer coefficient in both external and internal-loop types of airlift reactors may be increased further by using static mixers. In draft-tube sparged reactors, Kenics-type twisted ribbon static mixers placed in the draft-tube have been shown to enhance the mass transfer coefficient by  $\sim 20\%$  relative to operation without the mixers (17).

The various correlations developed for solid–liquid mass transfer coefficient in internal-and external-loop types of airlift reactors are noted in Table 20 (115, 120–122). These correlations require a knowledge of the energy dissipation rate per unit mass of fluid;  $E$  is calculated using the equation

$$E = \frac{gU_{Gr}}{1 + \frac{A_d}{A_r}} \quad (117)$$

where  $U_{Gr}$  is the superficial gas velocity in the riser (7,72).

*Fluidized Beds.* Mass transfer coefficient for spherical particles suspended in a gas or liquid fluidized bed can be estimated using

$$Sh = \frac{0.4548 Re^{0.5931} Sc^{1/3}}{\phi_f} \quad (118)$$

where  $\phi_f$  is the void fraction of the bed. Equation 118 is suitable for  $10 \leq Re \leq 4000$ . Another similar correlation is

$$Sh = \left[ 0.01 + \frac{0.863}{Re^{0.58} - 0.483} \right] \frac{Re Sc^{1/3}}{\phi_f} \quad (119)$$

which applies for  $10 < Re < 2000$ . A correlation applicable only to liquid fluidized beds is

$$Sh = \frac{1.1068 Re^{0.28} Sc^{1/3}}{\phi_f} \quad (120)$$

which is suitable for  $1 \leq Re \leq 10$ . Gas–solid mass transfer in gas fluidized beds has been discussed by Yusuf and co-workers (123).

Mass transfer from the vessel wall to the fluid in a liquid fluidized bed (no gas) is aided by suspended solids that disturb the boundary layer at the wall of the reactor. The liquid-film mass transfer coefficient at the wall of such systems has been correlated (124) with the following equation:

$$\frac{k_L d_p}{D_L} = 0.14 \left( \frac{d_p U_L \rho_L}{\mu_L} \right)^{1/3} \left( \frac{\mu_L}{\rho_L D_L} \right)^{1/3} + 0.13(1 - \phi_f)(\phi_f - \phi_b) \left( \frac{\mu_L^2}{\rho_L^2 U_L d_p D_L} \right)^{1/3} \left( \frac{d_p^3 (\rho_S - \rho_L) \rho_L g}{\mu_L^2} \right)^{1/3} \quad (121)$$

Equation 121 applies when  $0.9 \leq \left( \frac{d_p U_L \rho_L}{\mu_L (1 - \phi_f)} \right) \leq 1652$  and  $151 \leq \left( \frac{\mu_L}{\rho_L D_L} \right) \leq 7021$ . In equation 121,  $\phi_f$  is the bed voidage and  $\phi_b$  is the void fraction of the settled bed.

**External Mass Transfer and Heterogeneous Reaction.** At steady state, the rate of mass transfer of a reactant being consumed at the surface of a non-porous particle equals the rate of consumption; thus,

$$k_L a_s (C_B - C_{Sb}) = R \quad (122)$$

where  $a_s$  is the solid–liquid interfacial area per unit liquid volume,  $R$  is the overall rate of reaction, and  $C_B$  and  $C_{Sb}$  are reactant concentrations in the bulk fluid and at the solid's surface, respectively. Because  $R$  is a function of the reactant concentration  $C_{Sb}$ ,  $R$  tends to a maximum when the concentration at the interface approaches that in the bulk fluid, ie, the mass transfer rate or the  $k_L a_s$  is large. In this situation, the rate of reaction is maximum and it is controlled by the intrinsic kinetics and not by mass transfer effects. At the other extreme, when the mass transfer rate is low compared to the reaction rate, the reactant concentration at the interface approaches zero, and the reaction is mass transfer controlled. Because now  $C_{Sb} = 0$ , the reaction rate is

$$R = k_L a_s C_B \quad (123)$$

Thus, the observed rate of a mass transfer controlled reaction will be influenced by changes in  $C_B$ ,  $k_L$ , or the specific solid–liquid interfacial area  $a_s$ . Indeed, observing influence of these parameters on the reaction rate provides methods for determining if the reaction is mass transfer limited. In addition, because the activation energy for mass transfer is much smaller than that of chemical reactions, the observed rate of a mass transfer controlled reaction is not as sensitive to temperature changes as the rate of reaction when it is not limited by transport effects. In a batch stirred vessel, an increase in the rate of a solid-phase catalyzed reaction with increasing agitation implies a mass transfer limited reaction. Similarly, in a packed bed reactor, the rate of a mass transfer controlled reaction will increase as the flow rate is increased but the contact time is kept unchanged (ie, the depth of the bed is increased proportionately).

The solid–liquid mass transfer correlations given earlier in this monograph may be used to estimate  $k_L$  in bubble columns, packed beds, fluidized beds, and other geometries of reactors. External mass transfer in immobilized enzyme systems has been discussed in greater detail by Goldstein (125).

**Intraparticle Mass Transfer.** In heterogeneous catalysis, transport within pores is largely diffusion-controlled. When the rate of mass transfer in the catalyst pores is less than or equal to the rate of consumption by the reaction, the catalyst is not fully active and the reaction is said to be controlled by internal diffusion. A regime of kinetic control of reaction rate occurs when the rates of mass transfer outside and within the catalyst particle exceed the rate of consumption by the reaction. An intermediate regime of catalysis occurs when the rate of mass transfer just balances consumption on the surface of the catalyst and no reaction takes place within pores. If the rate of transport to the surface of the catalyst is insufficient, concentration gradients develop in the fluid layer surrounding the particle and the reaction is controlled by external mass transfer. Reactions in gas fluidized beds of catalyst particles of 0.05–0.25-mm diameter generally occur in the kinetic regime. Because of small values of diffusivities in liquids, the kinetic regime does not usually obtain in packed beds of particles catalyzing a typical chemical reaction in the liquid phase.

In microporous particles, in the absence of convective transport, the main internal mass transfer parameter is the effective diffusivity  $D_e$  in the particle. The effective diffusivity is related to the unconfined bulk liquid- or gas-phase diffusivity as follows

$$D_e = \frac{p}{\tau} D_L \quad (124)$$

In equation 124,  $p$  is the porosity (ie, the void fraction within the particle), and  $\tau$  is the tortuosity of the porous matrix. The tortuosity also corrects for changes in cross-sectional area of the pore. Equation 124 applies to gases and liquids when the ratio of the mean free path and the pore diameter (ie, the dimensionless Knudsen number) is  $< 0.01$ . Tortuosity of many porous solids (eg, silica gel and alumina) are in the range  $2 \leq \tau \leq 6$  (1). For activated carbon,  $5 \leq \tau \leq 65$  (1).

For low pressure gases diffusing in narrow pores, the mean free path of the molecules is significantly longer than the pore diameter so that molecular collisions with the pore walls control diffusion. This is the Knudsen diffusion regime. The effective Knudsen diffusivity in pores ( $D_{K,e}$ ) is given by the equation:

$$D_{K,e} = \frac{p}{\tau} D_K \quad (125)$$

where

$$D_K = 48.5 d_{\text{pore}} \left( \frac{T}{M_G} \right)^{1/2} \quad (126)$$

Both Knudsen diffusion and bulk diffusion can be important at intermediate values of pressure. Diffusion of fluids in pores usually controls mass transfer during drying, ion exchange, adsorption, leaching, and heterogeneous catalysis. In large pores, diffusion is similar to ordinary or bulk diffusion, except that it is hindered by the pore walls (1).

In macroporous particles, changes in local fluid velocity outside the particle create pressure fluctuations within the larger pores and this leads to some agitation of the fluid held in the pores. In this situation, the apparent effective diffusivity ( $D_{e\text{ ap}}$ ) is greater than that predicted by equation 124. For example, the apparent effective diffusivity of oxygen in pellets of *Aspergillus niger* has been reported to be  $\sim 10^{-8}$  m<sup>2</sup>/s, or  $\sim 10$ -fold greater than in water, which suggests a level of fluid movement within the pellet possibly because of turbulence induced elastic structural deformations of the loose floc.

For porous particles in packed beds, the apparent effective diffusivity has been observed to depend on the effective diffusivity (no convection) and the Peclet number ( $Pe$ ); thus,

$$D_{e\text{ ap}} = \frac{D_e}{\frac{3}{Pe} \left( \frac{1}{\tanh Pe} - \frac{1}{Pe} \right)} \quad (127)$$

where the  $Pe$  number is given as

$$Pe = \frac{d_p U_L}{(1 - \phi) D_e} \quad (128)$$

In equation 128,  $d_p$  is the diameter of the particle,  $U_L$  is the superficial fluid velocity through the bed, and  $\phi$  is its void fraction.

More complete treatments of intraparticle mass transfer have been provided by Chisti and Moo-Young (9), Radovich (126), Willaert and co-workers (127), Pitcher (128), Bailey and Ollis (129), and Pilkington and co-workers (130). Mass transfer effects during osmotic dehydration of foods and other biological matrices have been discussed by Shi and Le Maguer (131). Gervais and Beney (132) have discussed osmotic mass transfer in the yeast *Saccharomyces cerevisiae*. Combined heat and mass transfer during freezing processes, eg, those commonly encountered in the food industry, has been discussed by Delgado and Sun (133).

## 7. High Rates of Mass Transfer

All the correlations for mass transfer coefficient given in this monograph apply for low mass transfer rates and equimolar counter diffusion. For high mass transfer cases, the mass transfer coefficient calculated from the correlations must be corrected for "diffusion-induced bulk flow". If  $k_G$  is the low-mass transfer value for the gas film coefficient, then the corresponding value of the coefficient for high transfer rate is represented as  $k'_G$ ;  $k_G$  and  $k'_G$  are related as follows:

$$k'_G = k_G \left\{ \frac{(1 - y_i) - (1 - y_b)}{\ln \left( \frac{1 - y_i}{1 - y_b} \right)} \right\} \quad (129)$$

where  $y_i$  and  $y_b$  are the mole fractions of the diffusing component at the gas-liquid interface and in the bulk gas, respectively.

## 8. Relationship Among Transfer Processes

The mass transfer process is quite similar to transfer of heat and momentum. Convective transfer of mass, heat, and momentum are all linked with flow. Consequently, the heat transfer coefficient, the mass transfer coefficient, and the drag coefficient in a given flow device can often be related by the following relationship:

$$j_M = j_H = \frac{C_{Dx}}{2} \quad (130)$$

where  $j_M$  and  $j_H$  are the  $j$ -factors for mass and heat transfer, respectively, and  $C_{Dx}$  is the local drag coefficient. Equation 130 is known as the Chilton–Colburn analogy. The  $j$ -factors and  $C_{Dx}$  are calculated, as follows:

$$j_M = \frac{k_L Sc^{2/3}}{2U_{av}} \quad (131)$$

$$j_H = \frac{h_H Pr^{2/3}}{C_p \rho_L U_{av}} \quad (132)$$

$$C_{Dx} = \frac{0.646}{Re_x^{0.5}} \quad (133)$$

Equation 133 applies to a laminar boundary layer on a flat plate. In equation 132,  $Pr$  is Prandtl number. In these equations,  $U_{av}$  is the free-stream velocity or the average velocity of turbulent flow in a pipe or channel. The Chilton–Colburn analogy derives from a consideration of transport in laminar boundary layers, but it is a useful approximation for turbulent flow in the absence of form drag. If form drag occurs,  $j_M \approx j_H$  (but  $j_M$  and  $j_H \neq C_{Dx}/2$ ) so long as  $0.6 < Sc < 2500$  and  $0.6 < Pe < 100$ .

## 9. Nomenclature

---

$A$	Surface area of tube ( $m^2$ )
$A_d$	Cross-sectional area of downcomer ( $m^2$ )
$A_r$	Cross-sectional area of riser ( $m^2$ )
$A_s$	Total solid–liquid interfacial area ( $m^2$ )
$a_D$	Gas–liquid interfacial area per unit volume of dispersion ( $m^{-1}$ )
$a_L$	Gas–liquid interfacial area per unit liquid volume ( $m^{-1}$ )
$a_{Lc}$	Liquid–liquid interfacial area per unit volume of continuous phase ( $m^{-1}$ )
$a_s$	Solid–liquid interfacial area per unit liquid volume ( $m^{-1}$ )
BOD	Biochemical oxygen demand
$Bo$	Bond number (–)
$C$	Concentration ( $kg/m^3$ )
$C^*$	Saturation concentration of transferring gas or solute in liquid ( $kg/m^3$ )
$\Delta C$	Concentration gradient ( $kg/m^3$ )
$C_B$	Solute or reactant concentration in bulk liquid ( $kg/m^3$ )
$C_{Dx}$	Local drag coefficient at distance $x$ (–)
$C_G$	Concentration in the gas phase ( $kg/m^3$ )

## 46 MASS TRANSFER

$C_{Ge}$	Solute concentration in gel layer ( $\text{kg/m}^3$ )
$C_{Gi}$	Interfacial concentration of the diffusing component in the gas phase ( $\text{kg/m}^3$ )
$C_L$	Instantaneous concentration of transferring component in liquid ( $\text{kg/m}^3$ )
$C_{L0}$	Initial dissolved oxygen (or gas) concentration at time $t_0$ ( $\text{kg/m}^3$ )
$C_{Lc}$	Equilibrium concentration of solute in continuous phase ( $\text{kg/m}^3$ )
$C_{Ld}$	Equilibrium concentration of solute in dispersed phase ( $\text{kg/m}^3$ )
$C_{Li}$	Interfacial concentration of the diffusing component in the liquid-phase ( $\text{kg/m}^3$ )
$C_S$	Concentration of solids in slurry (% wt/vol or $\text{kg/m}^3$ )
$C_{Sb}$	Substrate or reactant concentration at solid–liquid interface ( $\text{kg/m}^3$ )
$C_{in}^*$	Saturation concentration of oxygen in equilibrium with ingoing gas ( $\text{kg/m}^3$ )
$C_{out}^*$	Saturation concentration of oxygen in equilibrium with the exhaust gas ( $\text{kg/m}^3$ )
$C_p$	Specific heat of the fluid ( $\text{J kg}^{-1} \text{ } ^\circ\text{C}^{-1}$ )
$D$	Diffusivity ( $\text{m}^2/\text{s}$ )
$D_A$	Diffusivity of A in water ( $\text{m}^2/\text{s}$ )
$D_{AA}$	Self diffusivity of A ( $\text{m}^2/\text{s}$ )
$D_{AB}$	Diffusivity of A in B ( $\text{m}^2/\text{s}$ )
$D_{AP}$	Diffusivity of A in protein solution ( $\text{m}^2/\text{s}$ )
$D_{BB}$	Self-diffusivity of B ( $\text{m}^2/\text{s}$ )
$D_D$	Diffusivity of dispersed phase ( $\text{m}^2/\text{s}$ )
$D_e$	Effective diffusivity in particle ( $\text{m}^2/\text{s}$ )
$D_{e \text{ ap}}$	Apparent effective diffusivity in particle ( $\text{m}^2/\text{s}$ )
$D_G$	Diffusivity in gas ( $\text{m}^2/\text{s}$ )
$D_{\text{gas}}$	Diffusivity of gas in liquid ( $\text{m}^2/\text{s}$ )
$D_K$	Knudsen diffusivity ( $\text{m}^2/\text{s}$ )
$D_{K, e}$	Effective Knudsen diffusivity in pores ( $\text{m}^2/\text{s}$ )
$D_L$	Diffusivity of gas or solute in liquid ( $\text{m}^2/\text{s}$ )
DMEM	Dulbecco's modified Eagle's medium
$D_{\text{oxygen}}$	Diffusivity of gas in liquid ( $\text{m}^2/\text{s}$ )
$d$	Characteristic length dimension (m)
$d^*$	Diameter number defined by equation 42 (–)
$d_B$	Sauter mean bubble diameter (m)
$d_D$	Diameter of drop (m)
$d_F$	Maximum diameter of flask (m)
$d_H$	Diameter of sparger hole (m)
$d_h$	Hydraulic diameter (m)
$d_{hi}$	Hydraulic diameter in packed bed as defined in Table 19 (m)
$d_i$	Diameter of impeller (m)
$d_o$	Outer diameter of tubing (m)
$d_p$	Diameter of particle (m)
$d_{\text{pore}}$	Pore diameter (m)
$d_r$	Diameter of riser (m)
$d_T$	Diameter of tank or column (m)
$E$	Energy dissipation rate per unit mass (W/kg)
EDTA	Ethylenediaminetetraacetic acid
$E_L$	Overall axial dispersion coefficient of liquid ( $\text{m}^2/\text{s}$ )
$e$	Absolute roughness (m)
$\hat{e}$	Eccentricity of shaker platform (–)
$F$	Mass flow rate of gas ( $\text{kg/s}$ )
$Fr$	Froude number (–)
$f$	Parameter (–)
$G$	Mass flux of gas in column ( $\text{kg}\cdot\text{s}^{-1}\cdot\text{m}^{-2}$ )
$G_g$	Molar flux of gas ( $\text{kmol}\cdot\text{s}^{-1}\cdot\text{m}^{-2}$ )
$Gr$	Grashof number (–)
$g$	Gravitational acceleration ( $\text{m/s}^2$ )
$H$	Dimensionless Henry's law constant (–)
HPLC	High performance liquid chromatography

$HTU$	Height of an overall transfer unit (m)
$HTU_G$	Height of gas phase transfer unit defined by equation 76 (m)
$HTU_L$	Height of liquid-phase transfer unit defined by equation 77 (m)
$h$	Height of channel (m)
$h_D$	Height of dispersion (m)
$h_H$	Heat transfer coefficient ( $\text{W}\cdot\text{m}^{-2}\cdot^\circ\text{C}^{-1}$ )
$h_L$	Height of gas-free liquid (m)
$h_T$	Height of liquid on tray (cm)
$I$	Ionic strength ( $\text{kg ion m}^{-3}$ )
$J$	Mass flux ( $\text{kg}\cdot\text{m}^{-2}\cdot\text{s}^{-1}$ or $\text{kmol}\cdot\text{m}^{-2}\cdot\text{s}^{-1}$ ) or permeate flux (m/s)
$j_H$	Chilton–Colburn factor for heat transfer, defined by equation 132 (–)
$j_M$	Chilton–Colburn factor for mass transfer, defined by equation 131 (–)
$K$	Consistency index of fluid ( $\text{Pa}\cdot\text{s}^n$ )
$K_L$	Overall mass transfer coefficient based on liquid film (m/s)
$K_P$	Mass transfer coefficient for plug ( $\text{mol}\cdot\text{O}_2\cdot\text{atm}^{-1}\cdot\text{h}^{-1}$ )
$K_p$	Partition coefficient of solute defined by equation 34 (–)
$K_S$	Mass transfer coefficient at surface ( $\text{mol}\cdot\text{O}_2\cdot\text{atm}^{-1}\cdot\text{h}^{-1}$ )
$k$	Mass transfer coefficient (m/s)
$k_B$	Boltzman constant ( $8.9308 \times 10^{-10} \text{ g}\cdot\text{equiv}\cdot\Omega\cdot\text{s}^{-1}$ )
$k_{G_i}$	Gas film mass transfer coefficient (m/s)
$k_G$	Gas film mass transfer coefficient for high transfer rate (m/s)
$k_g$	Gas film mass transfer coefficient defined by equation 74 (cm/s)
$k_H$	Thermal conductivity of the fluid ( $\text{W m}^{-1}\cdot^\circ\text{C}^{-1}$ )
$k_i$	Impeller-dependent constant in equation 54 (–)
$k_L$	Liquid film mass transfer coefficient (m/s)
$k_{LaL}$	Overall gas–liquid volumetric mass transfer coefficient ( $\text{s}^{-1}$ )
$(k_{LaL})_r \text{ or } d$	Overall volumetric mass transfer coefficient in riser or downcomer ( $\text{s}^{-1}$ )
$k_{Lc}$	Liquid film mass transfer coefficient in continuous phase (m/s)
$k_{Ld}$	Liquid-film mass transfer coefficient in dispersed phase (m/s)
$L$	Length of circulation loop, pipe, plate, or flow channel (m)
$L_L$	Molar flux of liquid ( $\text{kmol}\cdot\text{s}^{-1}\cdot\text{m}^{-2}$ )
$L_m$	Mass flux of liquid in column ( $\text{kg}\cdot\text{s}^{-1}\cdot\text{m}^{-2}$ )
$l$	Length of impeller blade (m)
$M_A$	Molar mass of A ( $\text{kg}/\text{kmol}$ )
$M_B$	Molar mass of B ( $\text{kg}/\text{kmol}$ )
$M_G$	Molar mass of gas ( $\text{kg}/\text{kmol}$ )
$M_L$	Molecular weight of liquid ( $\text{kg}/\text{kmol}$ )
$Mo$	Morton number (–)
$N$	Rotational speed ( $\text{s}^{-1}$ )
$n$	Flow behavior index (–)
$P$	Power input (W)
PEG	Poly(ethylene glycol)
$Pe$	Peclet number (–)
$P_G$	Gassed power input (W)
$P_g$	Pressure (Pa)
$P_o$	Power number (–)
$Pr$	Prandtl number, $C_p\mu/k_H$ (–)
$Ps$	Poiseuille number (–)
$p$	Porosity of particle (–)
$p_{\text{atm}}$	Partial pressure of oxygen in the atmosphere outside flask (atm)
$p_L$	Partial pressure of oxygen in liquid in flask (atm)
$Q_G$	Volume flow rate of gas ( $\text{m}^3/\text{s}$ )
$q_{\text{O}_2}$	Specific oxygen consumption rate ( $\text{s}^{-1}$ )
$R$	Overall rate of reaction ( $\text{kg}\cdot\text{m}^{-3}\cdot\text{s}^{-1}$ )
$Ra$	Rayleigh number (–)
$R_b$	Ratio of bubble diameter to its width (–)
$R_G$	Gas constant ( $8314.4 \text{ J}\cdot\text{kmol}^{-1}\text{K}^{-1}$ )

## 48 MASS TRANSFER

$Re$	Reynolds number (–)
$Re_C$	Reynolds number for the continuous phase (–)
$Re_d$	Reynolds number based on $d_{hi}$ as in Table 19 (–)
$Re_G$	Reynolds number of gas (–)
$Re_i$	Reynolds number based on impeller (–)
$Re_L$	Reynolds number of liquid (–)
$Re_t$	Reynolds number based on terminal settling velocity of particle (–)
$Re_x$	Local value of Reynolds number at distance $x$ from leading edge (–)
RPMI	Cell culture medium
$Sc$	Schmidt number (–)
SDS	Sodium dodecyl sulfate
$Sh$	Sherwood number (–)
$Sh_x$	Local value of Sherwood number at distance $x$ from leading edge (–)
$Sh_G$	Sherwood number of gas (–)
$Sh_L$	Sherwood number of liquid (–)
SLS	Sodium lauryl sulfate
$St$	Stanton number (–)
$T$	Temperature (°C) or absolute temperature (K)
$T_b$	Normal boiling point (K)
$t$	Instantaneous time (s)
$t_C$	Contact time of droplets (s)
$t_m$	Mixing time (s)
$t_R$	Residence time of gas in liquid (s)
$U$	Velocity (m/s)
$U_{av}$	Free stream velocity or average velocity of turbulent flow (m/s)
$U_B$	Bubble rise velocity (m/s)
$U_G$	Superficial gas velocity based on outer column cross-sectional area (m/s)
$U_{Gr}$	Superficial gas velocity in the riser (m/s)
$U_L$	Mean superficial liquid velocity in the reactor or pipe (m/s)
$U_{Lr}$	Superficial liquid velocity in the riser (m/s)
$U_{max}$	Liquid flow velocity at gas–liquid interface (m/s)
$U_p$	Velocity of particle (m/s)
$U_t$	Terminal settling velocity of a single particle in liquid (m/s)
$u$	Gas velocity (cm/s)
$V_A$	Molar volume of A at its boiling point or at critical point (m <sup>3</sup> /kmol)
$V_b$	Molar volume at normal boiling point (cm <sup>3</sup> /mol)
$V_G$	Molar volume of gas (m <sup>3</sup> /kmol)
$V_L$	Volume of liquid or slurry (m <sup>3</sup> )
$V_{Lc}$	Volume of continuous phase (m <sup>3</sup> )
$V_M$	Molar volume of solute at its boiling point (m <sup>3</sup> /kmol)
$v_A$	Diffusion volume of A (cm <sup>3</sup> /mol)
$v_B$	Diffusion volume of B (cm <sup>3</sup> /mol)
$W$	Width of impeller blade (m)
$We$	Weber number (–)
$Wi$	Weissenberg number (–)
$X$	Viable biomass concentration (kg/m <sup>3</sup> )
$x$	Distance (m)
$x_i$	Mass fraction of oxygen in inlet gas stream (–)
$x_o$	Mass fraction of oxygen in exhaust gas (–)
$y_b$	Molar fraction of diffusing component in bulk gas (–)
$y_i$	Molar fraction of diffusing component at gas–liquid interface (–)

---



## 10. Greek Symbols

---

$\alpha$	Parameter; parameter in equation 87 ( $\text{m}^{-\beta} \cdot \text{s}^{-(\beta+1)}$ )
$\alpha_H$	Thermal diffusivity ( $\text{m}^2/\text{s}$ )
$\alpha_M$	Value of $\alpha$ (equation 87) in presence of static mixers ( $\text{m}^{-\beta} \cdot \text{s}^{-(\beta+1)}$ )
$\beta$	Parameter (—)
$\gamma$	Parameter or shear rate ( $\text{s}^{-1}$ )
$\delta$	Film thickness (m)
$\delta_G$	Thickness of gas film (m)
$\delta_L$	Thickness of liquid film (m)
$\delta_w$	Wall thickness of tube (m)
$\varepsilon$	Characteristic Lennard-Jones energy given by equation 10
$\varepsilon_A$	Characteristic Lennard-Jones energy of A
$\varepsilon_B$	Characteristic Lennard-Jones energy of B
$\varepsilon_G$	Overall gas holdup (—)
$\varepsilon_{Gr}$	Gas holdup in the riser (—)
$\varepsilon_S$	Volume fraction or holdup of solids in three-phase systems (—)
$\theta$	Parameter in equation 94 (—)
$\lambda$	Characteristic time or relaxation time of viscoelastic fluid (s)
$\lambda_m$	Mean free path (m)
$\mu$	Viscosity (Pa·s)
$\mu_{ap}$	Apparent viscosity of non-newtonian fluid (Pa·s)
$\mu_B$	Viscosity of B (Pa·s)
$\mu_C$	Viscosity of the continuous phase (Pa·s)
$\mu_D$	Viscosity of the dispersed phase (Pa·s)
$\mu_G$	Viscosity of the gas (Pa·s)
$\mu_L$	Viscosity of the liquid (Pa·s)
$\mu_{SL}$	Viscosity of the slurry (Pa·s)
$\mu_w$	Viscosity of water (Pa·s)
$\zeta$	Association parameter (—)
$\pi$	Pi (—)
$\rho$	Density ( $\text{kg}/\text{m}^3$ )
$\rho_C$	Density of continuous phase ( $\text{kg}/\text{m}^3$ )
$\rho_D$	Density of dispersed phase ( $\text{kg}/\text{m}^3$ )
$\rho_G$	Density of gas ( $\text{kg}/\text{m}^3$ )
$\rho_L$	Density of the liquid ( $\text{kg}/\text{m}^3$ )
$\rho_P$	Density of the particles ( $\text{kg}/\text{m}^3$ )
$\rho_S$	Density of solids ( $\text{kg}/\text{m}^3$ )
$\rho_{SL}$	Density of slurry ( $\text{kg}/\text{m}^3$ )
$\Delta\rho$	Density difference between phases ( $\text{kg}/\text{m}^3$ )
$\sigma$	Interfacial tension (liquid–liquid) ( $\text{kg}/\text{s}^2$ )
$\sigma_A$	Characteristic length of A (Å)
$\sigma_B$	Characteristic length of B (Å)
$\sigma_{AB}$	Characteristic length defined by equations 7 and 8 (Å)
$\sigma_i$	Characteristic length of i (Å)
$\sigma_L$	Interfacial tension ( $\text{kg}/\text{s}^2$ )
$\tau$	Tortuosity of pores (—)
$\phi$	Void fraction of the packed bed (—)
$\phi_b$	Voidage of settled bed (—)
$\phi_f$	Voidage of fluidized bed (—)
$\phi_S$	Volume fraction of solids in gas-free slurry (—)
$\chi$	Parameter (—)
$\Omega_D$	Parameter defined by equation 9

---

## BIBLIOGRAPHY

“Mass Transfer” in *ECT* (online), posting date: May 17, 2002, by Y. Chisti, Massey University; in *ECT* 5th ed., Vol. 15, pp. 670–740, by Y. Chisti, Massey University.

## CITED PUBLICATIONS

1. J. G. Knudsen, H. C. Hottel, A. F. Sarofim, P. C. Wankat, and K. C. Knaebel, in R. H. Perry and D. W. Green, eds., *Perry's Chemical Engineers' Handbook*, 7th ed., McGraw-Hill, New York, 1997, pp. 5.1–5.79.
2. C. J. Geankoplis, *Transport Processes and Unit Operations*, 3rd ed., Prentice Hall, Englewood Cliffs, 1993.
3. H. R. C. Pratt, in T. C. Lo, M. H. I. Baird and C. Hanson, eds., *Handbook of Solvent Extraction*, John Wiley & Sons, Inc., New York, 1983, pp. 91–123.
4. C. R. Wilke and P. Chang, *AIChE J.* **1**, 264 (1955).
5. Y. Chisti, in M. C. Flickinger and S. W. Drew, eds., *Encyclopedia of Bioprocess Technology: Fermentation, Biocatalysis, and Bioseparation*, Vol. **3**, John Wiley & Sons, Inc., New York, 1999, pp. 1607–1640.
6. Y. Chisti, in R. Robinson, C. Batt and P. Patel, eds., *Encyclopedia of Food Microbiology*, Academic Press, London, 1999, pp. 663–674.
7. Y. Chisti, *Airlift Bioreactors*, Elsevier, London, 1989, pp. 350.
8. K. Van't Riet, *Ind. Eng. Chem. Process Des. Dev.* **18**, 357 (1979).
9. Y. Chisti and M. Moo-Young, in V. Moses and R. E. Cape, eds., *Biotechnology: The Science and the Business*, Harwood Academic Publishers, New York, 1991, pp. 167–209.
10. J. L. Casas López, E. M. Rodríguez Porcel, I. Oller Alberola, M. M. Ballesteros Martín, J. A. Sánchez Pérez, J. M. Fernández Sevilla, and Y. Chisti, *Ind. Eng. Chem. Res.* **45**, 1167 (2006).
11. C. S. Ho and J. F. Shanahan, *CRC Crit. Rev. Biotechnol.* **4**, 185 (1986).
12. P. H. Calderbank and M. B. Moo-Young, *Chem. Eng. Sci.* **16**, 39 (1961).
13. P. H. Calderbank and A. C. Lochiel, *Chem. Eng. Sci.* **19**, 485 (1964).
14. Y. Chisti and M. Moo-Young, *Biotechnol. Bioeng.* **34**, 1391 (1989).
15. E. M. Grima, Y. Chisti, and M. Moo-Young, *J. Biotechnol.* **54**, 195 (1997).
16. L. K. Shi, J. P. Riba, and H. Angelino, *Chem. Eng. Commun.* **89**, 25 (1990).
17. Y. Chisti, *Appl. Mech. Rev.* **51**, 33 (1998).
18. Y. Chisti, in M. C. Flickinger and S. W. Drew, eds., *Encyclopedia of Bioprocess Technology: Fermentation, Biocatalysis, and Bioseparation*, Vol. **5**, John Wiley & Sons, Inc., New York, 1999, pp. 2379–2406.
19. Y. Chisti, *Trends Biotechnol.* **18**, 420 (2000).
20. Y. Chisti, *Crit. Rev. Biotechnol.* **21**, 67 (2001).
21. M. Reuss, in H.-J. Rehm and G. Reed, eds., *Biotechnology*, Vol. **3**, 2nd ed., VCH, Weinheim, 1993, pp. 185–217.
22. M. Moo-Young and H. W. Blanch, *Adv. Biochem. Eng.* **19**, 1 (1981).
23. T. Oolman and H. W. Blanch, *CRC Crit. Rev. Biotechnol.* **4**, 133 (1986).
24. Y. Chisti, *Trends Biotechnol.* **21**, 89 (2003).
25. Y. Chisti and M. Moo-Young, *J. Chem. Technol. Biotechnol.* **58**, 331 (1993).
26. S. Yamada, M. Wada, and I. Chibata, *J. Ferment. Technol.* **56**, 20 (1978).
27. J. G. Aunins and H.-J. Henzler, in H.-J. Rehm and G. Reed, eds., *Biotechnology*, Vol. **3**, 2nd ed., VCH Weinheim, 1993, pp. 219–281.
28. A. Gupta and G. Rao, *Biotechnol. Bioeng.* **84**, 351 (2003).

29. U. Maier and J. Büchs, *Biochem. Eng. J.* **7**, 99 (2001).
30. J. G. Aunins, B. A. Woodson, Jr., T. K. Hale, and D. I. C. Wang, *Biotechnol. Bioeng.* **34**, 1127 (1989).
31. M. Lavery and A. W. Nienow, *Biotechnol. Bioeng.* **30**, 368 (1987).
32. Y. Kato, S. Hiraoka, Y. Tada, K. Sato, and T. Ohishi, *J. Chem. Eng. J.*, **30**, 362 (1997).
33. H.-J. Henzler and D. J. Kauling, *Bioproc. Eng.* **9**, 61 (1993).
34. J. F. Perez and O. C. Sandall, *AIChE J.* **20**, 770 (1974).
35. Y. Kawase and M. Moo-Young, *Trans. Inst. Chem. Eng.* **68**, 189 (1990).
36. R. E. Farritor and G. A. Hughmark, *AIChE J.* **20**, 1027 (1974).
37. K. A. Bin, *Chem. Eng. Commun.* **31**, 155 (1984).
38. Y. Chisti and U. J. Jauregui-Haza, *Biochem. Eng. J.* **10**, 143 (2002).
39. C. H. E. Nielsen, S. Kiil, H. W. Thomsen, and K. Dam-Johansen, *Chem. Eng. Sci.* **53**, 495 (1998).
40. P. L. Spedding and M. T. Jones, *Chem. Eng. J.* **37**, 165 (1998).
41. A. W. Nienow, *Appl. Mech. Rev.* **51**, 3 (1998).
42. A. Bakker, J. M. Smith, and K. J. Myers, *Chem. Eng.*, **101**(12), 98 (1994).
43. C. S. Shin, M. S. Hong, and J. Lee, *Biotechnol. Techn.* **10**, 679 (1996).
44. Y. Chisti, *Bioproc. Eng.* **9**, 191 (1993).
45. H. Taguchi and F. Yoshida, *J. Ferment. Technol.* **46**, 814 (1968).
46. H. Yagi and F. Yoshida, *Ind. Eng. Chem. Process Des. Dev.* **14**, 488 (1975).
47. Y. Kawase and M. Moo-Young, *Chem. Eng. Res. Des.* **66**, 284 (1988).
48. K. Chandrasekharan and P. H. Calderbank, *Chem. Eng. Sci.* **36**, 819 (1981).
49. G. Ascanio, B. Castro, and E. Galindo, *Chem. Eng. Res. Des.* **82**, 1282 (2004).
50. Y. T. Shah, B. G. Kelkar, S. P. Godbole, and W.-D. Deckwer, *AIChE J.* **28**, 353 (1982).
51. W.-D. Deckwer, *Bubble Column Reactors*, John Wiley & Sons, Inc., New York, 1992.
52. W.-D. Deckwer and A. Schumpe, *Chem. Eng. Sci.* **48**, 889 (1993).
53. J. J. Heijnen and K. Van't Riet, *Chem. Eng. J.* **28**, B21 (1984).
54. J. R. Fair, *Chem. Eng.* **74** July 3, 67 (1967).
55. K. Akita and F. Yoshida, *Ind. Eng. Chem. Process Des. Dev.* **12**, 76 (1973).
56. G. A. Hughmark, *Ind. Eng. Chem. Process Des. Dev.* **6**, 218 (1967).
57. M. Nakano and F. Yoshida, *Ind. Eng. Chem. Process Des. Dev.* **19**, 190 (1980).
58. A. Schumpe, C. Singh, and W.-D. Deckwer, *Chem. -Ing. -Techn.* **57**, 988 (1985).
59. Y. Kawase, B. Halard, and M. Moo-Young, *Chem. Eng. Sci.* **42**, 1609 (1987).
60. H. Hikita, S. Asai, K. Tanigawa, K. Segawa, and M. Kitao, *Chem. Eng. J.* **22**, 61 (1981).
61. W.-D. Deckwer, K. Nguyen-Tien, A. Schumpe, and Y. Serpemen, *Biotechnol. Bioeng.* **24**, 461 (1982).
62. S. P. Godbole, A. Schumpe, Y. T. Shah, and N. L. Carr, *AIChE J.* **30**, 213 (1984).
63. J. Dudley, *Wat. Res.* **29**, 1129 (1995).
64. G.-Q. Li, S.-Z. Yang, Z.-L. Cai, and J.-Y. Chen, *Chem. Eng. J.* **56**, B101 (1995).
65. K. Koide, H. Sato, and S. Iwamoto, *J. Chem. Eng. Jpn.*, **16**, 407 (1983).
66. K. Koide, K. Horibe, H. Kawabata, and S. Ito, *J. Chem. Eng. Jpn.*, **18**, 248 (1985).
67. P. Verlaan, J.-C. Vos, and K. van't Riet, *J. Chem. Technol. Biotechnol.* **45**, 181 (1989).
68. I.-S. Suh, A. Schumpe, and W.-D. Deckwer, *Biotechnol. Bioeng.* **39**, 85 (1992).
69. K. Koide, K. Shibata, H. Ito, S. Y. Kim, and K. Ohtaguchi, *J. Chem. Eng. Jpn.*, **25**, 11 (1992).
70. E. E. Petersen and A. Margaritis, *Crit. Rev. Biotechnol.* **21**, 233 (2001).
71. P. A. Kilonzo and A. Margaritis, *Biochem. Eng. J.* **17**, 27 (2004).
72. Y. Chisti and M. Moo-Young, *Chem. Eng. Commun.* **60**, 195 (1987).
73. A. B. Russell, C. R. Thomas, and M. D. Lilly, *Bioproc. Eng.* **12**, 71 (1995).
74. F. C. Rubio, J. L. Garcia, E. Molina, and Y. Chisti, *Chem. Eng. Sci.* **54**, 1711 (1999).

75. F. C. Rubio, J. L. Garcia, E. Molina, and Y. Chisti, *Chem. Eng. J.* **84**, 43 (2001).
76. Y. Chisti and M. Moo-Young, *Chem. Eng. Prog.*, **89**(6), 38 (1993).
77. K. Koide, K. Horibe, H. Kitaguchi, and N. Suzuki, *J. Chem. Eng. Jpn.*, **17**, 547 (1984).
78. Y. Chisti, M. Kasper, and M. Moo-Young, *Can. J. Chem. Eng.* **68**, 45 (1990).
79. W. Zhou, K. Holzhauser-Rieger, and K. Schügerl, *J. Biotechnol.* **28**, 165 (1993).
80. J. Audet, J. Thibault, and A. LeDuy, *Biotechnol. Bioeng.* **52**, 507 (1996).
81. M. Lounes, J. Audet, J. Thibault, and A. LeDuy, *Bioproc. Eng.* **13**, 1 (1995).
82. X. Ni, S. Gao, and D. W. Pritchard, *Biotechnol. Bioeng.* **45**, 165 (1995).
83. F. G. A. Fernández, J. M. F. Sevilla, J. A. S. Pérez, E. M. Grima, and Y. Chisti, *Chem. Eng. Sci.* **56**, 2721 (2001).
84. E. M. Grima, F. G. A. Fernández, F. G. Camacho, and Y. Chisti, *J. Biotechnol.* **70**, 231 (1999).
85. E. M. Grima, J. Fernández, F. G. A. Fernández, and Y. Chisti, *J. Biotechnol.* **92**, 113 (2001).
86. H. Ziegler, I. J. Dunn, and J. R. Bourne, *Biotechnol. Bioeng.* **22**, 1613 (1980).
87. J. C. VandenHeuvel, P. G. Verschuren, and S. P. P. Ottengraf, *Wat Sci. Technol.* **36**, 311 (1997).
88. K. Muroyama and L.-S. Fan, *AIChE J.* **31**, 1 (1985).
89. K. Nguyen-Tien, A. N. Patwari, A. Schumpe, and W.-D. Deckwer, *AIChE J.* **31**, 194 (1985).
90. V. Y. Loh, S. R. Richards, and P. Richmond, *Proceedings: International Conference on Bioreactor Fluid Dynamics*, 15–17 April, 1986, BHRA, Cambridge, England.
91. B. C. Smith and D. R. Skidmore, *Biotechnol. Bioeng.* **35**, 483 (1990).
92. D. G. Karamanev, T. Nagamune, and I. Endo, *Chem. Eng. Sci.* **47**, 3581 (1992).
93. M. A. Winkler, *Biological Treatment of Waste-Water*, Ellis Horwood, Chichester, 1981.
94. W. Sittig, *J. Chem. Technol. Biotechnol.* **32**, 47 (1982).
95. K. Schügerl, *Solvent Extraction in Biotechnology: Recovery of Primary and Secondary Metabolites*, Springer-Verlag, New York, 1994.
96. S. Martin, P. Soucaille, and J.-S. Condoret, *Bioproc. Eng.* **13**, 293 (1995).
97. E. Dumont and H. Delmas, *Chem. Eng. Proc.* **42**, 419 (2003).
98. S. S. Save, R. B. Desai, S. B. Sawant, and J. B. Joshi, *Trans. Inst. Chem. Eng.* **74C**, 171 (1996).
99. Y. Chisti, in M. C. Flickinger and S. W. Drew, eds., *Encyclopedia of Bioprocess Technology: Fermentation, Biocatalysis, and Bioseparation*, Vol. **5**, John Wiley & Sons, Inc., New York, 1999, pp. 2446–2462.
100. D. K. Edwards, V. E. Denny, and A. F. Mills, *Transfer Processes*, Holt, Rinehart and Winston, Inc., New York, 1973.
101. P. N. Dwivedi and S. N. Upadhyay, *Ind. Eng. Chem. Process Des. Develop.* **16**, 157 (1977).
102. F. Larachi, L. Belfares, I. Iliuta, and B. P. A. Grandjean, *Ind. Eng. Chem. Res.* **42**, 222 (2003).
103. G. Q. Wang, X. G. Yuan, and K. T. Yu, *Ind. Eng. Chem. Res.* **44**, 8715 (2005).
104. Q. Li, E. W. Grandmaison, C. C. Hu, D. Taylor, and M. F. A. Goosen, *Bioseparation* **5**, 189 (1995).
105. K. Miyabe and G. Guiochon, *J. Sep. Sci.* **26**, 155 (2003).
106. G. Carta, A. R. Ubiera, and T. M. Pabst, *Chem. Eng. Technol.* **28**, 1252 (2005).
107. Y.-K. Lee and H.-K. Hing, *Appl. Microbiol. Biotechnol.* **31**, 298 (1989).
108. R. S. Tutunjian, *Biotechnol.* **3**, 615 (1985).
109. S. Ripperger, *Chem. Eng. Technol.* **11**, 17 (1988).

110. M. H. V. Mulder, in R. D. Noble and S. A. Stern, eds., *Membrane Separations Technology: Principles and Applications*, Elsevier, Amsterdam, The Netherlands, 1995, pp. 45–84.
111. W. S. W. Ho and K. K. Sirkar, eds., *Membrane Handbook*, Van Nostrand Reinhold, New York, 1992.
112. K. Brindle and T. Stephenson, *Biotechnol. Bioeng.* **49**, 601 (1996).
113. Y. Kawase, A. V. Shenoy, and K. Wakabayashi, *Can. J. Chem. Eng.* **72**, 798 (1994).
114. H. Nagaoka, *Wat. Sci. Technol.* **36**, 329 (1997).
115. H. H. Mao, Y. Chisti, and M. Moo-Young, *Chem. Eng. Commun.* **113**, 1 (1992).
116. W.-D. Deckwer and A. Schumpe, *Ger. Chem. Eng.* **7**, 168 (1984).
117. D. C. Hempel, in R. K. Finn, P. Präve, M. Schlingmann, W. Crueger, K. Esser, R. Thauer, F. Wagner, eds., *Biotechnology Focus 1: Fundamentals, Applications, Information*, Hanser, New York, 1988, pp. 51–94.
118. V. G. Pangarkar, A. A. Yawalkar, M. M. Sharma, and A. A. C. M Beenackers, *Ind. Eng. Chem. Res.* **41**, 4141 (2002).
119. P. Sängler and W.-D. Deckwer, *Chem. Eng. J.* **22**, 179 (1981).
120. S. Goto, Y. Matsumoto, and P. Gaspillo, *Chem. Eng. Commun.* **85**, 181 (1989).
121. K. B. Kushalkar and V. G. Pangarkar, *Chem. Eng. Sci.* **49**, 139 (1994).
122. P. D. Gaspillo and S. Goto, *J. Chem. Eng. Jpn.* **24**, 680 (1991).
123. R. Yusuf, M. C. Melaaen, and V. Mathiesen, *Chem. Eng. Technol.* **28**, 13 (2005).
124. S. Schmidt, J. Büchs, C. Born, and M. Biselli, *Chem. Eng. Sci.* **54**, 829 (1999).
125. L. Goldstein, *Methods Enzymol.* **44**, 397 (1976).
126. J. M. Radovich, *Enzyme Microbial. Technol.* **7**, 2 (1985).
127. R. G. Willaert, G. V. Baron, and L. De Backer, eds., *Immobilised Living Cell Systems: Modelling and Experimental Methods*, John Wiley & Sons, Inc., Chichester, 1996.
128. W. H. Pitcher, Jr., *Adv. Biochem. Eng.* **10**, 1 (1978).
129. J. E. Bailey and D. F. Ollis, *Biochemical Engineering Fundamentals*, 2nd ed., McGraw-Hill, New York, 1986, pp. 204–220.
130. F. H. Pilkington, A. Margaritis, and N. A. Mensour, *Crit. Rev. Biotechnol.* **18**, 237 (1998).
131. J. Shi and M. Le Maguer, *Food Rev. Int.* **18**, 305 (2002).
132. P. Gervais and L. Beney, *Cell. Mol. Biol.* **47**, 831 (2001).
133. A. E. Delgado and D. W. Sun, *J. Food Eng.* **47**, 157 (2001).

YUSUF CHISTI  
Massey University

Table 1. Typical Magnitude of Diffusivity in Various Phases

Continuous phase	Diffusivity, m <sup>2</sup> /s
gas (atmospheric pressure)	10 <sup>-5</sup>
liquid	10 <sup>-9</sup>
liquid held in a solid matrix	10 <sup>-10</sup>
polymers	10 <sup>-12</sup>
solid	10 <sup>-14</sup>

Table 2. Diffusivities of Some Common Solutes in Dilute Liquids

Solute	Solvent	Temperature, °C	$D, \times 10^9 \text{ m}^2/\text{s}$
acetic acid	water	25	1.26
acetic acid	benzene	25	2.09
acetone	water	25	1.28
benzoic acid	water	25	1.21
carbon dioxide	water	20	1.50
carbon dioxide	water	25	2.00
chloroform	benzene	20	2.11
chloroform	ethanol	20	1.23
ethanol	water	25	1.24
glucose	water	20	0.60
glycerol	water	20	0.83
methanol	water	15	1.26
nitrogen	water	20	1.64
oxygen	water	20	1.80
oxygen	water	25	2.41
phenol	water	20	0.84
phenol	ethanol	20	0.80
sodium chloride	water	20	1.35
sucrose	water	20	0.45
urea	water	25	1.38
water	ethanol	25	1.13

Table 3. Diffusivities of Some Large Molecules (Globular Proteins) in Dilute Aqueous Solutions

Protein	Molecular weight, kg/kmol	Temperature, °C	$D \times 10^{11} \text{ m}^2/\text{s}$
bovine serum albumin	67,500	25	6.81
urease	482,700	25	4.01
human serum albumin	72,300	20	5.93
human fibrinogen	339,700	20	1.98

Table 4. Association Parameters for Some Solvents<sup>a</sup>

Solvent	Association Parameter, $\xi$
water	2.6 <sup>b</sup>
methanol	1.9
ethanol	1.5
propanol	1.2
benzene	1.0
ether	1.0
heptane	1.0
other unassociated solvents	1.0

<sup>a</sup>Ref. 4.<sup>b</sup>A value of 2.26 better described the data, as shown in later publications.

Table 5. Diffusivities of Some Gases and Vapors in Air at 25 °C

Solute	$D, \times 10^6 \text{ m}^2/\text{s}$
acetic acid	13.3
ammonia	28.0
benzene	8.8
butanol	9.0
carbon dioxide	16.4
carbon disulfide	10.7
ethanol	11.9
hydrogen	71.0
oxygen	20.6
toluene	8.4
water	25.6

Table 6. Factors Influencing Gas–Liquid Mass Transfer

temperature	concentration of solids
pressure	hydrophobicity of solids
diffusivity	morphology of solids
viscosity	shear rate or power input
density	aeration velocity
surface tension	pH
presence of surfactants	geometry of the gas–liquid
and ions	contactor
ionic strength	flow parameters of non-newtonian
	fluids

Table 7. Possible Ways of Expressing Mass Flux and Mass Transfer Coefficient

Flux, $J$	Driving force	Units of $K_L$
$\text{kg}\cdot\text{s}^{-1}\text{m}^{-2}$	concentration difference, $\text{kg}/\text{m}^3$	$\text{m}/\text{s}$
$\text{kg}\cdot\text{s}^{-1}\text{m}^{-2}$	mole fraction difference	$\text{kg}\cdot\text{s}^{-1}\text{m}^{-2}$
$\text{kg}\cdot\text{s}^{-1}\text{m}^{-2}$	partial pressure difference	$\text{kg}\cdot\text{s}^{-1}\text{m}^{-2}$
$\text{kmol}\cdot\text{s}^{-1}\text{m}^{-2}$	concentration difference, $\text{kg}/\text{m}^3$	$\text{m}/\text{s}$
$\text{kmol}\cdot\text{s}^{-1}\text{m}^{-2}$	mole fraction difference	$\text{kmol}\cdot\text{s}^{-1}\text{m}^{-2}$
$\text{kmol}\cdot\text{s}^{-1}\text{m}^{-2}$	partial pressure difference	$\text{kmol}\cdot\text{s}^{-1}\text{m}^{-2}$
$\text{m}^3\text{m}^{-2}\text{s}^{-1}$ (for transfer of a gas)	partial pressure difference	$\text{m}/\text{s}$

Table 8. Alternative Methods of Expressing Dimensionless Groups

Group	Alternative expressions
Reynolds number, $Re$	$\frac{\rho_L U_L d}{\mu_L}$ , or $\frac{\rho_G U_G d}{\mu_G}$ (in pipes and channels) $\frac{\rho_L N d_i^2}{\mu_L}$ (stirred tanks) $\frac{\rho_L U_L L}{\mu_L}$ , or $\frac{\rho_G U_G L}{\mu_G}$ (flow past a plate) $\frac{\rho_L U_L d_p}{(1-\phi)\mu_L}$ , or $\frac{\rho_G U_G d_p}{(1-\phi)\mu_G}$ (flow past particles in packed beds)
Sherwood number, $Sh$	$\frac{k_L d}{D_L}$ , or $\frac{k_G d}{D_G}$ ( $d$ may be diameter of a particle, flow channel, etc)
Froude number, $Fr$	$\frac{U_L^2}{gh_L}$ , or $\frac{U_G^2}{gh_L}$ (in bubble columns and airlift reactors) $\frac{N d_i^2}{gh_L}$ , or $\frac{N^2 d_i}{g}$ (in stirred tanks)
Peclet number, $Pe$	$\frac{U_L h_L}{D_L}$ , or $\frac{U_B d_B}{D_L}$ (in bubble columns and airlift reactors) $\frac{N d_i^2}{D_L}$ (in stirred tanks)



Table 9. Other Dimensionless Groups Relevant to Mass Transfer and Related Fluid Mechanics

Group	Definition	Physical significance
Bond number, $Bo$	$\frac{gd_p^2 \Delta \rho}{\sigma_L}$	$\frac{\text{gravity force}}{\text{surface tension force}}$
Peclet number, $Pe$	$\frac{U_L L}{D_L}$ or $\frac{U_G L}{D_G}$	$\frac{\text{bulk mass transport}}{\text{diffusional mass transport}}$
Poiseuille number, $Ps$	$\frac{\mu_L U_p}{\rho_L g d_p^2 \Delta \rho}$ or $\frac{\mu_G U_p}{\rho_G g d_p^2 \Delta \rho}$	$\frac{\text{viscous force}}{\text{gravity force}}$
Power number, $Po$	$\frac{P}{\rho_L N^3 d_i^5}$	
Rayleigh number, $Ra$	$Gr \cdot Sc$	
Stanton number, $St$	$\frac{Sh}{Re \cdot Sc}$	
Weber number, $We$	$\left( \frac{U_p^2 \rho_L d_p}{\sigma_L} \right)^{1/2}$	$\frac{\text{inertial force}}{\text{surface tension force}}$

## 58 MASS TRANSFER

Table 10. **Correlations for Liquid-Phase Mass Transfer Coefficient at Free Surface in Baffled Stirred Tanks (No Vortex)**

---

$k_L = 5.11 \times 10^{-3} \left[ \frac{11^{n-1} K}{\rho_L} \left( \frac{3n+1}{4n} \right)^n \right]^{-0.426} D_L^{0.5} d_i^{0.852} N^{1.352-0.426n}$	Perez and Sandall <sup>a</sup>
$k_L = 0.322 Sc^{-2/3} N^{0.7} d_i^{0.4} (\mu_L / \rho_L)^{0.3}$	Hikita and Ishikawa <sup>b</sup>
$k_L = 0.0256 Sc^{-1/2} \frac{Po^{1/3} N d_i^2}{(\pi d_T^2 h_L / 4)^{1/3}}$	Farritor and Hughmark <sup>c</sup>
$k_L = \left\{ 0.432 \left( \frac{d_i}{d_T} \right) - 0.13 \right\} \left( \frac{E \rho_L}{\mu_L} \right)^{1/3} D_L^{1/2}$	Bin <sup>d</sup>
$\frac{k_L d_i}{D_L} = 0.04 \left( \frac{N d_i^2 \rho_L}{\mu_L} \right) \left( \frac{N^2 d_i^3 \rho_L}{\sigma_L} \right)^{1/2} \left( \frac{\mu_L}{\rho_L D_L} \right)^{1/2}$	Kataoka and Miyauchi <sup>b</sup>

---

<sup>a</sup>Ref. 34.

<sup>b</sup>Ref. 35.

<sup>c</sup>Ref. 36.

<sup>d</sup>Ref. 37.

Table 11. Mass transfer Correlations for Stirred Tanks

Correlation	Ranges
1. Taguchi and Yoshida (45) $\frac{k_L a_L}{N} = 0.113 \left( \frac{d_T^2 h_L}{W(d_i - W)} \right)^{1.437} (N t_m)^{-1.087} (d_i/d_T)^{1.021}$	pseudoplastic paper pulp slurries (1.6 % wt/vol pulp). Disk turbine stirred vessel
2. Yagi and Yoshida (46) $\frac{k_L a_L d_i^2}{D_L} = 0.06 \left( \frac{d_i^2 N \rho_L}{\mu_L} \right)^{1.5} \left( \frac{d_i N^2}{g} \right)^{0.19} \left( \frac{\mu_L}{\rho_L D_L} \right)^{0.5}$ $\times \left( \frac{\mu_L U_G}{\sigma_L} \right)^{0.6} \left( \frac{N d_i}{U_G} \right)^{0.32} \left[ 1 + 2\sqrt{\lambda N} \right]^{-0.67}$ <p>for non-newtonian fluids use apparent viscosity instead of <math>\mu_L</math>. <math>\lambda</math> is the characteristic time or relaxation time of viscoelastic fluids; <math>\lambda = 0</math> for nonviscoelastics</p>	viscous newtonian and non-newtonian liquids, including viscoelastic fluids
3. Perez and Sandall (34) $\frac{k_L a_L d_i^2}{D_L} = 21.2 \left( \frac{\rho_L N d_i^2}{\mu_{ap}} \right)^{1.11} \left( \frac{\mu_{ap}}{\rho_L D_L} \right)^{0.5} \left( \frac{U_G d_i}{\sigma_L} \right)^{0.447} \left( \frac{\mu_G}{\mu_{ap}} \right)^{0.694}$ $\mu_{ap} = K(11N)^{n-1} \left( \frac{3n+1}{4n} \right)^n$	carbon dioxide absorption in water and non-Newtonian power law solutions
4. Kawase and Moo-Young (47) $k_L a_L = 0.675 \sqrt{D_L} \frac{\rho_L^{3/5} E^{9+4n/10(1+n)}}{(K/\rho_L)^{1/2(1+n)} \sigma_L^{3/5}} \left( \frac{U_G}{U_B} \right)^{0.5} \left( \frac{\mu_{ap}}{\mu_w} \right)^{-0.25}$	Newtonian and non-newtonian power law fluids
5. Niebelschütz (21) $k_L a_L \left( \frac{V_L}{Q_G} \right) Sc^{0.3} = 0.103 \left( \frac{P_G}{Q_G \rho_L (g \mu_L / \rho_L)^{2/3}} \right)^{0.53}$	non-newtonian power law slurries and polymer solutions; $0.035 \leq V_L \text{ (m}^3\text{)} \leq 0.070$ , $0.02 \leq \mu_L \text{ (Pa}\cdot\text{s)} \leq 3.1$ ; $\mu_L$ was calculated at a shear rate value of $10^4/\text{s}$
6. Reuss (21) $\frac{k_L a_L}{U_G} \left( \frac{\mu_L^2}{g \rho_L^2} \right)^{1/3} Sc^{0.3} = 5.5 \times 10^{-4} \left( \frac{P_G}{V_L U_G \rho_L g} \right)^{0.7}$	newtonian fluids; $\mu_L \leq 12 \times 10^{-3} \text{ Pa}\cdot\text{s}$ , $0.05 \leq V_L \text{ (m}^3\text{)} \leq 1.9$
7. Chandrasekharan and Calderbank (48) $k_L a_L = \left( \frac{0.0248}{d_T^4} \right) \left( \frac{P_G}{V_L} \right)^{0.551} Q_G^{0.551/\sqrt{d_T}}$	air–water

## 60 MASS TRANSFER

Table 12. Values of  $\alpha$  and  $\beta$  for Use in Equation<sup>a</sup>

Sparger	$d_H$ , mm	$\alpha$	$\beta$	Range
frit	0.01	$6.0 \times 10^{-5}$	0.4	$0.001 \leq U_G(\mu_L g / \rho_L)^{-1/3} \leq 0.1$
	0.02	$6.3 \times 10^{-5}$	0.2	
perforated pipe	0.5	$4.2 \times 10^{-5}$	0.2	$0.01 \leq U_G(\mu_L g / \rho_L)^{-1/3} \leq 0.2$
	2.0	$2.2 \times 10^{-5}$	0.17	

<sup>a</sup>Ref. 33.

Table 13. Gas–Liquid Mass Transfer Correlations for Bubble Columns

Correlation	Ranges
1. Chisti (7) $k_L a_L = 2.39 \times 10^{-4} (P_G/V_L)^{0.86}$	air–water, $d_T \geq 0.1$ m, $200 \leq P_G/V_L$ (W/m <sup>3</sup> ) $\leq 1000$ , $h_L/d_T$ up to 25
2. Heijnen and Van't Riet (53) $k_L a_L = 0.32 U_G^{0.7}$	air–water at 20 °C, $0.08 < d_T$ (m) < 11.6, $0 < U_G$ (m/s) < 0.3, $0.3 < h_L$ (m) < 21 perforated pipe or perforated plate spargers producing 4–6-mm bubbles
3. Fair (54) $k_L a_D = 3.31 \left( \frac{D_L \varepsilon_G}{d_B^2} \right) \left( \frac{\mu_L}{\rho_L D_L} \right)^{1/3} \left( \frac{d_B \rho_L U_G}{\mu_L} \right)^{0.5}$	newtonian fluids
4. Akita and Yoshida (55) $\frac{k_L a_D d_T^2}{D_L} = 0.6 \left( \frac{\mu_L}{\rho_L D_L} \right)^{0.5} \left( \frac{g d_T^2 \rho_L}{\sigma_L} \right)^{0.62} \left( \frac{g d_T^3 \rho_L^2}{\mu_L^2} \right)^{0.31} \varepsilon_G^{1.1}$	air–water and other newtonian fluids; $\mu_L$ $\leq 21 \times 10^{-3}$ Pa·s, $U_G$ and $U_L$ up to 0.4 m/s
5. Akita and Yoshida (55) $\frac{k_L d_B}{D_L} = 0.5 \left( \frac{\mu_L}{\rho_L D_L} \right)^{0.5} \left( \frac{g d_B^3 \rho_L^2}{\mu_L^2} \right)^{0.25} \left( \frac{g d_B^2 \rho_L}{\sigma_L} \right)^{3/8}$	air–water and other newtonian fluids, $\mu_L \leq 21 \times 10^{-3}$ Pa·s, $U_G$ and $U_L$ up to 0.4 m/s
6. Chisti (7) $k_L = 5.63 \times 10^{-5} \left( \frac{g \rho_L^2 D_L \sigma_L}{\mu_L^3} \right)^{0.5} d_B e^{-0.131 C_S^2}$	air–water, and slurries of paper pulp in salt solutions; bubble and churn turbulent flow; $0 \leq C_S$ (wt/vol %) $\leq 3$
7. Hughmark (56) $\frac{k_L d_B}{D_L} = 2 + 0.0187 \times \left[ \left( \frac{\mu_L}{\rho_L D_L} \right)^{0.339} \left( \frac{d_B U_G \rho_L}{\mu_L} \right)^{0.484} \left( \frac{d_B g^{1/3}}{D_L^{2/3}} \right)^{0.072} \right]^{1.61}$	newtonian fluids, $0.0009 \leq \mu_L$ (Pa·s) $\leq 0.152$

## 62 MASS TRANSFER

Table 13. (*Continued*)

Correlation	Ranges
<p>8. Nakanoh and Yoshida (57)</p> $\frac{k_L a_D d_T^2}{D_L} = 0.09 \left( \frac{\mu_L}{\rho_L D_L} \right)^{0.5} \left( \frac{g d_T^2 \rho_L}{\sigma_L} \right)^{0.75} \left( \frac{g d_T^3 \rho_L^2}{\mu_L^2} \right)^{0.39} \left( \frac{U_G^2}{g d_T} \right)$ $\times \left( 1 + \chi \left( \frac{U_B \lambda}{d_B} \right) \right)^{-0.45}$ <p><math>\chi = 0</math> (inelastic fluids) or 0.133 (elastic fluids). For non-newtonian power law fluids <math>\mu_L = \mu_{ap} = K (5000 U_G)^{n-1}</math></p>	<p>newtonian, non-newtonian and viscoelastic fluids, <math>0.005 \leq \mu_L</math> (Pa·s) <math>\leq 0.06</math>, <math>U_G &lt; 0.1</math> m/s</p>
<p>9. Schumpe and co-workers (58)</p> $\frac{k_L a_D d_T^2}{D_L} = 0.021 \left( \frac{\mu_L}{\rho_L D_L} \right)^{0.5} \left( \frac{g d_T^2 \rho_L}{\sigma_L} \right)^{0.21} \left( \frac{g d_T^3 \rho_L^2}{\mu_L^2} \right)^{0.60} \left( \frac{U_G}{\sqrt{g d_T}} \right)^{0.49}$ <p><math>\mu_L</math> is the apparent viscosity of the power law fluid</p>	<p>non-newtonian media</p>
<p>10. Kawase and co-workers (59)</p> $\frac{k_L a_D d_T^2}{D_L} = 0.555 \left( \frac{K d_T^{1-n}}{\rho_L D_L U_G^{1-n}} \right)^{0.5} \left( \frac{g d_T^2 \rho_L}{\sigma_L} \right)^{3/5} \left( \frac{d_T^n U_G^{2-n}}{K / \rho_L} \right)$ $\times \left( \frac{U_G^2}{g d_T} \right) \frac{(2+n)(2n-3)}{20(1+n)^2} \varepsilon_G^{0.5}$	<p>newtonian and non-newtonian power law fluids. For newtonian fluids <math>K = \mu_L</math> and <math>n = 1</math></p>
<p>11. Hikita and co-workers (60)</p> $k_L a_L = \frac{14.9 g f}{U_G} \left( \frac{U_G \mu_L}{\sigma_L} \right)^{1.76} \left( \frac{\mu_L^4 g}{\rho_L \sigma_L^3} \right)^{-0.248} \left( \frac{\mu_G}{\mu_L} \right)^{0.243} \left( \frac{\mu_L}{\rho_L D_L} \right)^{-0.604}$ <p><math>f</math> is 1.0 for nonelectrolytes; <math>f = 10^{0.0681I}</math> for ionic strength <math>I &lt; 1.0</math> kg ion/m<sup>3</sup>; and <math>f = 1.114 \times 10^{0.021}</math> for <math>I &gt; 1.0</math> kg ion/m<sup>3</sup></p>	<p>low viscosity newtonian media: water and various gases (air, oxygen, carbon dioxide, hydrogen, methane), sucrose solution, aqueous electrolytes, alcohols, <math>0.0008 \leq \mu_L</math> (Pa·s) <math>\leq 0.011</math>, <math>0.042 \leq U_G</math> (m/s) <math>\leq 0.38</math></p>
<p>12. Deckwer and co-workers (61)</p> $k_L a_D = 3.15 \times 10^{-3} U_G^{0.59} \left[ K (5000 U_G)^{n-1} \right]^{-0.84}$	<p>non-newtonian power law fluids, slug flow (<math>U_G &gt; 0.02</math> m/s)</p>
<p>13. Godbole and co-workers (62)</p> $k_L a_D = 8.35 \times 10^{-4} U_G^{0.44} \left[ K (5000 U_G)^{n-1} \right]^{-1.01}$	<p>non-newtonian power law fluids</p>

Table 14. Gas–Liquid Volumetric Mass Transfer Coefficient Correlations for Airlift Reactors

Configuration	Equation	Ranges
concentric-tube internal-loop vessels (annulus sparged)	$\frac{k_L a_D \sigma_L}{D_L g \rho_L} = 2.25 \left( \frac{\mu_L}{\rho_L D_L} \right)^{0.500} \left( \frac{\rho_L \sigma_L^3}{g \mu_L^4} \right)^{0.136} \left( \frac{d_H}{d_T} \right)^{-0.0905} \varepsilon_G^{1.26}$ Average estimation error was 12% for 175 measurements Koide and co-workers (65)	newtonian media, $3.71 \times 10^2 \leq \mu_L / \rho_L D_L \leq 6.00 \times 10^4$ , $1.18 \times 10^6 \leq \rho_L \sigma_L^3 / g \mu_L^4 \leq 5.93 \times 10^{10}$ , $0.471 \leq d_i / d_T \leq 0.743$ , $7.14 \times 10^{-3} \leq d_H / d_o \leq 2.86 \times 10^{-2}$ , $0.0302 \leq \varepsilon_G \leq 0.305$ , $6 \leq$ aspect ratio $\leq 15$ , $0.52 \leq A_d / A_r \leq 1.23$
concentric-tube internal-loop vessels (draft- tube sparged) external-loop reactor	$\frac{k_L a_D d_T^2}{D_L} = 2.66 \left( \frac{\mu_L}{\rho_L D_L} \right)^{0.500} \left( \frac{g d_T^2 \rho_L}{\sigma_L} \right)^{0.715} \left( \frac{g d_T^3 \rho_L^2}{\mu_L^2} \right)^{0.251} \left( \frac{d_i}{d_T} \right)^{-0.429} \varepsilon_G^{1.34}$ Koide and co-workers (66) $\frac{k_L a_L L}{U_{Lr}} = 14.5 \left( \frac{U_{Gr}}{U_{Lr}} \right)^{0.83} Pe^{-0.6}$ <i>Pe</i> -value is for the entire loop Verlaan and co-workers (67)	newtonian media, $\rho_L = 997\text{--}1182 \text{ kg/m}^3$ , $\mu_L = (0.894\text{--}17.0) \times 10^{-3} \text{ Pa}\cdot\text{s}$ , $\sigma_L = (51.7\text{--}73.0) \times 10^{-3} \text{ N/m}$ , $D_L = (0.145\text{--}2.42) \times 10^{-9} \text{ m}^2/\text{s}$ , $A_r / A_d = 0.3\text{--}0.8$ , aspect ratio = 6–15 air–water in 0.165-m <sup>3</sup> reactor, aspect ratio = 16 (based on riser), $A_r / A_d = 4$ , no gas in downcomer, $0.01 \leq U_{Gr}$ (m/s) $\leq 0.14$ , $Pe = U_L L / E_L$ , $Pe = 40\text{--}60$ (increased with gas flow rate)
a bubble column and a draft- tube sparged concentric- tube airlift vessel	$\frac{k_L a_L d_T^2}{D_L} = 0.018 \left( \frac{K (2800 U_G)^{n-1}}{\rho_L D_L} \right)^{0.5} \left( \frac{g d_T^2 \rho_L}{\sigma_L} \right)^{0.20} \left( \frac{U_G}{\sqrt{g d_T}} \right)^{0.51}$ $\times \left( \frac{g d_T^3 \rho_L^2}{[K (2800 U_G)^{n-1}]^2} \right)^{0.62} (1 + 0.12 Wi)^{-1}$	non-newtonian fluids. Bubble column (0.05 m <sup>3</sup> , aspect ratio $\approx 19$ ); airlift reactor (1.2 m <sup>3</sup> , $A_r / A_d = 1$ , aspect ratio $\approx 12$ )
concentric-tube internal-loop (draft-tube sparged)	<i>Suh</i> and co-workers (68) $k_L a_L = 3.43 \times 10^{-2} U_{Gr}^{0.524} \mu_{-ap}^{-0.255}$ $\mu_{-ap}$ was calculated by assuming the shear rate to equal $5000 \cdot U_{Gr}$ for $U_{Gr} \geq 0.04 \text{ m/s}$ , or $1000 \cdot (U_{Gr})^{0.5}$ for $U_{Gr} < 0.04 \text{ m/s}$ . Li and co-workers (64)	aqueous carboxymethyl cellulose ( $K = 0.286\text{--}11.5 \text{ Pa}\cdot\text{s}^n$ ; $n = 0.441\text{--}0.617$ ), $0.055 \text{ m}^3$ vessel, $A_r / A_d = 0.618$ , aspect ratio $\sim 26$ . $0.020 \leq \mu_{ap} \leq 0.85 \text{ (Pa}\cdot\text{s)}$

Table 14. (Continued)

Configuration	Equation	Ranges
concentric-tube internal-loops (draft-tube sparged)	$\frac{k_L a_D d_T^2}{D_L} = 2.66 \left( \frac{\mu_L}{\rho_L D_L} \right)^{0.500} \left( \frac{g d_T^2 \rho_L}{\sigma_L} \right)^{0.715} \left( \frac{g d_T^3 \rho_L^2}{\mu_L^2} \right)^{0.251} \left( \frac{d_i}{d_T} \right)^{-0.429} \epsilon_G^{1.34}$ $\times \left( 1 + 0.099 \left( \frac{C_S}{\rho_S} \right)^{0.069} \left( \frac{\rho_L \sigma_L^3}{g \mu_L^4} \right)^{0.023} \left( \frac{U_t}{U_G} \right)^{0.046} \right)^{-1}$ <p>average estimation error was within 17% for 383 measurements. Koide and co-workers (66)</p>	<p>suspensions of glass or bronze spheres, 3.71 <math>\times 10^2 \leq \mu_L/\rho_L D_L \leq 9.92 \times 10^4</math>, <math>1.36 \times 10^3 \leq g d_T^2/\rho_L \sigma_L \leq 1.22 \times 10^4</math>, <math>1.29 \times 10^8 \leq g d_T^3 \rho_L^2/\mu_L^2 \leq 1.26 \times 10^{11}</math>, <math>0.471 \leq d_i/d_T \leq 0.743</math>, <math>3.99 \times 10^{-2} \leq \epsilon_G \leq 2.73 \times 10^{-1}</math>, <math>1.69 \times 10^{-11} \leq g \mu_L^4/\rho_L \sigma_L^3 \leq 2.55 \times 10^{-6}</math>, <math>0 \leq C_S/\rho_S \leq 8.00 \leq 10^{-2}</math>, <math>1.17 \times 10^{-2} \leq U_t/U_G \leq 0.844</math>, <math>A_r/A_d = 0.3-0.8</math>, aspect ratio = 6-15</p>
concentric-tube internal-loop reactors (draft-tube sparged)	$\frac{k_L a_D d_T^2}{D_L} = \frac{4.04}{1 + 2\phi_S^{1.3}} \left( \frac{\mu_L}{\rho_L D_L} \right)^{0.5} \left( \frac{g d_T^2 \rho_L}{\sigma_L} \right)^{0.67} \left( \frac{g d_T^3 \rho_L^2}{\mu_L^2} \right)^{0.26} \left( \frac{d_i}{d_T} \right)^{-0.047} \epsilon_G^{1.34}$ <p>average error of estimation was 14% for 260 data; <math>U_G</math> is based on the diameter <math>d_T</math> of the outer column. The <math>k_L a_D</math> values in water and salt solutions were similar. Koide and co-workers (69)</p>	<p>suspensions of relatively low density calcium alginate beads in water, aqueous glycerol and aqueous salt solutions (0.10 or 0.27 kmol/m<sup>3</sup> barium chloride; 0.4 kmol/m<sup>3</sup> sodium sulfate), 0-20% vol/vol solids, 1.88-3.98-mm bead diameter, <math>A_r/A_d = 0.3-1.2</math>, aspect ratios = 6-16, <math>\mu = (0.894-12.5) \times 10^{-3}</math> Pa·s, <math>D_L</math> of oxygen = (0.194-2.42) <math>\times 10^{-9}</math> m<sup>2</sup>/s, <math>3.71 \times 10^2 \leq \mu_L/D_L \rho_L \leq 5.52 \times 10^4</math>, <math>2.66 \times 10^3 \leq \rho_L d_T^2 g/\sigma_L \leq 1.22 \times 10^8</math>, <math>2.35 \times 10^8 \leq \rho_L^2 d_T^3 g/\mu_L^2 \leq 3.29 \times 10^{11}</math>, <math>0.471 \leq d_i/d_T \leq 0.743</math>, <math>1.69 \times 10^{-11} \leq Mo \leq 6.67 \times 10^{-7}</math>, <math>3.79 \times 10^{-2} \leq \epsilon_G \leq 2.24 \times 10^{-1}</math>, <math>0 \leq \phi_S \leq 0.2</math>; where the Morton number is</p> $Mo = \frac{g(\rho_L - \rho_G)}{\sigma_L^3 \rho_L^2} K^4 \left( \frac{8U_L r}{d_r} \right)^{4(n-1)} \left( \frac{3n+1}{4n} \right)^{4n}$



Table 15. The Parameters in Equation 89 for Pulsed Baffle Reactors

Fluid	$\frac{\alpha_2}{s^{\beta+\gamma-1} m^{3\beta-\gamma} J^{-\beta}}$	$\beta (-)$	$\gamma (-)$	Ranges
water	4.86	0.364	1.55	$23 \leq P/V_L \text{ (W/m}^3\text{)} \leq 3620$ $0.0049 \leq U_G \text{ (m/s)} \leq 0.0099$ $h_L/d_T \approx 40$
water	0.281	0.632	1.138	$35 \leq P/V_L \text{ (W/m}^3\text{)} \leq 6600$ $0.0005 \leq U_G \text{ (m/s)} \leq 0.004$ $h_L/d_T \approx 1.87$
water–glycerol (1:1 by vol)	0.0039	0.735	0.668	$35 \leq P/V_L \text{ (W/m}^3\text{)} \leq 6600$ $0.0005 \leq U_G \text{ (m/s)} \leq 0.004$ $h_L/d_T \approx 1.87$
aqueous yeast slurry	4.8	0.268	1.184	$d_T = 0.05 \text{ m}$

Table 16. **Mass Transfer Coefficient Inside Mobile or Oscillating Drops in Liquid–Liquid Dispersions<sup>a</sup>**

Correlation	Range
$Sh \approx 16.7$	$Re < 50$
$Sh = 0.320Re^{0.68} \left( \frac{\sigma^3 \rho_C^2}{g\mu_C^4 \Delta\rho} \right)^{0.10} \left( \frac{4D_D t_C}{d_D^2} \right)^{-0.14}$	$Re > 150-200$
$Sh = 0.32Re^{0.63} Sc^{0.50} \left( 1 + \frac{\mu_D}{\mu_C} \right)^{-0.5}$	$10 \leq Re \leq 1000$ spherical drops
$Sh = 7.5 \times 10^{-5} Re_C^{2.0} Sc^{0.56} \left( 1 + \frac{\mu_D}{\mu_C} \right)^{-0.5}$	$100 \leq Re_C \leq 1500$ , larger oblate drops

<sup>a</sup>The  $Re$  number in these equations is based on drop diameter and relative velocity between phases; all other properties are for the drop phase unless otherwise noted. The density and viscosity in  $Re_C$  are for the continuous phase. The subscripts  $C$  and  $D$  refer to continuous and dispersed phases, respectively.

Table 17. **Continuous-Phase Mass Transfer Coefficient Correlations for Liquid–Liquid Dispersions<sup>a,b</sup>**

---

*Small, noncirculating drops*

$$Sh = 2 + 0.79 Re^{0.5} Sc^{0.33}$$

$$Sh = 2 + 0.76 Re^{0.5} Sc^{0.33}$$

$$Sh = 0.562 Re^{0.5} Sc^{0.33}$$

*Larger, mobile drops*

$$Sh = \frac{2}{\sqrt{\pi}} \left[ 1 - Re^{-0.5} \left( 2.89 + 2.15 \left( \mu_D / \mu_C \right)^{0.64} \right) \right]^{0.5} (Re \cdot Sc)^{0.5}$$

when  $Re < 120$ ,  $(\mu_D / \mu_C) \leq 2$ , and  $0 \leq (\rho_D / \rho_C) \leq 4$

$$Sh = -126 + 18 Re^{0.50} Sc^{0.33}$$

when  $8 \leq Re \leq 800$

$$Sh = -178 + 3.62 Re^{0.50} Sc^{0.33}$$


---

<sup>a</sup> Refs. 3, 95.

<sup>b</sup> The  $Re$  in these equations is based on drop diameter and relative velocity between phases; all other properties are for the continuous phase unless otherwise noted. The subscripts  $C$  and  $D$  refer to continuous and dispersed phases, respectively.

Table 18. **Properties of Some Oxygen Vectors<sup>a</sup>**

Property	<i>n</i> -Dodecane	Perfluorocarbon
oxygen solubility (mg/L)	59.4	118.0
density (kg/m <sup>3</sup> )	743	1750
interfacial tension (liquid–air) (N/m)	$24.6 \times 10^{-3}$	17.8
interfacial tension (liquid–water) (N/m)	$32.9 \times 10^{-3}$	25.0
boiling point (°C)	214	206

<sup>a</sup> Oxygen solubility data at 35°C; all other data at 30°C.

Table 19. Relationships for Estimating Solid–Liquid Mass Transfer Coefficients<sup>a</sup>

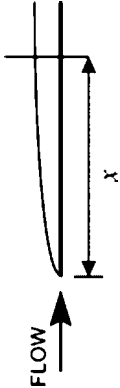


Flow geometry	Laminar flow	Flow transition	Turbulent flow
1. flow parallel to a flat plate	$Sh_x = 0.332 Re_x^{1/2} Sc^{1/3} \text{ } (Sc \geq 0.5)$	$Re_x \approx 5 \times 10^5$	$Sh_x = 0.0296 Re^{0.8} Sc^{0.6}$  ( $10.0 \geq Sc \geq 0.5$ )
	$Sh = 0.66 Re^{1/2} Sc^{1/3} \text{ } (Sc \geq 0.5)$		
2. fully developed flow in straight pipe	$Sh_x = 0.565 Re_x^{1/2} Sc^{1/2} \text{ } (Sc \leq 0.025)$ Subscript $x$ indicates <i>local</i> value a distance $x$ (characteristic length) from the leading edge of plate. Mean coefficient is given by the second equation where the whole length of the plate is used to calculate $Re$	$Re \approx 2300$	$Sh = 0.023 Re^{0.8} Sc^{0.33}$ ( $Sc > 0.5$ )
	use hydraulic diameter $d_h$ for noncircular section: $d_h = \frac{4 \times \text{flow area}}{\text{wetted perimeter}}$		$Sh = 0.0102 Re^{9/10} Sc^{1/3}$ ( $Sc \geq 10^3; Re \geq 3000$ )
3. fully developed flow between parallel plates	$Sh = 7.54 + 0.0234 \frac{Re \cdot Sc}{(L/d)}$	$Re \approx 2800$	$Sh = 0.023 Re^{0.8} Sc^{0.33}$ ( $Sc > 0.5$ )
			

Table 19. (Continued)

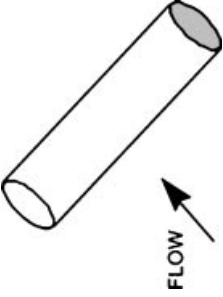

Flow geometry	Laminar flow	Flow transition	Turbulent flow
4. flow across a cylinder	$Sh = 0.43 + \alpha Re^\beta Sc^{0.31}$  $1000 \leq Re \leq 4000$ $(\alpha = 0.53, \beta = 0.5)$ $4000 \leq Re < 40000$ $(\alpha = 0.193, \beta = 0.618)$ $0.6 \leq Sc \leq 2.6$ (gases) $Sh = 0.600 Re^{0.513} Sc^{1/3}$ $1000 \leq Sc \leq 3000$ (liquids) $50 \leq Re \leq 50000$	$Re \approx 40,000$	$Sh = 0.43 + 0.0265 Re^{0.8} Sc^{0.31}$
			
5. flow across a sphere	$Sh = 2 + 0.37 Re^{0.6} Sc^{0.33}$  $Sh = 2 + 0.552 Re^{0.53} Sc^{1/3}$ (gases)  $0.6 \leq Sc \leq 2.7$ $1 \leq Re \leq 48,000$  $Sh = 2 + 0.95 Re^{0.50} Sc^{1/3}$ (liquids) $2 \leq Re \leq 2000$	$Re \approx 150,000$	
			

Table 19. (Continued)

Flow geometry	Laminar flow	Flow transition	Turbulent flow
6. flow through a packed bed of spheres	$Sh = 2 + 0.347 Re^{0.62} Sc^{1/3}$ (liquids)		
	$2000 \leq Re \leq 17000$		
	$St \cdot Sc^{2/3} = 1.625 Re_d^{-1/2}$	$Re_d = 120$	$St \cdot Sc^{2/3} = 0.687 Re_d^{-0.327}$
	$15 < Re_d < 120$		$120 < Re_d < 2000$
	$Re_d = \frac{\rho_L U_L d_{hi}}{\mu_L}$ , where		
$d_{hi} = \frac{6(1 - \phi) \cdot \text{flow area}}{\text{wetted perimeter}}$			
where $\phi$ is the void fraction and $St$ is the Stanton number:			
$St = \frac{Sh}{Sc} \frac{K_L}{Re} = \frac{K_L}{U_L}$			

<sup>a</sup> Refs, 2, 100.

Table 20. Solid–Liquid Mass Transfer Coefficient in Airlift Reactors

Reactor configuration	Correlation	Ranges
internal-loop reactors (draft-tube sparged)	$Sh = 2 + 0.064 \left( \frac{E \rho_L^3 d_p^4}{\mu_L^3} \right)^{0.165} Sc^{0.45}$ <p>Kushalkar and Pangarkar (121)</p>	0.5% wt benzoic acid granules, $d_p = 0.55\text{--}3$ mm, in air-water $A_r/A_d = 0.17\text{--}1.29$ , $U_G = 0.08\text{--}0.35$ m/s
internal-loop reactors (draft-tube sparged)	$Sh = 2 + 1.01 \left( \frac{E \rho_L^3 d_p^4}{\mu_L^3} \right)^{0.173} Sc^{0.33}$ <p>Goto and co-workers (120)</p>	Amberlyst 15 ion exchange resin, $d_p = 0.55\text{--}0.92$ mm, suspended in dilute aqueous sodium hydroxide. $A_r/A_d = 0.1\text{--}1.4$
internal-loop reactors with static mixers (draft-tube sparged)	$Sh = 2 + 1.68 \left( \frac{E \rho_L^3 d_p^4}{\mu_L^3} \right)^{0.133} Sc^{0.33}$ <p>Gaspillo and Goto (122)</p>	Kenics-type twisted ribbon static mixers were in draft tube
external-loop reactors	$Sh = 2 + 0.48 \left( \frac{E^{1/3} \rho_L d_p^{4/3}}{\mu_L} \right)^{0.72} Sc^{1/3}$ <p>Mao and co-workers (115)</p>	Benzoic acid coated particles, $d_p = 3.8$ mm, $\rho_s \approx 1080$ kg/m <sup>3</sup> , suspended in water



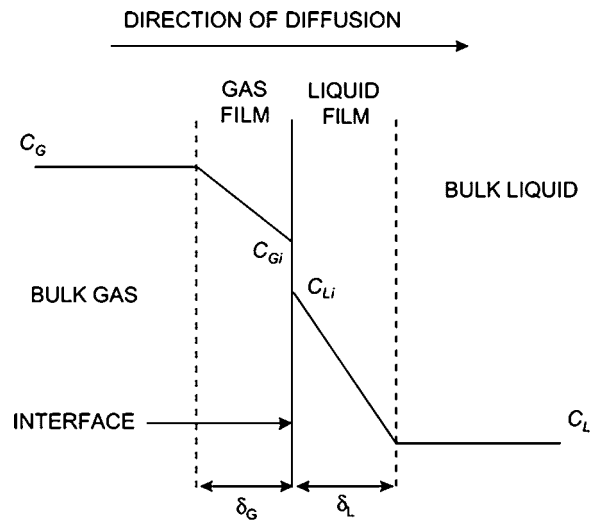


**Fig. 1.** Steady-state dissolved oxygen concentration profile in the vicinity of the gas-liquid interface.

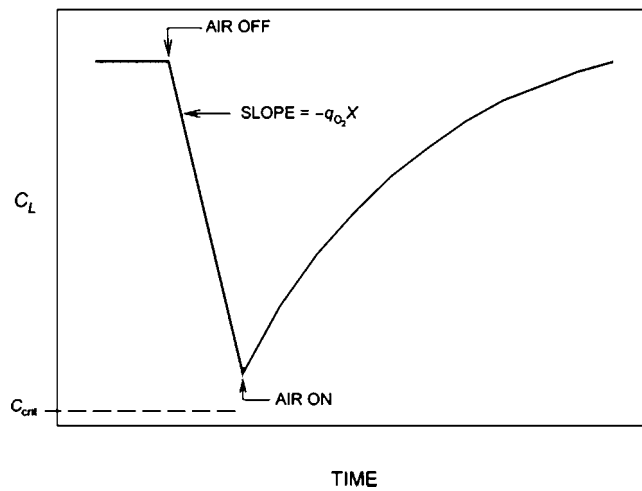


**Fig. 2.** Dissolved oxygen concentration as a function of time during dynamic determination of the overall volumetric gas-liquid mass transfer coefficient in a reactor.

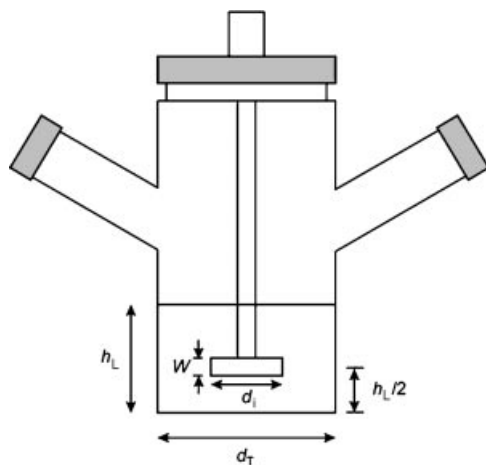


**Fig. 3.** Geometry of 500-mL Corning spinner flasks:  $h_L = 0.08$  m;  $d_T = 0.096$  m;  $d_i = 0.078$  m ( $W = 0.025$  m), or  $d_i = 0.053$  m ( $W = 0.019$  m).

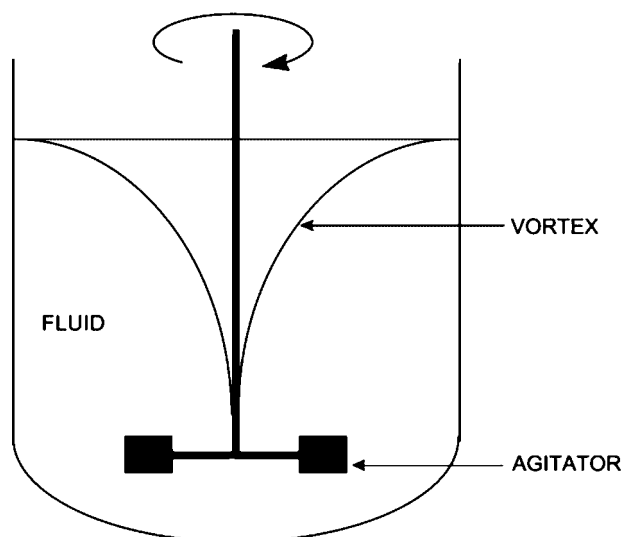


**Fig. 4.** Vortex aeration in a stirred reactor.

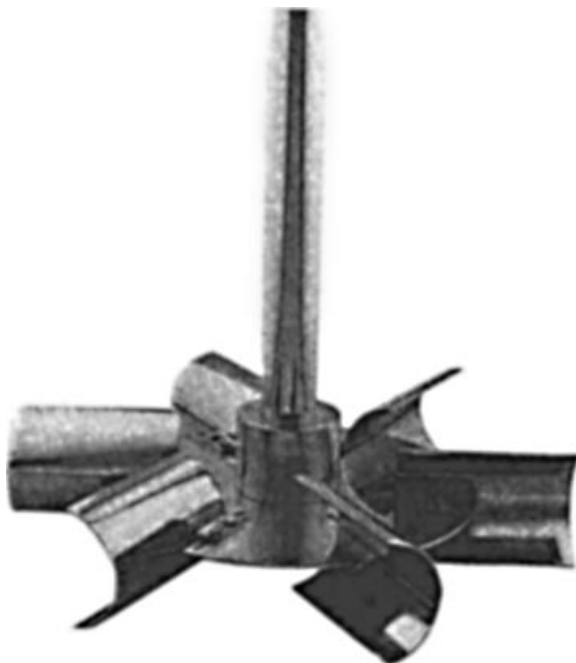


**Fig. 5.** A concave-blade impeller for dispersing gases in liquids. (Courtesy of Chemineer, Inc.)

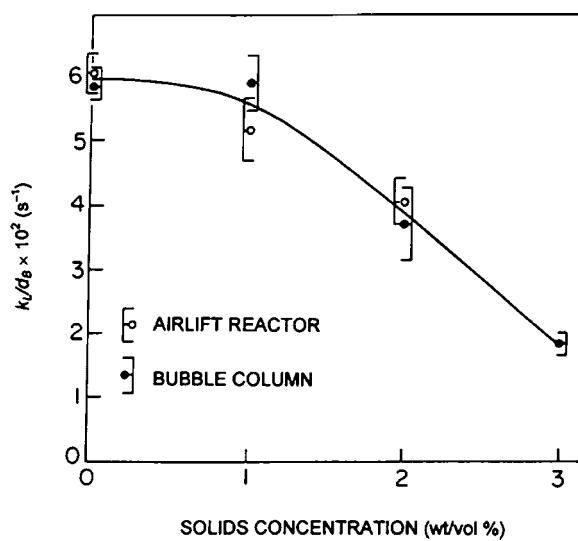


**Fig. 6.** Effect of concentration of cellulose fiber particles on the  $k_L/d_B$  ratio in aqueous salt solution (0.15 M NaCl) (7).

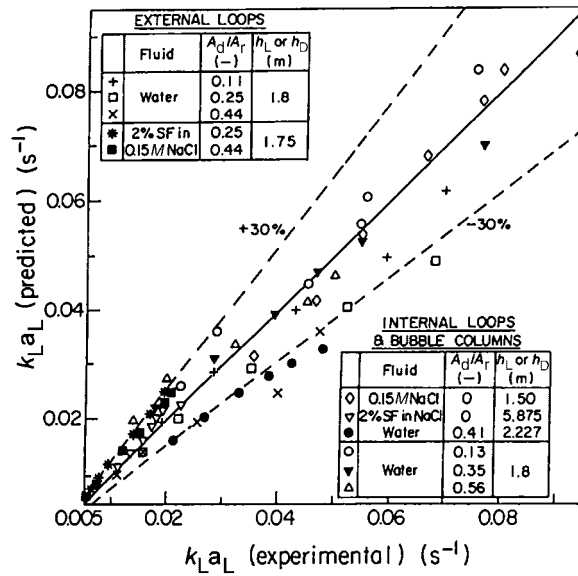


**Fig. 7.** Predicted versus measured overall volumetric gas-liquid mass transfer coefficient in bubble columns, external- and internal-loop airlift devices in Solka Floc (SF) cellulose fiber slurries and solids-free media (7). The solid line represents exact prediction.

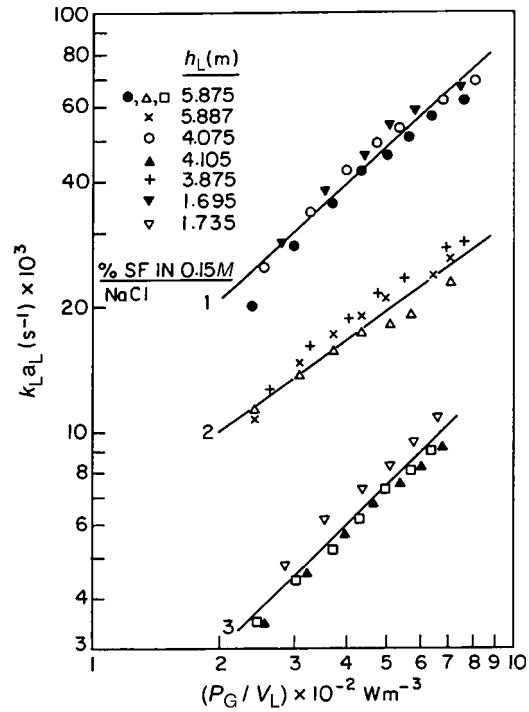


**Fig. 8.** The effect of SF cellulose pulp fibers on gas-liquid mass transfer coefficient in bubble columns at various static slurry heights  $h_L$ . The fibers were suspended in 0.15  $M$  sodium chloride in tap water (7). The  $k_L a_L$  is shown as a function of the specific power input.

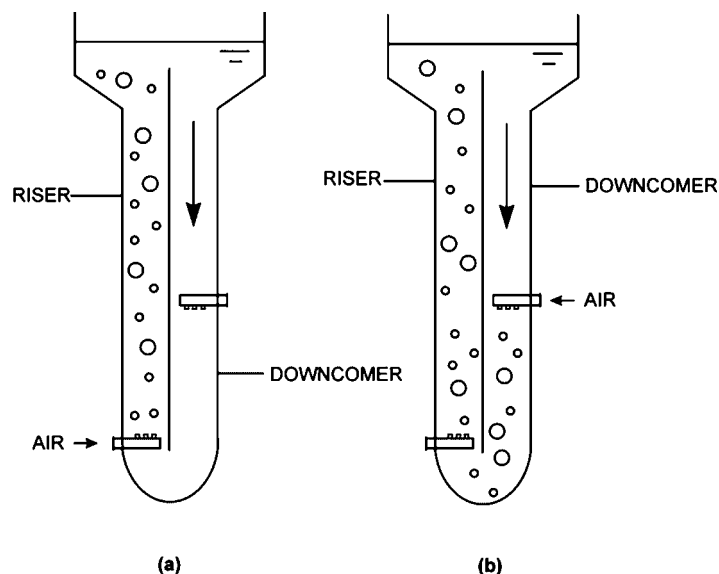


**Fig. 9.** Deep-shaft airlift reactor: (a) aeration in riser during start-up; (b) aeration in downcomer during normal operation. In case (b), no gas is being injected in the riser; all the gas bubbles in the riser are due to circulation from the downcomer.

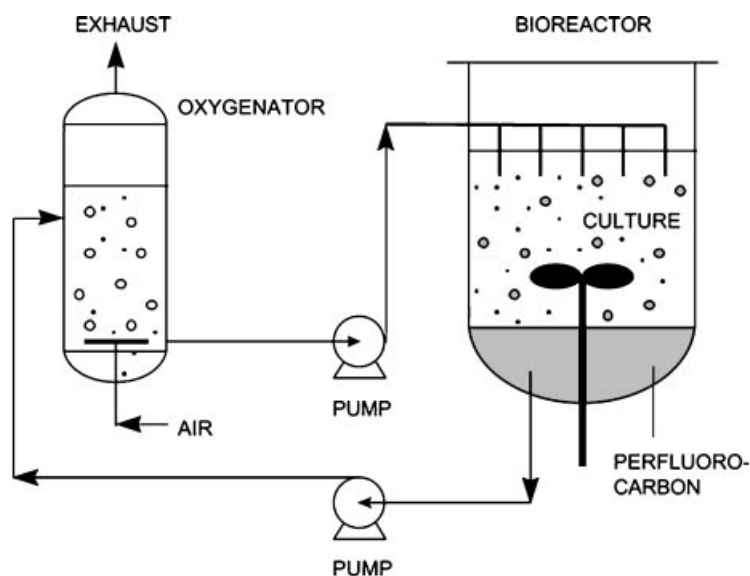


**Fig. 10.** Bubble-free aeration with perfluorocarbon oxygen vector in a bioreactor.

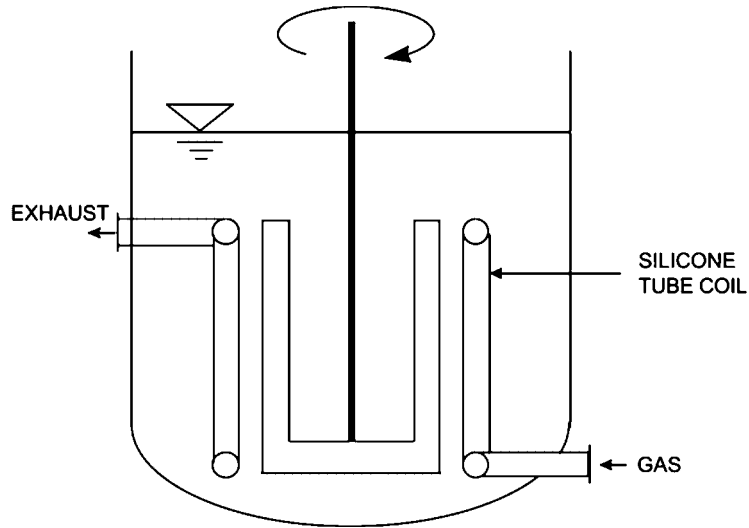


**Fig. 11.** Oxygen supply via silicone tubing.

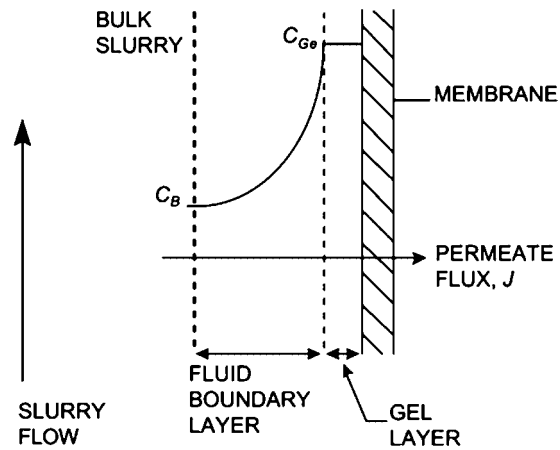


**Fig. 12.** Steady-state solute concentration profile in ultrafiltration and microfiltration processes.